PB93-217552

Center for Civil Engineering Earthquake Research

• Reno

Engineering Research and Development Center
College of Engineering
University of Nevada, Reno

Report Number CCEER-92-9

Effect of Hinge Restrainers on the Response of the Madrone Drive Undercrossing during the Loma Prieta Earthquake

D. N. O'Connor, M. "Saiid" Saiidi
and E. A. Maragakis

Prepared for

**California Department of Transportation,
National Science Foundation,
and Nevada Department of Transportation**

Center for Civil Engineering Earthquake Research
Department of Civil Engineering/258
University of Nevada
Reno, Nevada 89557

February 1993

Abstract

One of the most common seismic retrofitting techniques employed by the California Department of Transportation in recent years is the use of longitudinal restrainer cable systems. The Madrone Drive Undercrossing was retrofitted in 1985 with restrainer cables at the intermediate hinges and concrete shear keys at the abutments.

The October 1989 Loma Prieta earthquake caused extensive damage in the San Francisco Bay Area. Ground acceleration at the Madrone Drive Undercrossing was estimated at 0.65-g. This report describes the computer earthquake analysis conducted to determine the effect of the restrainer cables on the bridge's response.

Analysis cases examined include models with restrainer cables and without restrainer cables. Comparison of the results is made which provides an indication of the performance of the cables.

ACKNOWLEDGEMENTS

The study presented in this report was part of a project which has been mainly funded by the California Department of Transportation. Additional funds were provided by the National Science Foundation and the Nevada Department of Transportation (NDOT). All the funding agencies are thanked for providing their support. Messrs Jim Roberts, the Caltrans Chief Bridge Engineer, Jim Gates, a Caltrans senior bridge engineer, and Mark Yashinsky, the Caltrans project monitor are particularly thanked for their close interaction with the principal investigators and for providing advice in the course of this project. The assistance and promptness of Mr. Yashinsky in providing information to the researchers was much appreciated.

Dr. S. C. Liu, the program manager at the National Science Foundation, Mr. Floyd Marcucci, the Chief Bridge Engineer at NDOT, and Mr. R. Obisanya, a staff engineer at Caltrans, are also thanked for their support and comments.

Other members of the project team at the University of Nevada, Reno, provided significant assistance in the study. Mr. Saber Abdel-Ghaffar, a Doctoral student, and Dr. Shiping Feng, a visiting associate professor, are thanked for their valuable input.

Contents

List of Tables

List of Figures

Chapter 1
Introduction

1.1 Background

One of the most common seismic retrofitting techniques employed by the California Department of Transportation (Caltrans) in recent years is the use of longitudinal restrainer cable systems. Restrainer cables are believed to reduce the likelihood of bridge superstructures slipping off their supports. However, their effectiveness has not been extensively studied.

During the Loma Prieta earthquake of 17 October 1989, several highway bridges retrofitted with restrainer cables were subjected to relatively severe earthquake excitations. The dense network of strong-motion instrumentation in the area makes possible a detailed evaluation of the performance of these bridges.

1.2 Objective

This study represents one facet of a larger project funded by the California Department of Transportation, the National Science Foundation, and the Nevada Department of Transportation. The goals of the overall project include:

1. To develop detailed modeling elements for the currently used restrainer cables systems and incorporate them into available bridge dynamic analysis computer programs;
2. To perform a detailed survey of the response of retrofitted bridges during the Loma Prieta earthquake and classify these structures according to structure type, geometry, location, and sustained damage; and
3. To analyze representative structures using the techniques developed in phase (1), and evaluate the performance of the retrofit cables and their exact role on the overall performance of the bridges.

This report represents a part of the third objective, and presents the results of the study of restrainer cable effectiveness for the Madrone Drive Undercrossing.

Chapter 2
Bridge Description and Damage Summary

2.1 Description

The Madrone Drive Undercrossing, illustrated in Figure 2-1, is located in Santa Clara County, about five miles south of Los Gatos on California State Route 17. Built in 1938, the bridge is a three-span reinforced concrete T-beam structure with an overall length of 134 feet and a width of 59 feet. The bridge carries two 25-foot wide travel lanes, and has a 4-foot wide raised median to separate opposing traffic. The bridge elevation is 9.4 feet higher at the south abutment than at the north abutment (a vertical grade of 7 percent), and lies on a 700-foot radius curve with a superelevation rate of 10.4 percent. The bridge has no skew at the abutments or hinges.

The structure was designed in 1937 using the service load method to carry American Association of State Highway Officials (AASHO) H-15 live loads. Portland cement concrete used for the structure was specified to have a minimum compressive strength, f'_c, of 3000 psi; reinforcement was specified as Grade 50 steel.

The T-beam deck section consists of a 7.25-inch thick reinforced concrete slab and eight 15-inch wide by 41-inch deep rectangular girders spaced on 8.25-foot centers. The south end span is 43 feet long, the center span is 50 feet, and the north end span measures 41 feet long. Diaphragms are 18 inches thick at the abutments and at the intermediate deflection hinges. A 10-inch thick diaphragm is located at the midpoint of the center span. The deck section is enclosed by a steel mesh and gunite soffit. A cross-section of the deck is shown in Figure 2-2.

The center span is continuous over the two column bents with a short (7-foot long) cantilever section at each end. Each end span consists of a simply-supported deck section resting on a hinge-type deflection joint at the cantilever end and resting on five rocker bearings at each abutment.

The intermediate hinges consist of two opposing 5 inch by 3.5 inch by 0.75 inch steel angles with an overall seat width of 4.5 inches, held in place by 32 1-inch diameter shear bolts. The joint is located at mid-height of the deck section, and has a gap of 0.5

inch above the joint seat and 1 inch below the seat. The hinge is designed to allow rotation about the transverse axis of the deck, but to restrain translations and rotations in other directions. A detail of the hinge is shown in Figure 2-3.

The columns are tapered rectangular columns, with the smallest section at the column base. Figure 2-2 is a section of the bridge which shows the column bent. The foundation consists of 18, 12-inch diameter by approximately 30-foot long treated douglas fir piles; the outer six piles of each pier were driven at a 6-to-1 batter. Each column is connected to its concrete pile cap by 18 No. 9 dowels.

The seat-type abutments consist of a concrete seat 18 inches thick by 5 feet wide and a 12-inch thick, approximately 8-foot high concrete backwall. 12.75-foot long wingwalls project from either side of the backwall at a 4-to-12 slope. The abutment seat is stepped to follow the superelevation of the deck. The five rocker bearings which support the end spans are mounted on concrete pedestals measuring 18 inches deep by 29 inches wide by 34 inches high. An expansion joint gap of 1 inch is specified between the abutment backwall and the deck.

2.2 Seismic Retrofit

Since the 1971 San Fernando Earthquake, the California Department of Transportation (Caltrans) has been aggressively retrofitting highway bridges.[14] Damage from that earthquake showed that bridges were especially susceptible to collapse caused by joints pulling apart. The first phase of the retrofit was concerned with limiting movement of the superstructure. In 1985, the Madrone Drive Undercrossing was retrofitted as shown in Figure 2-4.

Two reinforced concrete shear pedestals were installed at each abutment to restrain movement in both the longitudinal direction and in the transverse direction. Each shear pedestal contains two 16-inch by 18-inch shear blocks, one on either side of the first interior girder; therefore, four shear blocks act to restrain movement in the longitudinal direction while only two blocks act simultaneously in the transverse direction. The shear blocks become effective after the ½-inch expansion gap has been closed. Two additional concrete pedestals, measuring 2 feet by 4 feet, were installed to act as "landing pads" in the event of a failure of the rocker bearings.

According to the retrofit plans, two sets of restrainer cables were installed at each intermediate hinge, on the first interior girders at each side, to prevent the end spans from dropping off the joint seats in the event of a failure of the shear bolts. Each cable unit consists of a 12-foot long ¾-inch steel cable with swaged ends and a turnbuckle. Two cable units are looped through holes cored through the girders and diaphragms on opposite sides of the hinge and connected to form a restrainer set. The turnbuckles were initially torqued to 20 foot-pounds to remove slack in the cable, then backed off 1-½ turns, at which time the jam nuts were tightened to prevent accidental adjustment.

2.3 Damage from the Loma Prieta Earthquake

The Madrone Drive Undercrossing is located approximately 8 miles from the epicenter of the Loma Prieta earthquake. Ground acceleration at the bridge site was estimated at 0.65-g, and was strongly transverse.[14]

During the earthquake, the north abutment underwent slight rotation, as evidenced by pavement cracking at the backwall paving notch, and the rocker bearings were knocked out of plumb. All of the retrofitted end-span shear blocks were severely damaged, producing large spalls and exposing the reinforcing steel.[10] The retrofit, however, appears to have contained the structure and prevented a catastrophic collapse of the end spans. The damage report makes no mention of any damage to the intermediate hinges or the restrainer cables.

Under an emergency contract, repairs to the structure were completed by March 1990. The madrone Drive Undercrossing is in essentially the same condition today as prior to the Loma Prieta earthquake.[10]

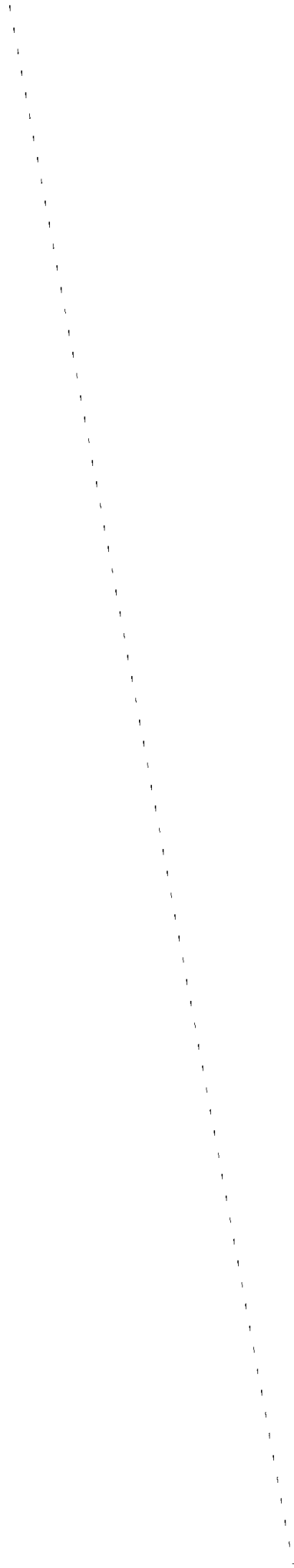

Chapter 3
Description of Computer Models

3.1 General Remarks

To determine the effect of the retrofit restrainer cables, two types of analysis were performed in this study: (1) a modal analysis to determine the first few mode shapes and the corresponding vibration periods, and (2) an earthquake analysis to evaluate the performance of the restrainer cables. The modal analysis was performed to obtain the structure's mass-proportional and stiffness-proportional damping factors, which are required as inputs to the earthquake analysis.

3.2 Computer Software for Analysis

3.2.1 Modal Analysis

The Madrone Drive Undercrossing modal analysis was performed using *Images-3D* from Celestial Software.[6] *Images-3D* is a three-dimensional general-purpose finite element analysis package for IBM and compatible personal computers. *Images-3D* can perform static, modal, and dynamic (response history) analyses. The modal analysis module can calculate the frequencies, mode shapes, modal weights, and participation factors for a given structure.

Images-3D supports the following element types:

1. Linear-elastic truss (axial force) and straight beam (flexural) elements;
2. Linear-elastic membrane and bending plates;
3. Linear-elastic springs between nodes and springs to ground; and
4. Linear-elastic cube, wedge, tetrahedron and axisymmetric solid elements.

Although *Images-3D* can perform time-history analyses, it does not support non-linear elements, and thus cannot be used to analyze a structure which is yielding.

3.2.2 Earthquake Analysis

The earthquake analysis for the Madrone Drive Undercrossing was performed using *NEABS* (*N*onlinear *E*arthquake *A*nalysis of *B*ridge *S*ystems) computer software.[7]

NEABS is a mainframe-based computer program written in FORTRAN IV that was developed for performing nonlinear dynamic analysis of bridges. *NEABS* evaluates the dynamic response time history to applied dynamic loadings or support excitations. The program uses a step-by-step integration procedure using either a constant acceleration or a linear acceleration method.

The *NEABS* program supports the following element types:

1. Linear-elastic and elasto-plastic (bilinear) straight beam (flexural) elements, shown in Figure 3-1;
2. Linear-elastic and elasto-plastic (bilinear) curved beam elements;
3. Linear-elastic foundation spring elements, shown in Figure 3-2;
4. Linear and bilinear expansion joint elements, shown in Figure 3-3; and
5. Nonlinear biaxial bending elements, shown in Figure 3-4.

The nonlinear biaxial bending elements, also called "five-spring elements," were added to the *NEABS* program during an earlier study conducted at the University of Nevada.[5] This element represents a column as a group of five axial springs, each spring representing the properties of the concrete and reinforcing steel. When employed in regions of plastic hinging in columns, five-spring elements allow a more realistic response to reinforced concrete columns subjected to biaxial bending than do linear-elastic or bilinear straight beam elements.

3.3 Simplifying Assumptions for the Madrone Drive Undercrossing

For ease in implementing the computer models, certain simplifying assumptions were made concerning the Madrone Drive Undercrossing:

1. The bridge lies on a 700-foot radius horizontal curve; the model is assumed to be straight.
2. The Madrone Drive Undercrossing has a superelevation of 10.4 percent to accommodate high-speed traffic on the horizontal curve; the model has no super-elevation.
3. The Madrone Drive Undercrossing has a vertical grade of -7.0 percent in the northbound direction; the model is assumed to have no vertical gradient.

These simplifications are illustrated in Figure 3-5.

3.4 Modal Analysis Model

3.4.1 Finite Element Mesh

The finite element model of the Madrone Drive Undercrossing used in the *Images-3D* analysis consists of 35 nodes, 34 linear-elastic beam elements, and 24 linear-elastic ground spring elements (Figure 3-6).

3.4.2 Element Properties

The Madrone Drive Undercrossing model is composed of several element types. This section describes the element properties employed to model the components of the structure.

Table 3-1 lists the material properties of the portland cement concrete used in the Madrone Drive Undercrossing.

3.4.2.1 Deck

The deck section, shown in Figure 3-5, is composed of a deck slab 7.25 inches thick by 59 feet wide, with eight girders measuring 15 inches wide by 40.75 inches high. Six-inch chamfers are included at acute angles between the deck and the girders. A 1.5-inch thick concrete slab extending the width of the deck section is included to model the wire mesh and gunite soffit.

The section properties for the deck are listed in Table 3-2.

3.4.2.2 Column Bent Cross-Beams

The bent cap-beams are also illustrated in Figure 3-5. Properties for these beams were calculated based on a T-beam section measuring 10.75 feet deep by 2.25 feet wide topped with a 9.5 foot wide section of the 7.25 inch deck slab. The width of the slab effective as a T-beam flange is based on the overhang limit of six times the deck thickness, as specified in the American Association of State Highway and Transportation Officials (AASHTO) bridge code.[1] Six-inch chamfers are included at acute angles of the section.

Section properties used in the *Images-3D* analysis are listed in Table 3-2. Bending inertia about the local *y*-axis was artificially increased to simulate the stiffening effect of the full-width deck, which is otherwise modeled as a point connection.

3.4.2.3 Column Caps and Rigid Members

Because of the elevation difference (4.6 feet) between the center of gravity of the deck section and the column bent cross-beams it was necessary to use a rigid beam to connect the elements. Rigid elements were also used to model the very-stiff upper joint region for each column. Section properties for these elements were chosen to ensure rigidity, and are listed in Table 3-2.

3.4.2.4 Columns

Each column bent is composed of two tapered columns (deeper at the top of the column). Each column is modeled with two linear-elastic beam elements sized to the average section properties. Table 3-2 lists the properties which were used in the *Images-3D* analysis.

3.4.2.5 Column Foundations

Each column is supported on 18 12-inch diameter Douglas Fir piles and a 2.25-foot thick pile cap. The piles are approximately 30 feet long and were driven to a pile loading of 21 tons. While the outer six piles were driven on a 6-to-1 batter, they were assumed vertical for this analysis. The column foundation was modeled using translational and rotational springs to ground.

The spring stiffnesses used are listed in Table 3-3. These parameters are described in detail in Section 3.5.2.5.

3.4.2.6 Abutment Expansion Joints

The expansion joint at each abutment consists of a rocker bearing; the shear blocks added as part of the seismic retrofit in 1985 were not included in the modal analysis. To simulate the rocker bearings, the deck end nodes are free to translate in the longitudinal direction and rotate about the transverse (z) axis.

3.4.2.7 Intermediate Hinges

In the *Images-3D* analysis, the intermediate hinges were modeled by releasing the moment about the transverse axis at nodes 4 and 10. The restrainer cables were not modeled because they would introduce nonlinearities which are incompatible with modal analysis.

3.5 Earthquake Analysis Model

3.5.1 Finite Element Mesh

The *NEABS* finite element analysis model of the Madrone Drive Undercrossing consisted of 43 element nodes, 20 auxiliary (direction) nodes, 34 linear-elastic straight beam elements, 4 five-spring nonlinear biaxial bending elements, 6 linear elastic foundation spring elements, and 18 expansion joint elements (Figure 3-7).

3.5.2 Element Properties

The Madrone Drive Undercrossing model is composed of several element types. This section describes the elements employed to model the components of the structure and, in several unconventional cases, why such elements were chosen. The properties of the various components are also described.

Table 3-1 lists the properties of the portland cement concrete used for each of the concrete element types.

3.5.2.1 Deck

The deck section, shown in Figure 3-5, is composed of a deck slab 7.25 inches thick by 59 feet wide, with eight girders measuring 15 inches wide by 40.75 inches high. Six-inch chamfers are included at acute angles between the deck and beams. A 1.5-inch thick concrete slab extending the width of the deck section is included to model the wire mesh and gunite soffit. The section properties for the deck are listed in Table 3-4.

3.5.2.2 Column Bent Cross-Beams

The column bent cap-beams are illustrated in Figure 3-5. Properties for these beams were calculated based on a T-beam section measuring 10.75 feet deep by 2.25 feet wide topped with a 9.5 foot wide section of the 7.25 inch deck slab. Six-inch chamfers are included at the acute angles of the section.

Section properties used in the *NEABS* analysis are listed in Table 3-4. Bending inertia about the y-axis was artificially increased to simulate the stiffening effect of the full-width deck, which is otherwise modeled as a point connection.

3.5.2.3 Column Caps and Rigid Members

Because of the difference in elevation between the deck section center of gravity and the column bent cross-beam center of gravity it was necessary to use a rigid beam to connect these elements. Rigid elements were also used to model the very-stiff upper joint region for each column. Section properties for these elements were empirically chosen to ensure rigidity, and are listed in Table 3-4.

3.5.2.4 Columns

Each column was modeled with two linear-elastic beam elements sized to the average section properties. Table 3-4 lists the properties which were used in the *NEABS* analysis.

To monitor column behavior in the plastic hinge region at the base of each column, five-spring non-linear biaxial bending elements were employed. No inelastic elements were assigned at the top of the columns because the column sections at the top are considerably stronger than the base and no plastic hinging is expected at these locations. The section properties used for the biaxial bending elements are listed in Table 3-5.

3.5.2.5 Column Foundations

The column foundation was modeled using *NEABS*' boundary spring elements, as shown in Figure 3-2. Piles were assumed to have a constant skin friction along the length of the pile. The vertical stiffness for each pile was calculated using[1]

$$k_v = \frac{2AE}{L}$$

where A is the cross-sectional area of the pile, E is the modulus of elasticity for Douglas Fir,[13] and L is the length of the pile. The vertical stiffness for the pile group is $K_v = 18k_v$; the pile cap was assumed to have no effect on vertical stiffness.

Horizontal stiffness was assumed to be a combined effect from piles, pile cap sliding, and pile cap embedment. Pile cap sliding was determined according to[3]

$$k_h = \beta_h (1 \quad \nu) G \sqrt{A}$$

where β_h is a shape factor whose value is approximately 2.0 for a length-to-width ratio of 5 or less, ν is the poisson's ratio for concrete, G is the shear modulus of elasticity for concrete, and A is the area of the pile cap. Using a depth-to-effective radius ratio of 1.25, Ref. [3] provides an embedment factor of 1.5. Horizontal stiffness of the piles was assumed to be 40 kips per inch.[2]

Rotational stiffness about the vertical axis was calculated using the pile horizontal stiffness value of 40 kips per inch. Rotational stiffness about the global x- and z-axes were calculated using a pile stiffness value of 942 kips per inch, obtained from the equation for vertical stiffness described above. Rotational stiffnesses were determined by calculating the counter-moment to a given rotation:

$$K_\theta = \frac{M}{\alpha} = \frac{\sum_{i=1}^{n} (l_i \ \alpha \ k_{pile})}{\alpha}$$

where l_i is the moment arm for pile i, α is the angle of rotation in radians (very small angle such that $\alpha \cong \sin \alpha$), and k_{pile} is the pile stiffness.

3.5.2.6 Abutment Expansion Joints

The expansion joint at each abutment consists of a rocker bearing and shear blocks which were added as part of the seismic retrofit in 1985. The abutment joints are modeled by three expansion joint elements each, one acting in the longitudinal

direction and two acting in the transverse direction. The *NEABS* expansion joint element is illustrated in Figure 3-3.

To simulate the rocker bearing, the deck end node is free to translate in the longitudinal and transverse directions. Each of the four longitudinal-acting shear blocks was modeled as a restrainer cable with the same stiffness and yield properties as the concrete block. In the transverse direction, two shear blocks act simultaneously in each direction; these two simultaneous blocks were modeled by a single restrainer. Since the two sets of blocks act in opposite directions, a second transverse expansion joint/restrainer element had to be included. A disadvantage of using separate restrainer elements in the longitudinal and transverse directions is that coupling effects cannot be modeled; for example, if a shear block yields in the longitudinal direction, the program will not utilize the post-yield stiffness in the transverse direction until yielding occurs separately in that direction.

The expansion joint element properties and restrainer properties are listed in Tables 3-7 and 3-8, respectively.

3.5.2.7 Abutment Foundations

The abutment foundation was modeled as a combination of linear boundary spring elements and restrainer (expansion joint) elements. This combination was necessary to simulate the non-linear characteristic of soil during yielding.

The longitudinal stiffness, soil yielding, and rotational stiffness about the vertical axis were calculated using Caltrans guidelines.[2] The longitudinal and rotational stiffnesses were calculated using a soil stiffness per linear foot, K_s, value of 100 kips per inch (standard 200 kips per inch adjusted for a 4-foot backwall break-away height); soil yielding was based on the maximum effective soil stress of 7.7 kips per square foot.[2]

Because *NEABS*' boundary spring elements are linear and, therefore, cannot simulate the effect of soil yielding, a pair of restrainer cables was used to simulate longitudinal soil mobilization. The distance between the restrainers was chosen to provide the calculated rotational stiffness about the vertical axis. Properties for the expansion joint/restrainer elements are listed in Tables 3-7 and 3-8.

Abutment movement in the transverse direction was assumed to be linear, and was modeled with a boundary spring element. The stiffness value, listed in Table 3-6, was calculated as described in Section 3.5.2.5 for pile cap sliding. Abutment degrees-of-freedom were restrained for vertical (y) translation and rotation about the global x- and z-axes.

3.5.2.8 Intermediate Hinges

The hinges were modeled with several expansion joint elements: one element to model frictional sliding and the cable restrainers, and others to model the shear bolts. Because the restrainer element is capable of one-way (tensile) loading only, two restrainers are required to model a two-way member. Thus, two expansion joints each were required to model longitudinal and transverse shear in the bolts. As discussed in section 3.5.2.6, the longitudinal and transverse restrainer elements are uncoupled, unlike the actual bolts.

The cable restrainer properties, listed in Table 3-8, were calculated according to Caltrans guidelines,[3] using a yield stress, F_y, equal to 176.1 ksi, an area of 0.222 in^2, and a modulus of elasticity of 10,000 ksi.

The restrainer properties for the shear bolts are also listed in Table 3-8. Because the information did not appear on construction plans, A307 bolts were assumed. The shear yield force was obtained from Ref. [9]. The shear stiffness was calculated assuming the bolt to be a cantilever beam:[4]

$$k_b = \frac{1}{\frac{L^3}{3EI} + \frac{f_s L}{GA}}$$

where L is the length of the cantilever, E is the modulus of elasticity, I is the section's moment of inertia, f_s is the form factor for shear ($^{10}/_9$ for round bars), G is the shear modulus of elasticity, and A is the area of the section. The cantilever length was taken as 1.25 inches, the distance between the shear force bearing points (centerlines of the opposing steel angles).

Chapter 4

Results of Analysis

4.1 General Remarks

During the 1989 Loma Prieta earthquake, the Madrone Drive Undercrossing experienced minor structural damage to the abutment joint rocker bearings and severe damage to the retrofitted end-span shear blocks. The retrofit, however, contained the structure and prevented a catastrophic collapse of the end spans.

To evaluate the effectiveness of the restrainer cable systems installed across the intermediate hinges in 1985, a modal analysis and a nonlinear earthquake analysis were conducted using *Images-3D* and *NEABS*.[6,7] This chapter presents the analytical results.

4.2 Modal Analysis

A modal analysis, using *Images-3D*, was conducted to determine the frequencies of the first two modes which are then used to evaluate mass-proportional and stiffness-proportional damping ratios, two values which are required inputs for the earthquake analysis. Period and frequency results from the analysis are shown in Table 4-1. Figures 4-1 through 4-3 illustrate the first three mode shapes. The relatively high stiffness in the transverse direction precludes a low frequency (long period) transverse mode shape: the first mode is in the longitudinal direction, while the next two are in the vertical direction.

The mass-proportional damping factor, α, and the stiffness-proportional damping factor, β, are determined from the system of equations[11]

$$\zeta_1 = \frac{1}{2\omega_1}\left(\alpha + \beta\omega_1^2\right)$$

$$\zeta_2 = \frac{1}{2\omega_2}\left(\alpha + \beta\omega_2^2\right)$$

in which ζ_1 and ζ_2 are the damping factors for the first two modes and ω_1 and ω_2 are the corresponding circular frequencies, in radians per second. For this analysis, ζ_1 and ζ_2 were both assumed equal to 5 percent.

Based on the frequencies of the first two modes, the values of α and β were determined using the above equations (Table 4-2).

4.3 Nonlinear Earthquake Analysis

The nonlinear earthquake analysis was performed using *NEABS*.[7] Several steps are involved in running a *NEABS* analysis: first, data concerning the bridge's structural system must be compiled, as described in the previous chapter, recorded in the input file, and the input file uploaded to the mainframe computer; second, the *NEABS* program is run; and finally, the program output must be downloaded for post-processing.

4.3.1 Loma Prieta Earthquake

The epicenter of the Loma Prieta earthquake was located approximately 8 miles from the Madrone Drive Undercrossing. The peak ground acceleration was estimated at 65 percent of the acceleration of gravity (0.65-g, where g is equal to 32.2 ft/s^2) and was strongly in the transverse direction of the bridge.[14]

Accelerograms from the nearest strong-motion detector station, Aloha Avenue in Saratoga (CSMIP station number 58065), were used as the ground motion input for the *NEABS* earthquake analysis.[12] This station was located approximately 17 miles from the earthquake epicenter. Figure 4-4 illustrates the acceleration record; both components are shown scaled to the estimated 0.65-g peak acceleration value in the east-west direction. The scale factor shown in the figure includes a conversion from centimeters per second per second (cm/s^2) to feet per second per second (ft/s^2).

Because of the large (1.0-g) spike that appears in the North-South component, that component was not used in the analysis. The east-west component was applied to the bridge model in both longitudinal and transverse directions (Figure 4-5).

As discussed in the following sections, the response of the model to the 0.65-g maximum acceleration produced damage greater than actually reported. To reduce this damage, a maximum acceleration of 0.5-g, as shown in Figure 4-6, was also employed.

4.3.2 Analysis Cases

The goal of the earthquake analysis was to develop a computer model which would simulate the damage actually experienced by the Madrone Drive Undercrossing during the Loma Prieta earthquake. Once the model was tailored to this purpose, the retrofit hinge restrainer cables could be removed in the analysis. A comparison of the structure's response would then give an indication of the effect of the restrainers.

As shown in Figure 2-3, each intermediate hinge is restrained against longitudinal and transverse translation with 32, 1-inch diameter bolts. Because these bolts are not observable, their condition could not be determined. Therefore, two extremes were explored: the first case with hinge bolts fully intact; the second case without bolts, relying only on friction to hold the hinge together. Including the cases at 0.65-g and 0.5-g and the cases with and without restrainer cables, a total of eight studies were performed.

4.3.3 Results of Analysis

4.3.3.1 Bridge Displacement Response

The maximum displacements for the eight case studies are listed in Table 4-3; Figures 4-7 through 4-14 present the response histories. Note that the displacements are relative to the ground displacement.

In general, the midspan displacements in both longitudinal and transverse directions were greater in the cases without restrainer cables. The displacements in the longitudinal direction were also generally larger for the cases with hinge bolts than without. This is attributed to the fact that, when the bolts are present, inertia forces from the end spans add to the earthquake forces of the middle span and result in larger movements.

The maximum displacement of 4.0 inches (southward) occurs in the case with 0.65-g acceleration, with hinge bolts, and without restrainer cables. At this point (approximately 3.9 seconds) both the south hinge and the south abutment joint gaps have closed and the abutment backwall has been driven into the soil.

4.3.3.2 Abutment Expansion Joints and Backwall

The maximum relative displacements of the south and north abutment expansion joint (nodes 1 and 2 and nodes 16 and 17 on Figure 3-7, respectively) are listed in Table 4-4. The complete histories are shown in Figures 4-15 through 4-30. The figures are arranged in order of 0.65-g and 0.5-g maximum acceleration, with and without hinge bolts, south and north joints, and longitudinal and transverse responses. Each figure compares the respective case with and without restrainer cables.

Because the expansion joint gap is built into the expansion joint elements, both nodes of each pair have identical coordinates. The figures show the movement of the "free" node (part of the deck) with respect to the movement of the node attached to the abutment. When the relative displacements reach 1 inch, the gap between the superstructure and the substructure closes and the relative displacements remains constant until the gap reopens. The spikes seen past the 1-inch limit (see for example Figure 4-15) are due to the linearization method used in the computer program *NEABS*.

In general, the maximum longitudinal and transverse relative displacements occur in the cases without restrainer cables. Exceptions to this occur in the longitudinal direction for the case with 0.65-g and without hinge bolts and for the case with 0.5-g and without hinge bolts. As with the midspan displacement, larger relative displacements tend to occur in the cases with hinge bolts than in the cases without hinge bolts.

The largest longitudinal relative displacements, 4.1 inches at the south abutment and 4.4 inches at the north abutment, occur in the case with 0.65-g, with hinge bolts, and without cables.

In the case with 0.65-g, with hinge bolts, and with cables, the maximum longitudinal relative displacement at the north abutment was 3.5 inches, larger than indicated in the Caltrans damage report. It was because of this, and the estimate that the earthquake was strongly transverse, that the 0.5-g maximum acceleration studies were conducted.

Figures 4-31 through 4-38 illustrate movements of the south and north abutments (Nodes 1 and 17, respectively) for the cases with 0.65-g and 0.5-g acceleration and with and without hinge bolts. For the south abutment, a negative displacement represents

movement into the soil; for the north abutment, movement into the soil is represented by a positive displacement.

4.3.3.3 Intermediate Hinges

The responses for the south and north intermediate hinge are listed in Table 4-4 and are shown in Figures 4-39 through 4-54. As with the abutment expansion joints, the figures are arranged in order of 0.65-g and 0.5-g maximum acceleration, with and without hinge bolts, south and north joints, and longitudinal and transverse response. Each figure compares the cases with and without restrainer cables.

In general, the intermediate hinge maximum relative displacements in the longitudinal direction were higher for the cases without restrainer cables than the cases with cables. A notable exception is the case with 0.65-g acceleration and without hinge bolts: the maximum relative displacements in the case without restrainer cables is approximately two-thirds of that for the case with cables.

The north and south end spans dropped off the hinge seats in the case with 0.65-g acceleration, with hinge bolts, and without restrainer cables. At this magnitude earthquake, the cable restrainers prevented structural failure. In the case with 0.65-g acceleration, without hinge bolts, and with restrainer cables, the maximum relative displacement at the south hinge is 4.5 inches, which is the width of the seat, and is in danger of end span drop-off. In the four cases with 0.5-g maximum acceleration, there was no danger of the end spans dropping.

4.3.3.4 Intermediate Hinge Restrainer Cables

The tensile load in the restrainer cables for the four cases 0.65-g and 0.5-g acceleration and with and without intermediate hinge bolts are shown in Figures 4-55 through 4-62. The figures are presented in the order of 0.65-g and 0.5-g maximum acceleration, presence and absence of hinge bolts, and south and north hinges.

In general, there is more cable loading activity in the cases without hinge bolts. This is expected, since some of the load is absorbed by the bolts. In all cases, at both 0.65-g and 0.5-g maximum accelerations, the cables reach their yield load; however,

yielding occurs only over very short durations, indicating that extensive post-yielding deformations are not occurring.

4.3.3.5 Abutment Retrofit Shear Blocks

During the Loma Prieta earthquake, the retrofit shear blocks were severely damaged. One goal of the computer analysis was to simulate this damage, thus ensuring a reliable model. Extensive damage to all shear blocks occurred in each of the eight cases studies.

Table 4-6 presents the maximum shear deformations for the south and north abutment shear blocks. Figures 4-63 through 4-78 present the complete deformation histories. The figures are arranged in order of 0.65-g and 0.5-g maximum acceleration, with and without hinge bolts, south and north abutment joints, and longitudinal and transverse deformation. Each figure compares the respective case with and without restrainer cables.

In general, the maximum shear deformation in both the longitudinal and transverse directions was greater for the cases without restrainer cables than with cables. In the four cases with hinge bolts, maximum transverse deformation of the north abutment blocks was nearly identical for cases with and without restrainer cables.

4.3.3.6 Column Hinging

No report was made concerning damage to the bottom of the columns caused by the Loma Prieta earthquake, possibly because these areas are below grade and not directly observable. To monitor behavior at the base of each column, "five-spring" non-linear biaxial bending elements were included in the *NEABS* model. The nonlinear elements were assigned only to the base of the columns because the column sections at the top were considerably stronger than the bases and no yielding of the steel at the top of the columns was expected.

To determine if plastic hinging (column yielding) occurred, column displacements from the eight cases were compared to the column yield displacements in both the longitudinal and transverse directions. The column yield displacements were calculated from curvature data obtained from the computer program *IAIUNR*. *IAIUNR*

is a personal computer-based FORTRAN program which calculates the interaction between axial load and bending moment for a reinforced concrete section at yielding of a given layer of steel reinforcement and a given concrete compressive strain. When multiplied by the effective depth (the assumed plastic hinge length) of the column section, the yield curvature produces the yield rotation, in radians. The yield rotation was then multiplied by the column length to find the yield displacement at that point. Elastic deformation of the column outside the plastic hinge was ignored to simplify the study.

Table 4-7 lists the yield curvature, yield rotation, and corresponding yield displacement for column bending in the longitudinal and transverse directions (about the global z- and x-axis, respectively). The yield displacement values correspond to a height on the column 11.45 feet above the foundation. This point was chosen for scrutiny, rather than the top of the column, because this is the point where the *NEABS* model changes column cross-sections; *IAIUNR* cannot analyze columns with variable cross-sections.

The nodal displacement values calculated by *NEABS* include components from foundation ground spring translation and rotation as well as column bending, as illustrated in Figure 4-79. The corrected displacement due to column bending, δ_{corr}, can be calculated as

$$\delta_{corr} = \delta_t - \delta_b - \theta_b l,$$

where δ_t is the nodal displacement reported by *NEABS*, δ_b is the displacement of the foundation ground spring, θ_b is the rotation of the ground spring, and l is the height of the column, 11.45 feet in this analysis. The foundation ground spring translation was relatively small; however, the rotations were not, accounting for nearly half of the total displacement.

Table 4-8 shows the comparison between the corrected displacement values and the yield displacements. For each case, the column with the largest displacement was used to ensure that the worst case was being examined.

Under a maximum acceleration of 0.65-g, the columns experienced plastic hinging in the longitudinal direction for all four cases. The magnitude of plastic hinge rotation was greater for cases without restrainer cables than with cables and greater for cases with hinge bolts than without bolts, following the trend found in the maximum midspan displacements. The maximum displacement ductility was 1.43 and 2.37 for the cases with and without restrainers, respectively.

With a maximum acceleration of 0.5-g, longitudinal plastic hinging occurs in both cases without restrainer cables. In the cases with restrainer cables, no column yielding occurred. Column yielding did not occur in the transverse direction in any of the eight cases.

4.4 Concluding Remarks

This chapter described the results of the analyses conducted to evaluate the performance of the Madrone Drive Undercrossing's restrainer cable system during the Loma Prieta earthquake of 1989. Two separate analyses were conducted, a modal analysis to obtain structure period data, and an earthquake analysis to evaluate the restrainer cables. The modal analysis was necessary to determine input parameters for the earthquake analysis.

Eight cases were examined in the earthquake analysis, four each, with restrainer cables and without restrainer cables; the presence or absence of intermediate hinge bolts and the magnitude of the input acceleration represent the other variables. A comparison between cases with and without restrainer cables gives an indication of the relative performance of the cables.

Results of the *NEABS* analyses indicate that the retrofit restrainer cables had a beneficial effect on the response of the intermediate hinges. In the case with hinge bolts and with the Loma Prieta earthquake record scaled to 0.65-g, the restrainer cables prevented failure of the structure. At a lower acceleration of 0.5-g, presence of the restrainer cables typically reduced hinge relative displacement by approximately 20 percent, reduced damage to the abutment shear blocks, and prevented yielding at the base of the columns.

Chapter 5
Summary and Conclusions

5.1 Summary

One of the most common seismic retrofitting techniques employed by the California Department of Transportation in recent years is the use of longitudinal restrainer cable systems. The Madrone Drive Undercrossing, located about five miles south of Los Gatos on California State Route 17, was retrofitted in 1985 with concrete pedestals and shear keys at the abutments and restrainer cables at the intermediate hinges.

The Loma Prieta earthquake, which occurred on 17 October 1989, caused extensive damage in the San Francisco Bay Area. Ground acceleration at the Madrone Drive Undercrossing was estimated at 0.65-g, and was strongly transverse to the bridge. During the earthquake, the north abutment underwent slight rotation, as evidenced by pavement cracking at the backwall paving notch, and the rocker bearings were knocked out of plumb. All of the retrofitted end-span shear blocks were severely damaged, producing large spalls and exposing the reinforcing steel.

This study was commissioned to determine the effect of the retrofit restrainer cables on the bridge's response. Two types of analyses were performed: a modal analysis to determine the first few mode shapes and the corresponding structure periods, and an earthquake analysis to evaluate the performance of the restrainer cables. The modal analysis was performed to obtain the structure's mass-proportional and stiffness-proportional damping factors, which are required as inputs to the earthquake analysis.

Eight cases were examined in the nonlinear earthquake analysis. The parameters were input earthquake amplitudes of 0.65-g and 0.5-g, presence or absence of intermediate hinge bolts, and restrainer cables or no restrainer cables. A comparison between cases with and without restrainer cables provides an indication of the performance of the cables.

5.2 Conclusions

Results of the earthquake analysis indicate that for the Loma Prieta earthquake, the retrofit restrainer cables may have had a substantial influence on the response of the Madrone Drive Undercrossing.

Analyses conducted with the input acceleration scaled to 0.65-g indicate that the presence of the restrainer cables may have prevented a catastrophic failure of the structure, with both south and north end spans dropping-off the hinge seats.

With the earthquake acceleration scaled to 0.65-g, damage to the retrofit shear blocks was greater than actually observed; therefore, the maximum acceleration experienced by the Madrone Drive Undercrossing in the longitudinal direction was probably less than 0.65-g. For this reason, analyses were also conducted with the earthquake record scaled to 0.5-g. In this case, the end spans were not in danger of failing. The restrainer cables, however, were still heavily loaded, and minimized relative displacements at the intermediate hinges by approximately 20 percent and prevented yielding at the base of the columns.

References

1. AASHTO. 1992. *Standard specifications for highway bridges*, 15ed. Washington, D.C.: American Association of State Highway and Transportation Officials.

2. Division of Structures. 1991. *Seismic design references*. Sacramento: California Department of Transportation.

3. Federal Highway Administration. 1981. "Seismic design of highway bridges: Workshop manual." *Report No. FHWA-IP-81-2*. Washington, D.C.: U.S. Department of Transportation.

4. Gere, J. M., and S. P. Timoshenko. 1984. *Mechanics of materials*. 2d ed. Boston: PWS Engineering.

5. Ghusn, G. E., and M. Saiidi. 1986. "A simple hysteretic element for biaxial bending of R/C columns and implementation in NEABS-86." *Report No. CCEER-86-1*. Reno, Nevada: University of Nevada, Department of Civil Engineering.

6. *Images-3D*. 1985. Berkeley, Calif.: Celestial Software.

7. Imbsen, R. A., and R. A. Schamber. 1983. "Earthquake resistant bridge bearings." *Report No. FHWA/RD-82/166*, Vol. 2. Washington, D.C.: U.S. Department of Transportation, Federal Highway Administration.

8. Lai, S. S. 1984. *Inelastic analysis of reinforced concrete space frame under biaxial earthquake motions*. Doctoral dissertation. Toronto: University of Toronto, Department of Civil Engineering.

9. *Manual of steel construction*, 8th ed. 1980. Chicago: American Institute of Steel Construction.

10. Nagai, E. 1989. "Madrone Drive Undercrossing supplementary bridge report." Sacramento: California Department of Transportation, Division of Structures.

11. Saiidi, M., and M. A. Sozen. 1979. "Simple and complex models for nonlinear seismic response of reinforced concrete structures." *Report No. UILU-ENG-79-2013*. Urbana, Ill.: University of Illinois, Department of Civil Engineering.

12. Shakal, A., M. Huang, M. Reichle, C. Ventura, T. Cao, R. Sherburne, M. Savage, R. Darrah, And C. Peterson. 1989. "CSMIP strong-motion records from the Santa Cruz Mountains (Loma Prieta), California earthquake of 17 October 1989." *Report No. OSMS-89-06*. Sacramento: California Department of Conservation, Division of Mines and Geology.

13. *Uniform building code*. 1988. Whitter, Calif.: International Conference of Building Officials.

14. Yashinsky, M. 1991. "Performance of retrofit measures on existing older bridges." Sacramento: California Department of Transportation, Division of Structures.

Table 3-1. Concrete Properties for Madrone Drive Undercrossing.

Property	Value
Compressive Strength, f'_c	432 ksf (3000 psi)
Modulus of Elasticity, E	450,000 ksf (3.122×10^6 psi)
Poisson's Ratio, ν	0.20
Mass Density, r	0 *

* Mass density is zero to bypass *Images-3D* and *NEABS* internal dead load calculations; dead loads are applied as discrete nodal loads.

Table 3-2. *Images-3D* Beam Element Section Properties.

	Cross-Sectional Area (ft^2)	Bending Inertia about Local y-Axis (ft^4)	Bending Inertia about Local z-Axis (ft^4)	Torsional Inertia (ft^4)
Deck	86.43	30,894	196.89	22.06
Column Bent Cross Beams	30.18	1×10^4 *	386.82	38.29
Upper Columns	27.92	17.60	245.53	58.65
Lower Columns	23.04	14.52	139.20	46.40
Rigid Elements	200 *	1×10^6 *	1×10^6 *	1×10^4 *

* Values chosen to ensure adequate rigidity.

Table 3-3. *Images-3D* Column Foundation Boundary Spring Properties.

Property	Value
Linear Stiffness, K_x (k/ft)	5.81×10^6
Linear Stiffness, K_y (k/ft)	5.81×10^6
Linear Stiffness, K_z (k/ft)	2.03×10^5
Rotational Stiffness, $K_{\theta x}$ (k-ft/rad)	7.42×10^6
Rotational Stiffness, $K_{\theta y}$ (k-ft/rad)	2.44×10^6
Rotational Stiffness, $K_{\theta z}$ (k-ft/rad)	2.09×10^5

Table 3-4. *NEABS* Beam Element Section Properties.

	Cross-Sectional Area (ft^2)	Shear Area in Local y-Direction (ft^2)	Shear Area in Local z-Direction (ft^2)	Bending Inertia about Local y-Axis (ft^4)	Bending Inertia about Local z-Axis (ft^4)	Torsional Inertia (ft^4)
Deck	86.43	33.33	29.70	30,894	196.89	22.06
Column Bent Cross Beams	30.18	20.16	20.16	1×10^4 *	386.82	38.29
Upper Columns	27.92	23.27	23.27	17.60	245.53	58.65
Lower Columns	23.04	19.20	19.20	14.52	139.20	46.40
Rigid Elements	200 *	— †	— †	1×10^6 *	1×10^6 *	1×10^4 *

* Values chosen to ensure adequate rigidity.
† Shear deformation effects not considered for these elements.

Table 3-5. *NEABS* 5-Spring Biaxial Bending Element Properties.

Property	Value
Concrete Compressive Strength, f'_c	432 ksf
Reinforcing Steel Yield Strength, f_y	7200 ksf
Gross Cross-Sectional Area of Column, A_g	20.84 ft^2
Area of Longitudinal Reinforcing Steel in Column, A_s	0.125 ft^2
Development Length of Longitudinal Reinforcing Steel, l_d	1.533 ft
Balanced Condition Average Axial Capacity, $P_{b/ave}$	3969.0 kips
Balanced Moment Capacity about local y-axis, M_{by}	3529.2 k-ft
Balanced Moment Capacity about local z-axis, M_{bz}	8909.3 k-ft
Stiffness Degradation Factor for Tension	0.4
Stiffness Degradation Factor for Compression	0.4

Table 3-6. *NEABS* Boundary Spring Properties.

	Abutment	Column Piles and Pile Caps
Linear Stiffness, K_x (k/ft)	3.54×10^4 *	5.81×10^6
Linear Stiffness, K_y (k/ft)	— †	5.81×10^6
Linear Stiffness, K_z (k/ft)	8.64×10^6	2.03×10^5
Rotational Stiffness, $K_{\theta x}$ (k-ft/rad)	— †	7.42×10^6
Rotational Stiffness, $K_{\theta y}$ (k-ft/rad)	5.22×10^5 *	2.44×10^6
Rotational Stiffness, $K_{\theta z}$ (k-ft/rad)	— †	2.09×10^5

* This degree-of-freedom is modeled with bilinear expansion joint restrainers; see Table 3-8.
† This degree-of-freedom is restrained.

Table 3-7. *NEABS* Expansion Joint Element Properties.

	Coefficient of Friction	Friction Stiffness (k/ft)	Tie Bar Gap (ft)	Seat Gap (ft)	Impact Stiffness (k/ft)
Abutment Foundation: Longitudinal and Vertical-Axis Rotation	n/a	n/a	0	0	1.0×10^{8} *
Abutment: Bearings with Retrofit Shear Blocks, Longitudinal	0.02	1.0	0.083	0.083	1.65×10^{5}
Abutment: Retrofit Shear Blocks, Transverse	n/a	n/a	0.042	n/a	n/a
Intermediate Hinge: Hinge and Cable Restrainers, Longitudinal	0.02	1.0	0	0.042	8.25×10^{4}
Intermediate Hinge: Shear Bolts, Longitudinal	n/a	n/a	0	n/a	n/a
Intermediate Hinge: Shear Bolts, Transverse	n/a	n/a	0	n/a	n/a

n/a—Not applicable.
* Required to restrain degree-of-freedom in direction away from soil.

Table 3-8. *NEABS* Non-Linear Expansion Joint Restrainer Properties.

	Linear Stiffness, K (k/ft)	Yield Force, F_y (kips)	Number of Restrainers	Restrainer Pair Moment Arm, D * (ft)
Abutment Foundation: Longitudinal and Vertical-Axis Rotation	1.77×10^4	908.6	2	7.68
Abutment: Retrofit Shear Blocks, Longitudinal	2.23×10^5	115.2	4	—
Abutment: Retrofit Shear Blocks, Transverse	4.04×10^5	230.4	1	—
Intermediate Hinge: Cable Restrainers, Longitudinal	444.0	78.2	2	—
Intermediate Hinge: Shear Bolts, Longitudinal	3.15×10^5	126.4	2	33.85
Intermediate Hinge: Shear Bolts, Transverse	6.30×10^5	252.8	1	—

* Distance required to provide proper rotational stiffness about y-axis.

Table 4-1. Madrone Drive Undercrossing Modal Analysis Results.

Mode	Direction	Period, T (sec.)	Frequency, ω (rad./sec.)
Mode 1	Longitudinal	0.735	8.54
Mode 2	Vertical	0.123	51.3
Mode 3	Vertical	0.094	66.8

Table 4-2. α and β Factors for Madrone Drive Undercrossing.

Mass-proportional damping factor, α	0.7323
Stiffness-proportional damping factor, β	0.001672

Table 4-3. Midspan Maximum Displacements.

Case			Node 9 Displacement	
			Longitudinal (inches)	Transverse (inches)
0.65-g	With Bolts	With Cables	2.5	0.34
		Without Cables	4.0	0.38
	Without Bolts	With Cables	2.3	0.37
		Without Cables	2.3	0.39
0.5-g	With Bolts	With Cables	1.6	0.27
		Without Cables	2.5	0.29
	Without Bolts	With Cables	1.4	0.32
		Without Cables	2.4	0.32

Table 4-4. Abutment Expansion Joint Maximum Relative Displacements.

Case			South Abutment		North Abutment	
			Longitudinal (inches)	Transverse (inches)	Longitudinal (inches)	Transverse (inches)
0.65-g	With Bolts	With Cables	3.3	3.2	3.5	3.6
		Without Cables	4.1	3.6	4.4	3.6
	Without Bolts	With Cables	2.6	3.9	2.3	3.8
		Without Cables	2.2	4.0	3.0	4.1
0.5-g	With Bolts	With Cables	2.0	1.9	2.2	2.2
		Without Cables	2.7	2.1	2.4	2.2
	Without Bolts	With Cables	1.7	2.8	1.9	3.0
		Without Cables	2.2	3.0	2.6	2.4

Table 4-5. Intermediate Hinge Maximum Relative Displacements.

Case			South Hinge		North Hinge	
			Longitudinal (inches)	Transverse (inches)	Longitudinal (inches)	Transverse (inches)
0.65-g	With Bolts	With Cables	2.2	3.1	4.3	3.6
		Without Cables	**4.9**	3.5	**5.6**	3.5
	Without Bolts	With Cables	**4.5**	3.8	3.4	3.8
		Without Cables	2.9	4.5	1.9	3.7
0.5-g	With Bolts	With Cables	3.1	1.9	2.4	2.2
		Without Cables	2.9	2.1	2.9	2.1
	Without Bolts	With Cables	2.0	2.9	2.6	3.1
		Without Cables	3.0	3.1	3.8	2.3

Note: Shaded cells indicate displacement greater than hinge seat width.

Table 4-6. Abutment Retrofit Shear Block Maximum Shear Deformations.

Case			South Abutment		North Abutment	
			Longitudinal (inches)	Transverse (inches)	Longitudinal (inches)	Transverse (inches)
0.65-g	With Bolts	With Cables	2.3	2.7	1.8	3.2
		Without Cables	3.0	3.1	3.3	3.1
	Without Bolts	With Cables	1.6	3.4	1.3	3.3
		Without Cables	1.2	4.0	2.0	3.6
0.5-g	With Bolts	With Cables	1.0	1.4	1.2	1.7
		Without Cables	1.3	1.6	1.4	1.7
	Without Bolts	With Cables	0.7	2.1	0.9	2.5
		Without Cables	1.2	2.3	1.3	1.8

Table 4-7. Column Yield Displacements for Checking Non-Linear Bending Elements.

Direction of Bending	Curvature at Yielding, ϕ_y (feet^{-1})	Effective Depth, d (feet)	Yield Rotation, θ_y (radians)*	Yield Displacement, δ_y (feet)†
Longitudinal (About z-axis)	1.032×10^{-3}	2.50	0.00258	0.0295
Transverse (About x-axis)	4.014×10^{-4}	5.98	0.0024	0.0275

* $\theta_y = \phi_y d$.
† $\delta_y = \theta_y l$, where l = 11.45 feet.

Table 4-8. Non-Linear Bending Element (5-Spring Element) Results.

Case			Direction of Bending	Corrected Displacement from NEABS, δ_{corr} (feet)	Calculated Yield Displacement, δ_y (feet)	Ductility Ratio
0.65-g	With Hinge Bolts	With Restrainer Cables	Longitudinal	0.0421	0.0295	**1.43**
			Transverse	0.0087	0.0275	0.32
		Without Restrainer Cables	Longitudinal	0.0698	0.0295	**2.37**
			Transverse	0.0089	0.0275	0.32
	Without Hinge Bolts	With Restrainer Cables	Longitudinal	0.0345	0.0295	**1.17**
			Transverse	0.0088	0.0275	0.32
		Without Restrainer Cables	Longitudinal	0.0402	0.0295	**1.36**
			Transverse	0.0057	0.0275	0.21

Table 4-8 (Continued). Non-Linear Bending Element (5-Spring Element) Results.

Case			Direction of Bending	Corrected Displacement from NEABS, δ_{corr} (feet)	Calculated Yield Displacement, δ_y (feet)	Ductility Ratio
0.5-g	With Hinge Bolts	With Restrainer Cables	Longitudinal	0.0274	0.0295	0.93
			Transverse	0.0071	0.0275	0.26
		Without Restrainer Cables	Longitudinal	0.0416	0.0295	**1.41**
			Transverse	0.0073	0.0275	0.27
	Without Hinge Bolts	With Restrainer Cables	Longitudinal	0.0268	0.0295	0.91
			Transverse	0.0090	0.0275	0.33
		Without Restrainer Cables	Longitudinal	0.0381	0.0295	**1.29**
			Transverse	0.0098	0.0275	0.36

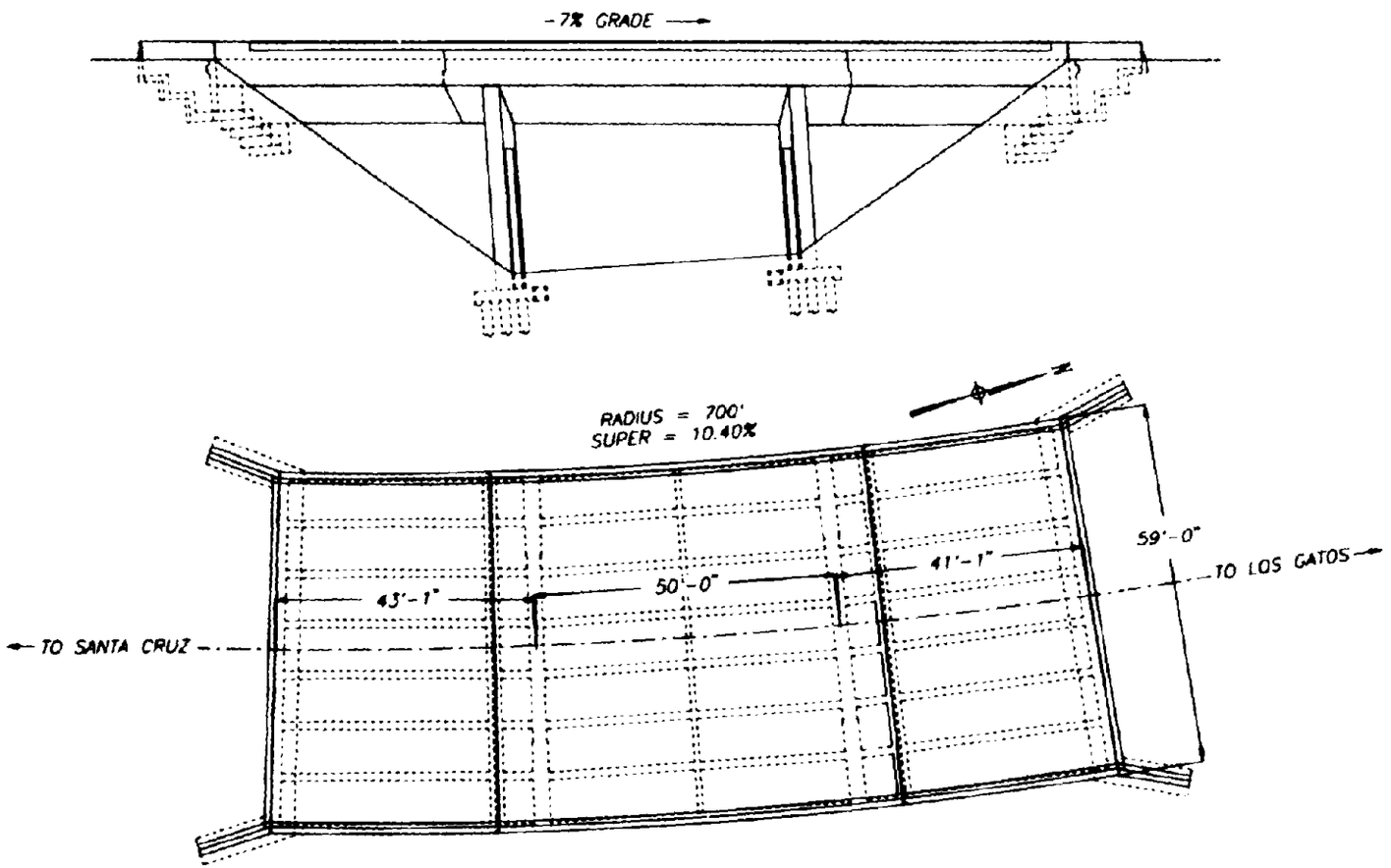

Figure 2-1. Madrone Drive Undercrossing.

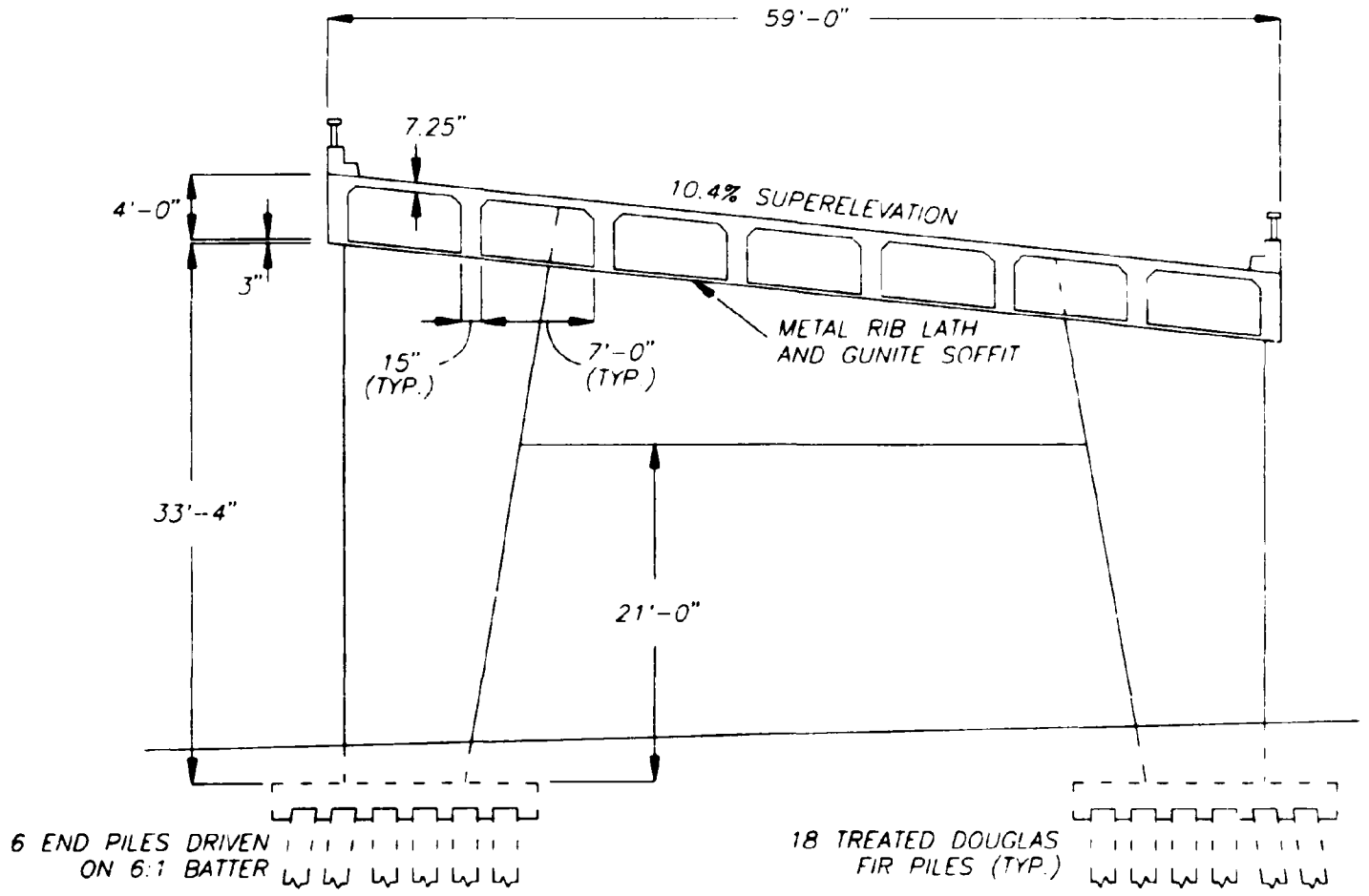

Figure 2-2. Section of Madrone Drive Undercrossing.

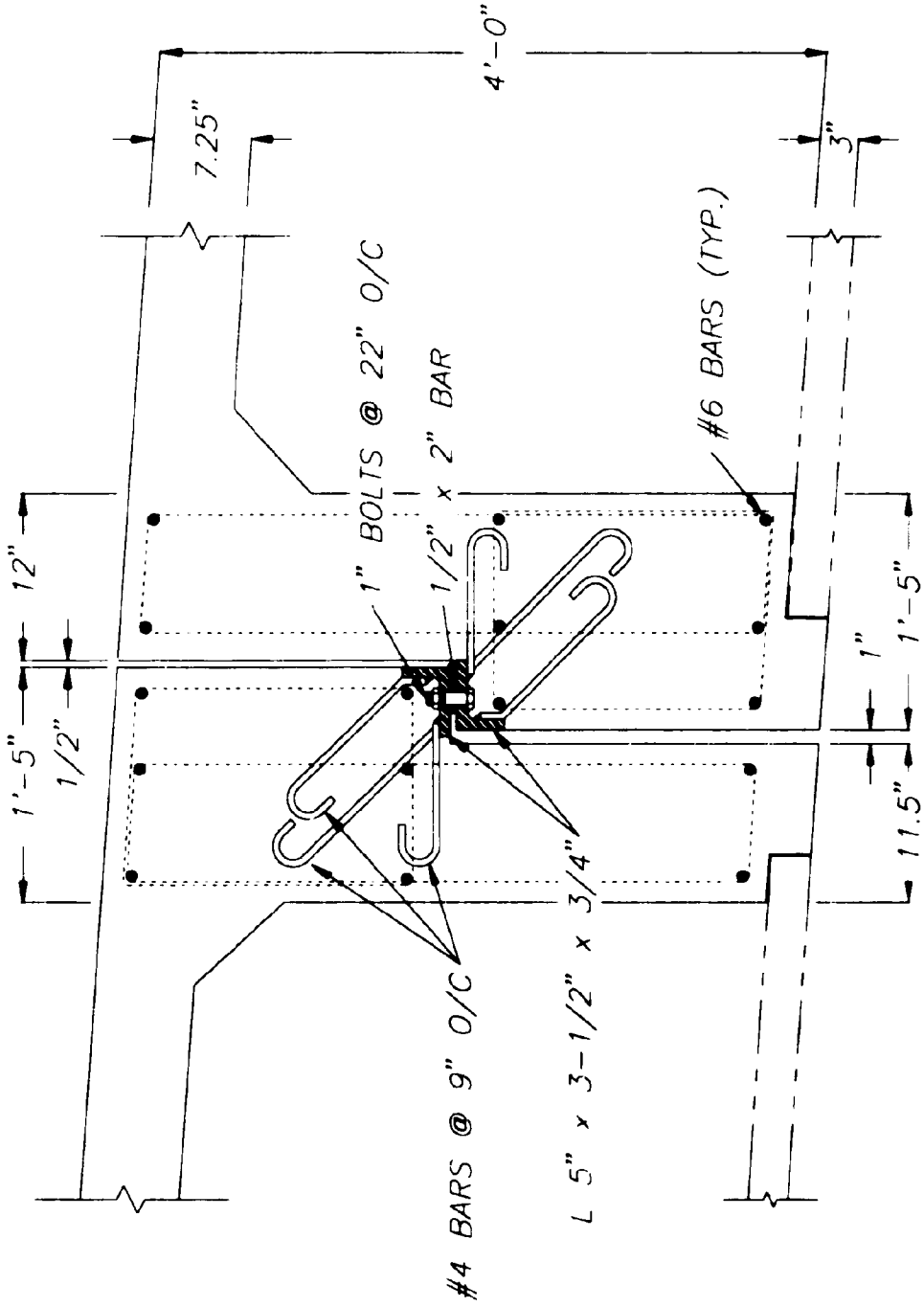

Figure 2-3. Detail of Intermediate Hinge.

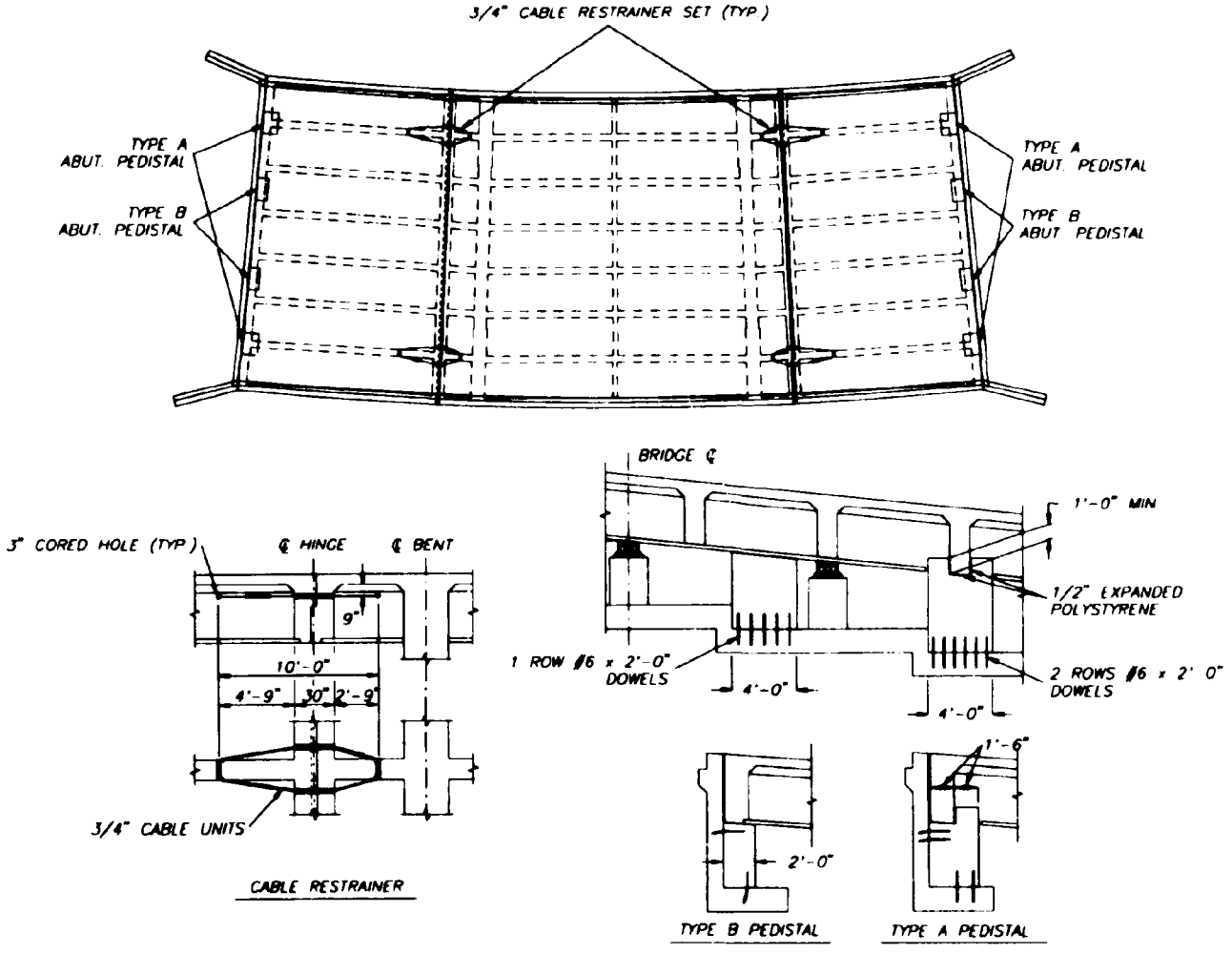

Figure 2-4. Seismic Retrofit of Madrone Drive Undercrossing.

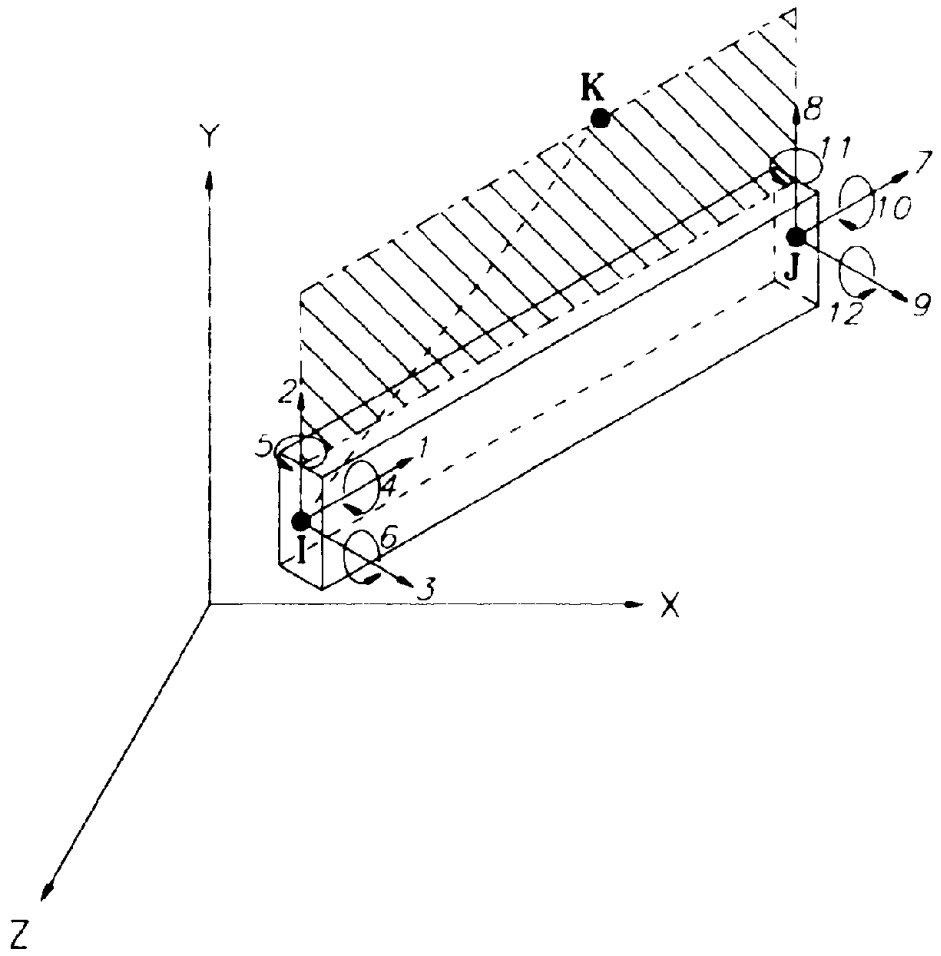

Figure 3-1. *NEABS* Beam Element Coordinate System.

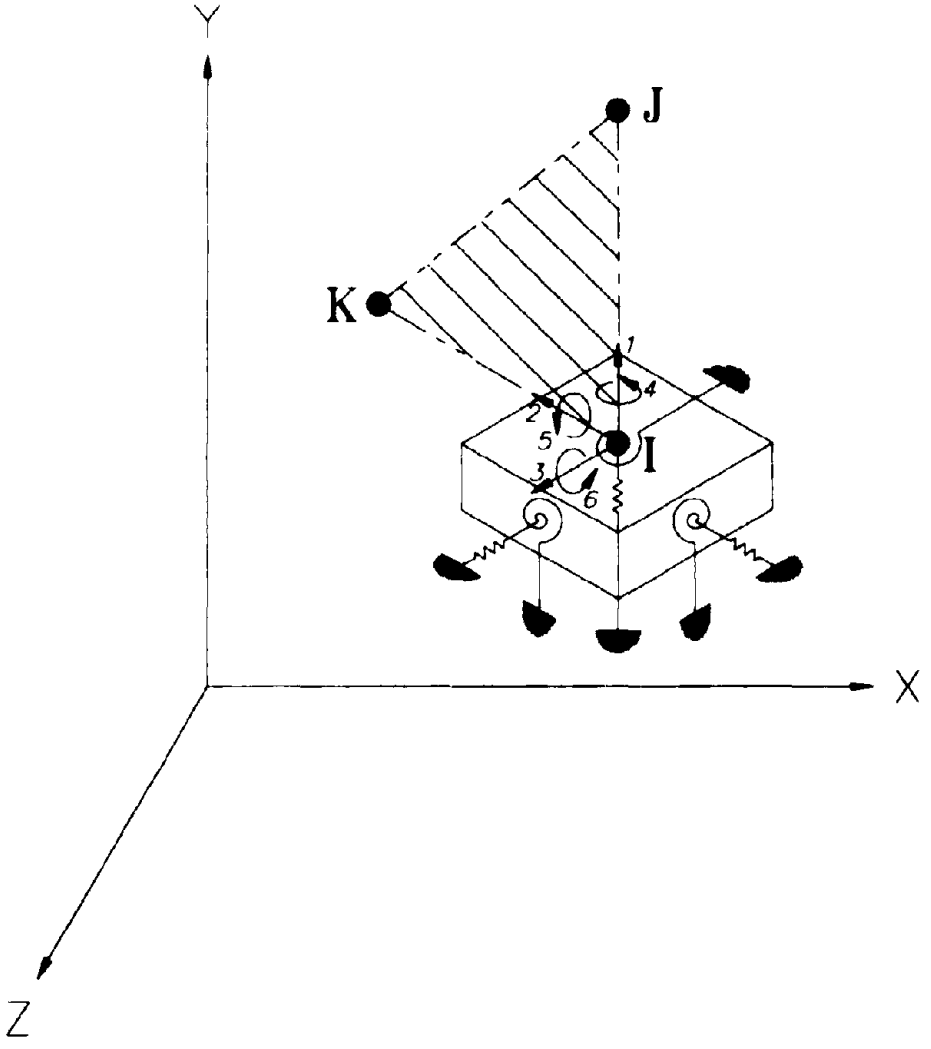

Figure 3-2. *NEABS* Boundary Spring Coordinate System.

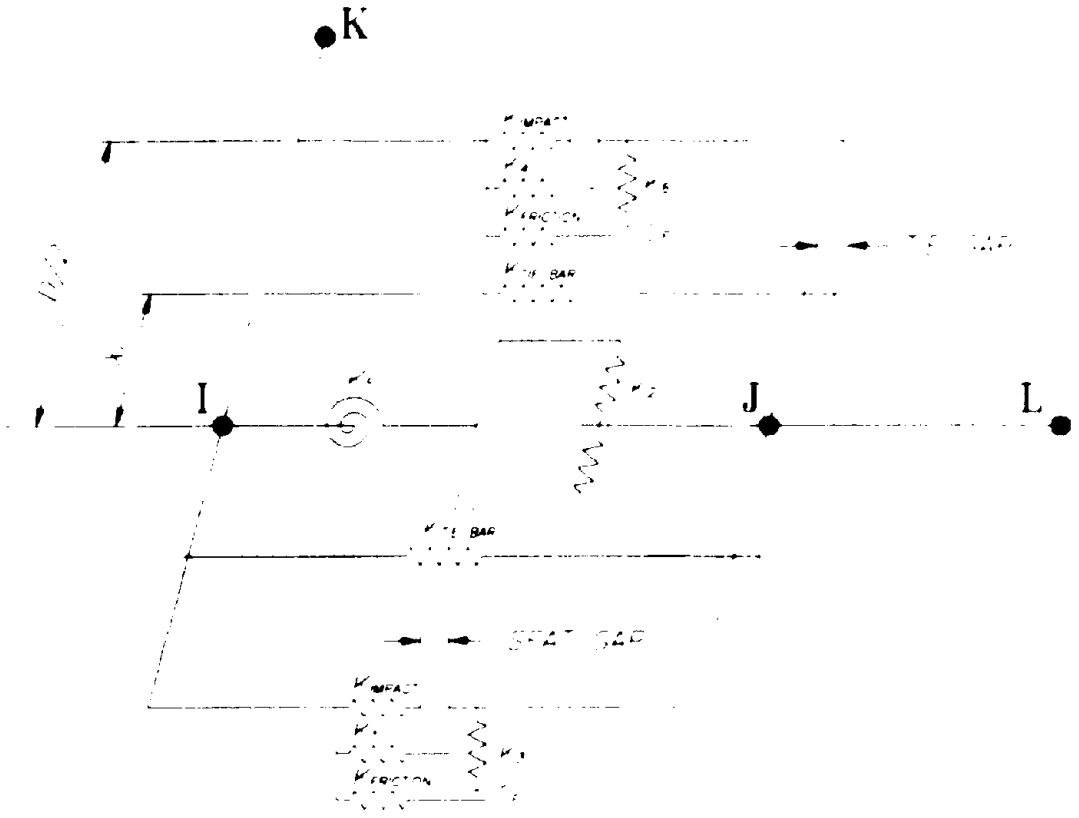

Figure 3-3. *NEABS* Expansion Joint Coordinate System.

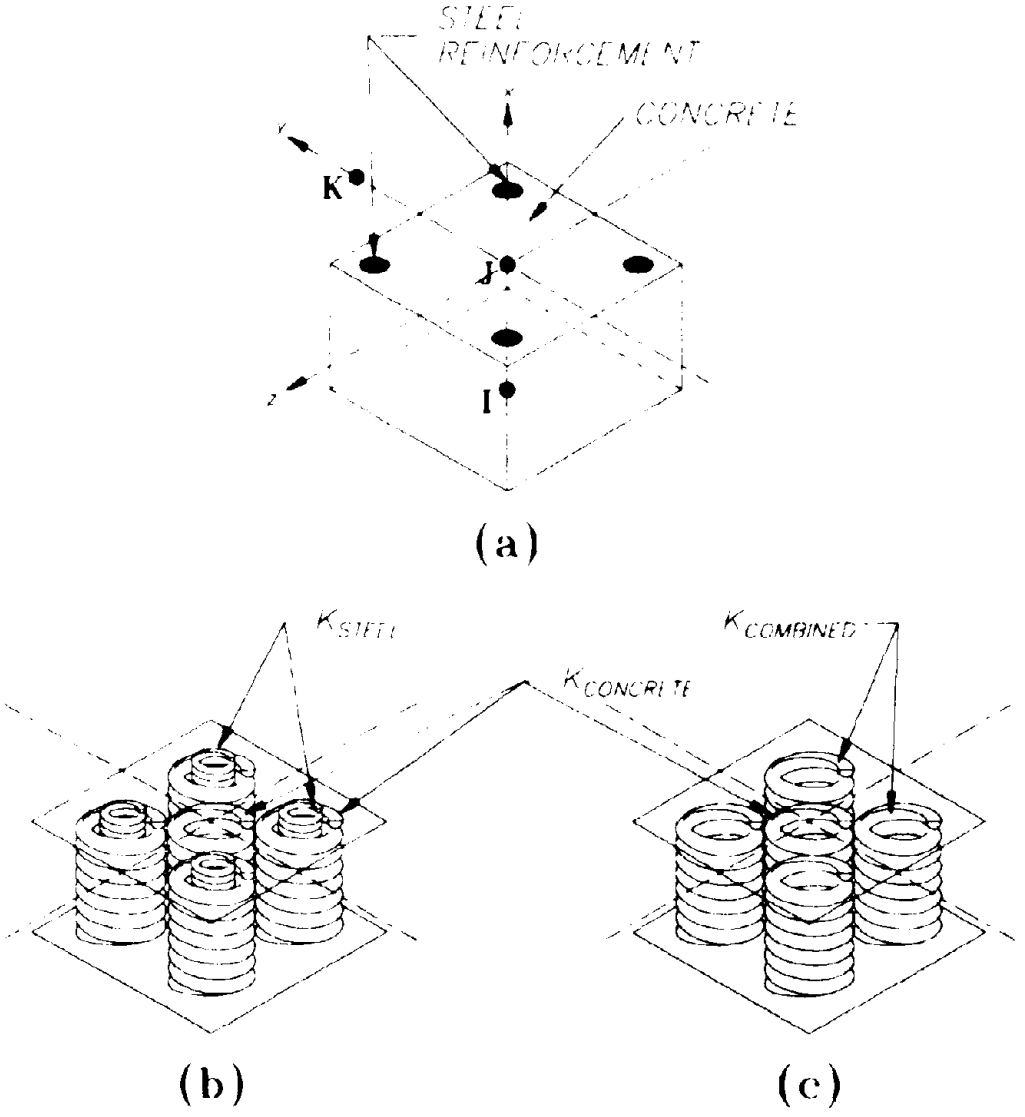

Figure 3-4. Non-Linear Column Section: (a) Coordinate System, (b) 9-Spring Element Model, (c) 5-Spring Element Model.

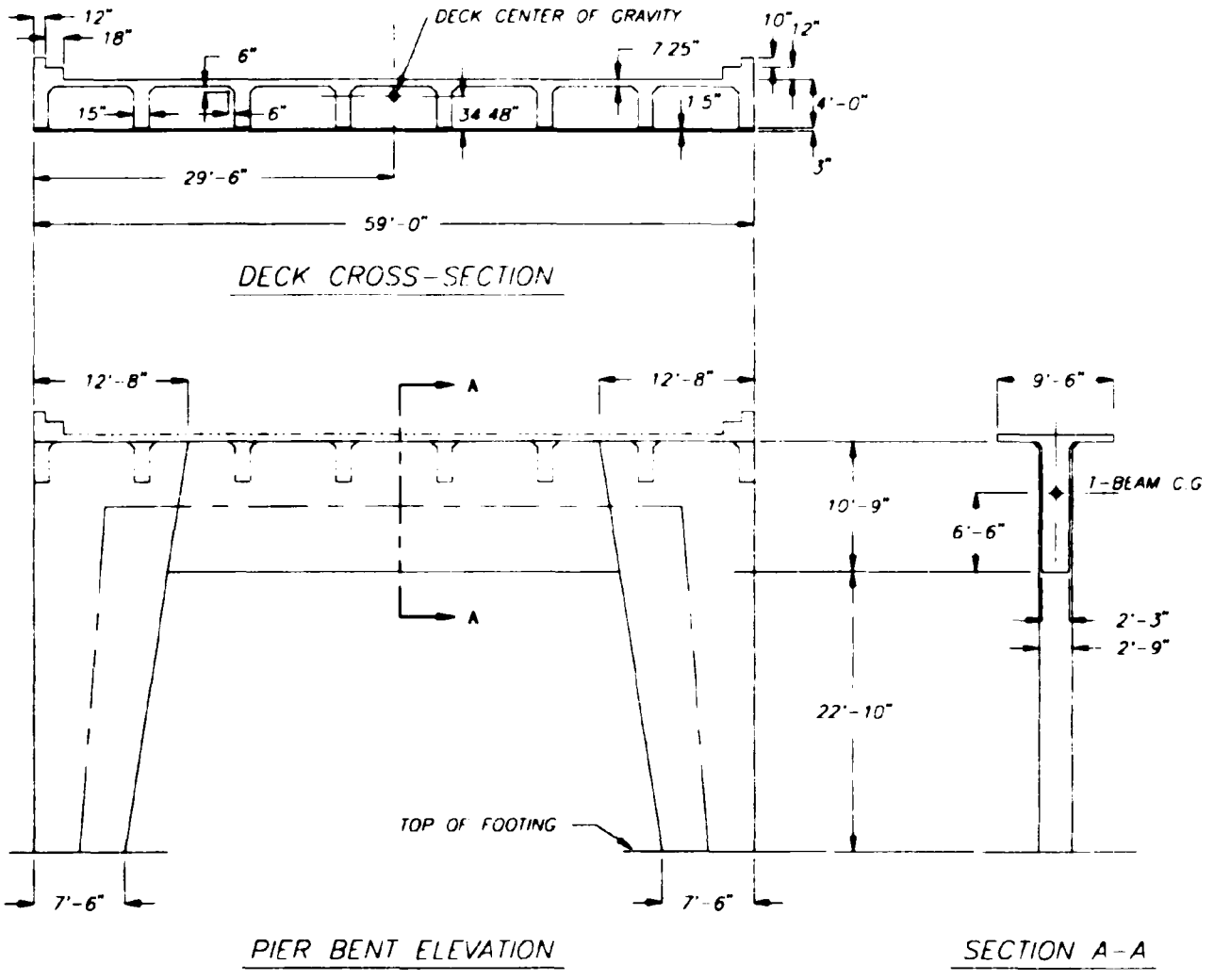

Figure 3-5. Simplified Model of the Madrone Drive Undercrossing.

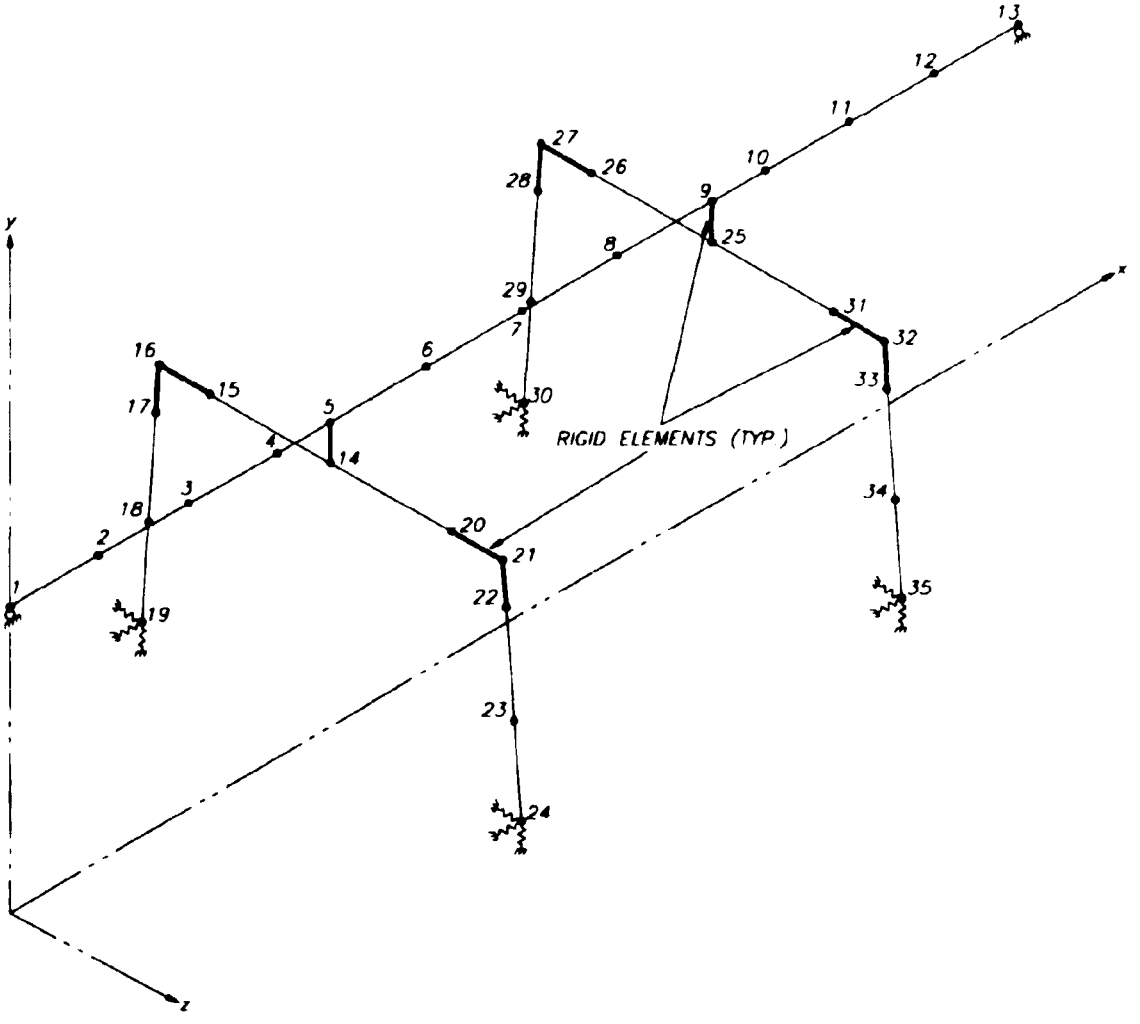

Figure 3-6. *Images 3-D* Finite Element Mesh for the Madrone Drive Undercrossing.

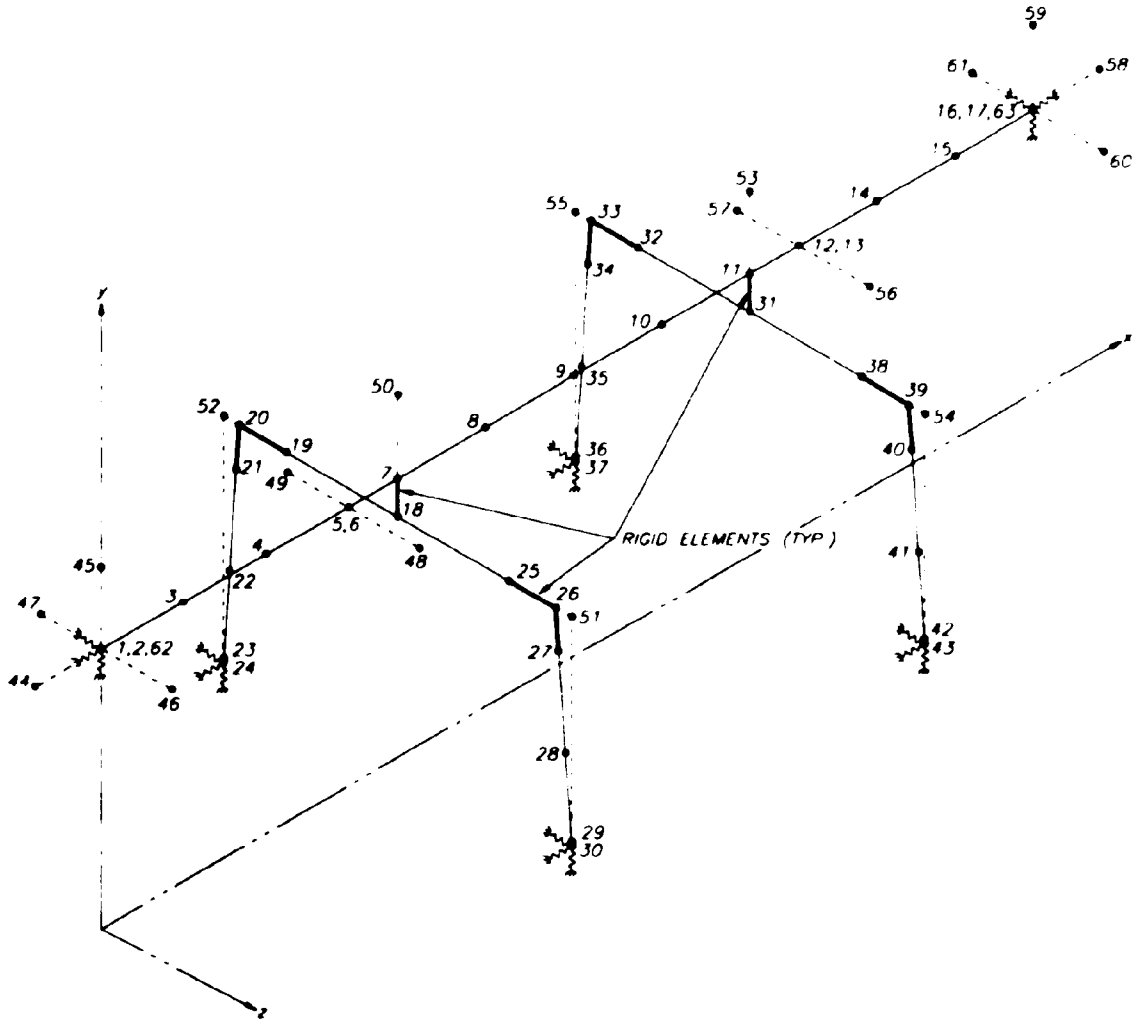

Figure 3-7. *NEABS* Finite Element Mesh for the Madrone Drive Undercrossing.

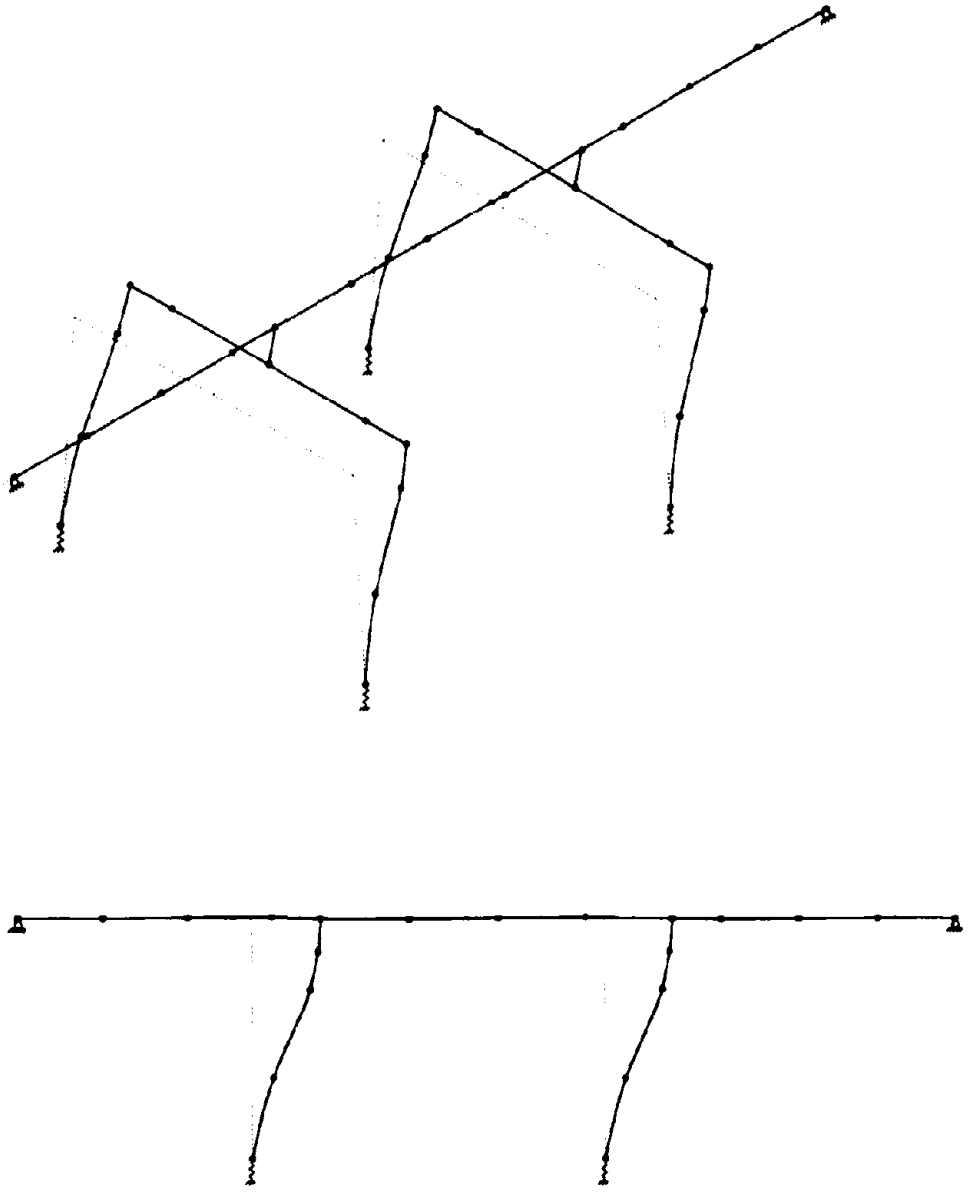

Figure 4-1. First Mode Shape for Madrone Drive Undercrossing (T_1 = 0.735 sec).

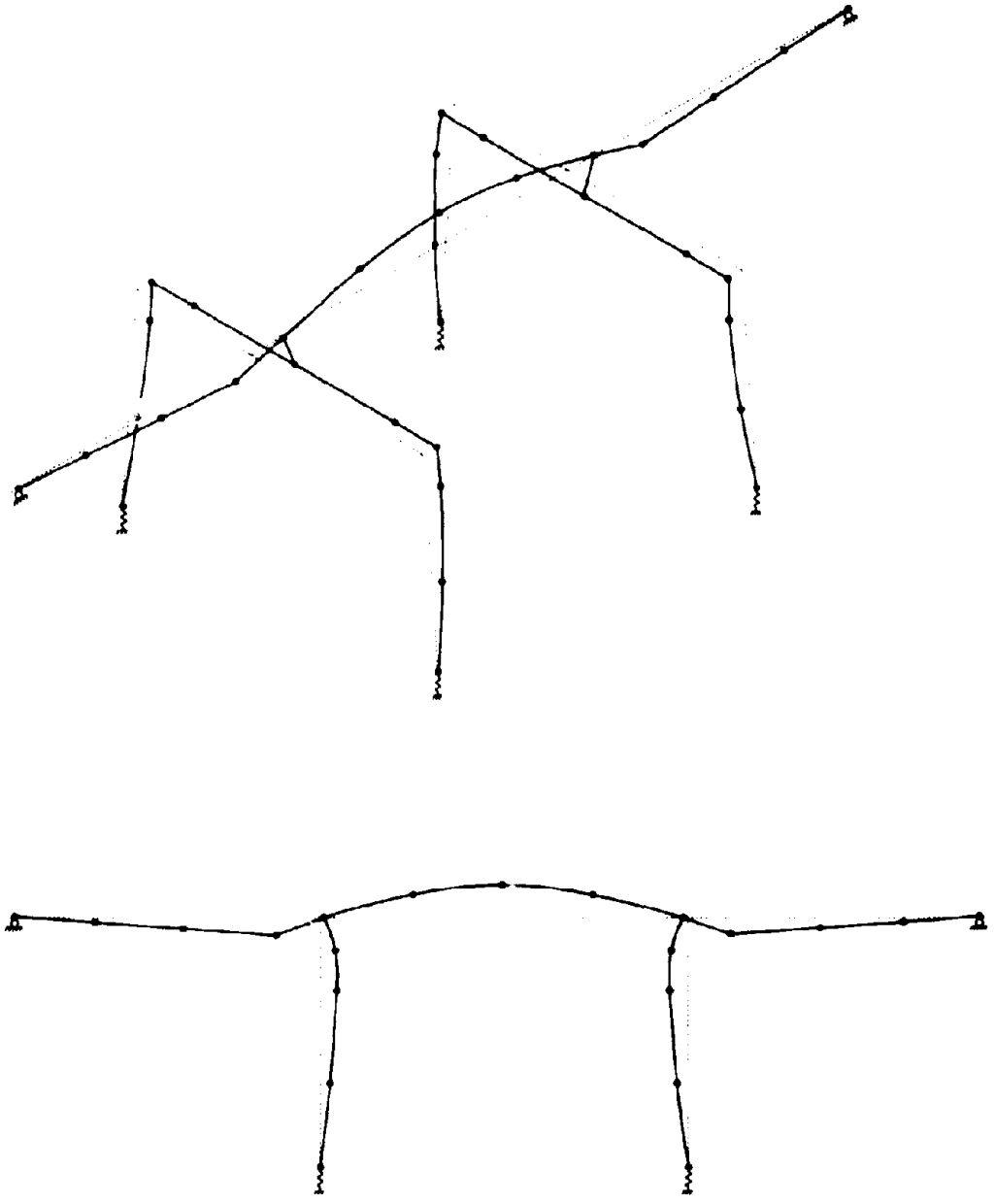

Figure 4-2. Second Mode Shape for Madrone Drive Undercrossing (T_2 = 0.123 sec).

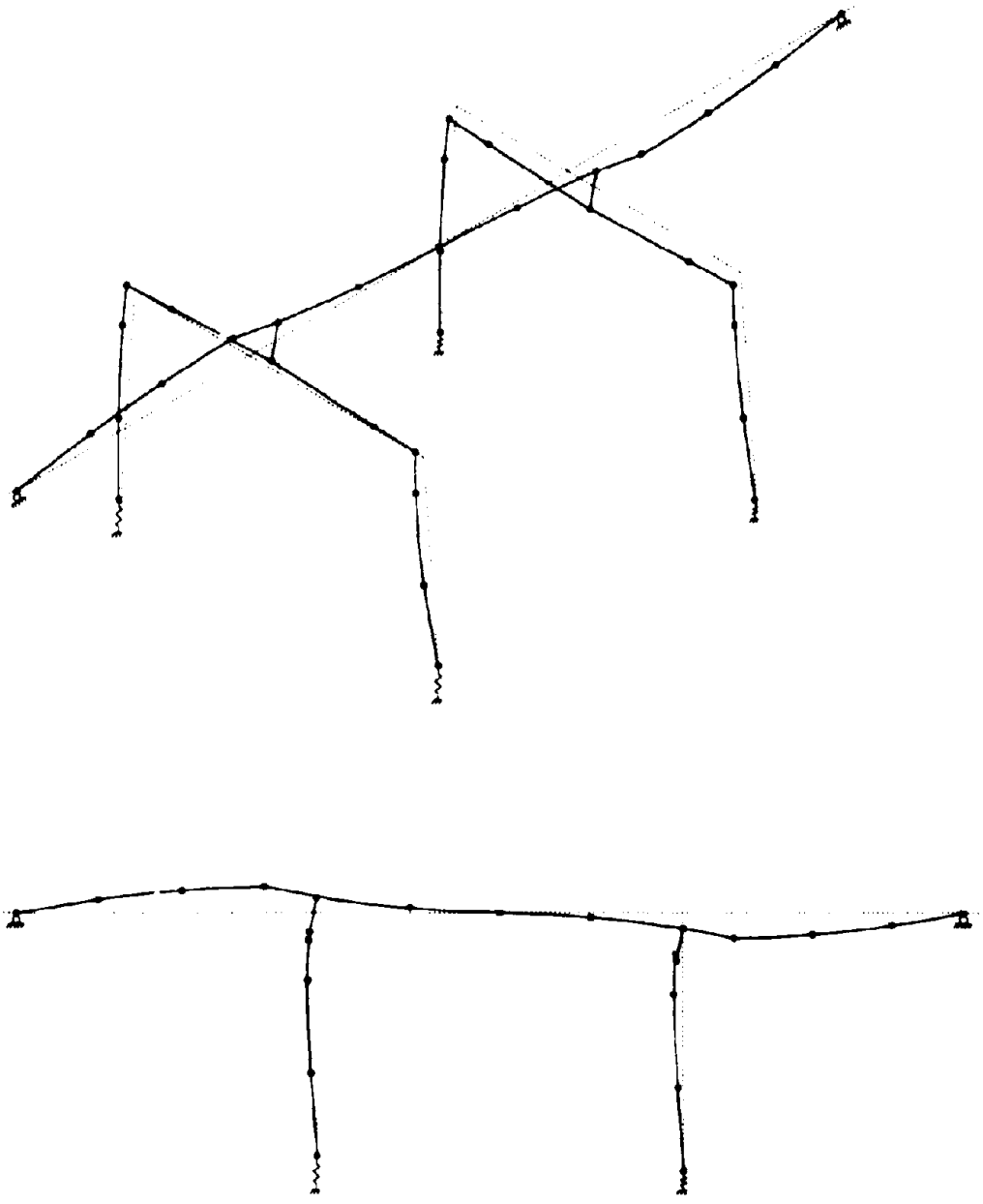

Figure 4-3. Third Mode Shape for Madrone Drive Undercrossing (T_3 = 0.094 sec).

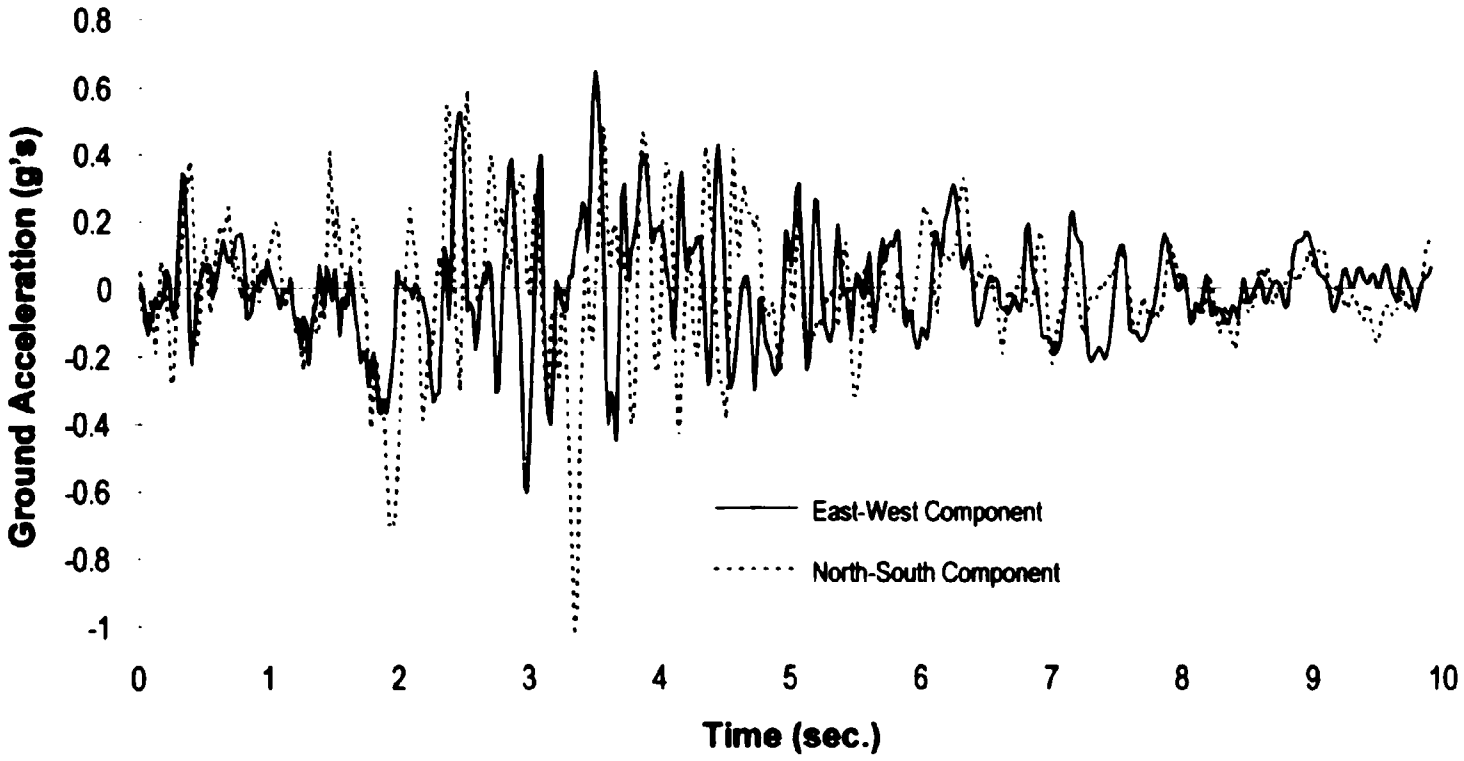

Figure 4-4. Accelerogram of the Loma Prieta Earthquake (Saratoga Station) East-West and North-South Components, East-West Component Scaled to 0.65-g (Scale Factor = 0.0662).

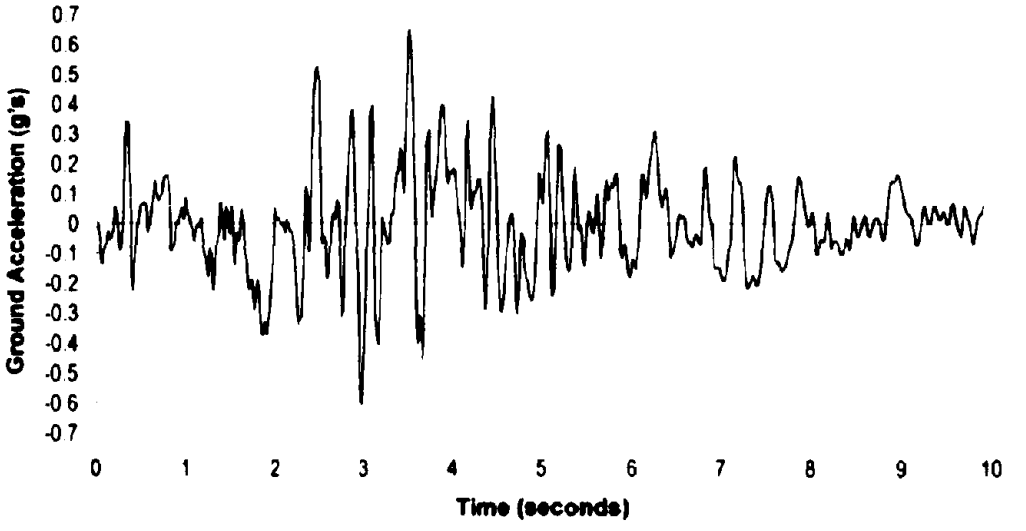

Figure 4-5. Accelerogram of the Loma Prieta Earthquake (Saratoga Station) East-West Component, Scaled to 0.65-g (Scale Factor = 0.0662).

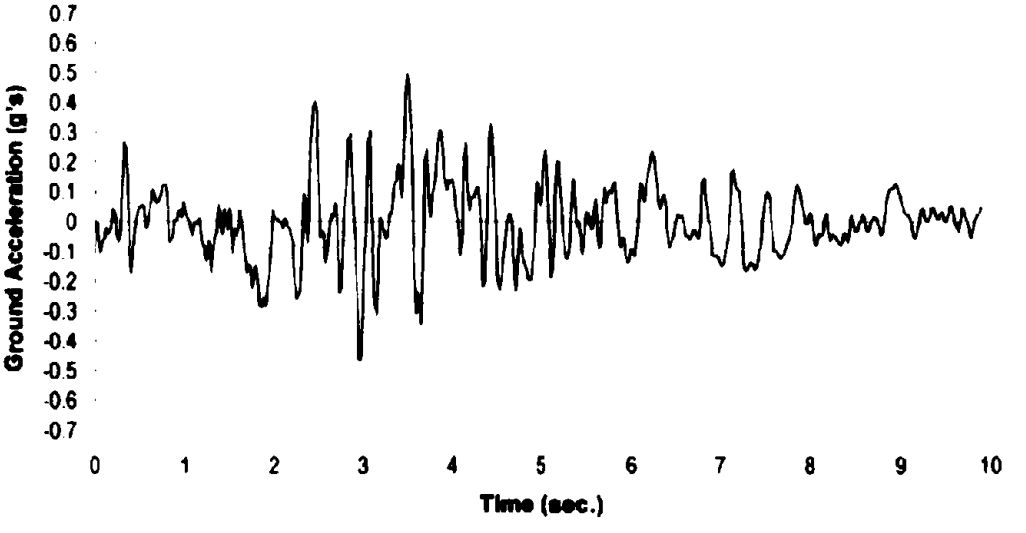

Figure 4-6. Accelerogram of the Loma Prieta Earthquake (Saratoga Station) East-West Component, Scaled to 0.5-g (Scale Factor = 0.0509).

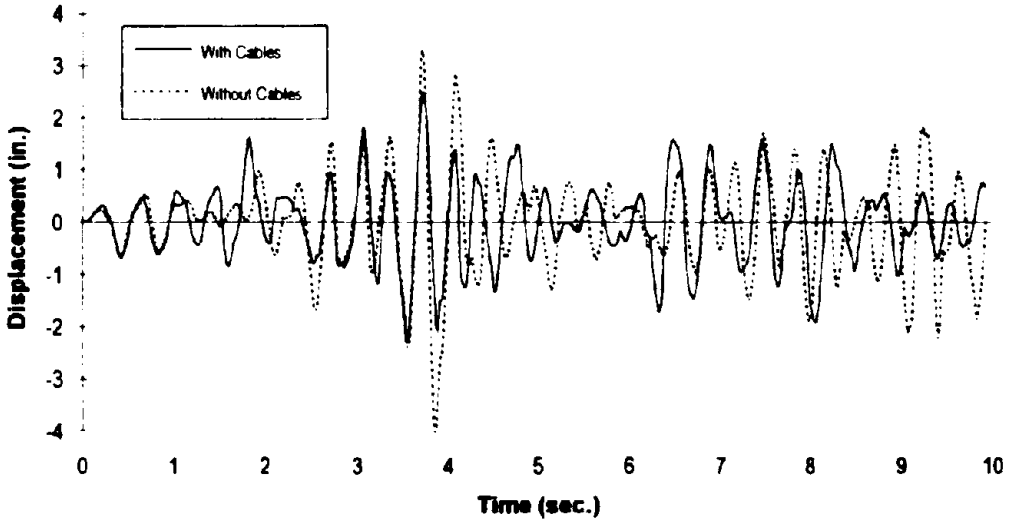

Figure 4-7. Midspan (Node 9) Longitudinal Response—0.65-g; with Hinge Bolts.

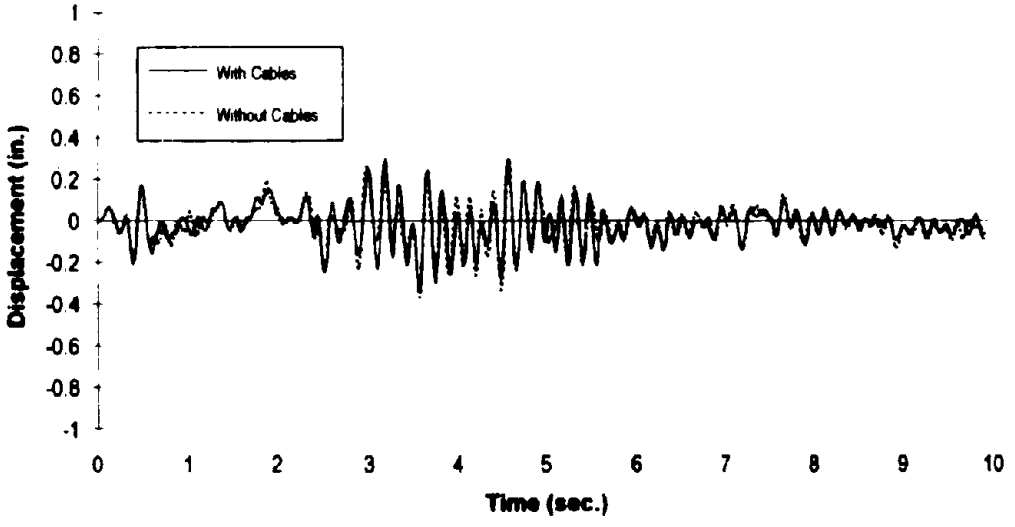

Figure 4-8. Midspan (Node 9) Transverse Response—0.65-g; with Hinge Bolts.

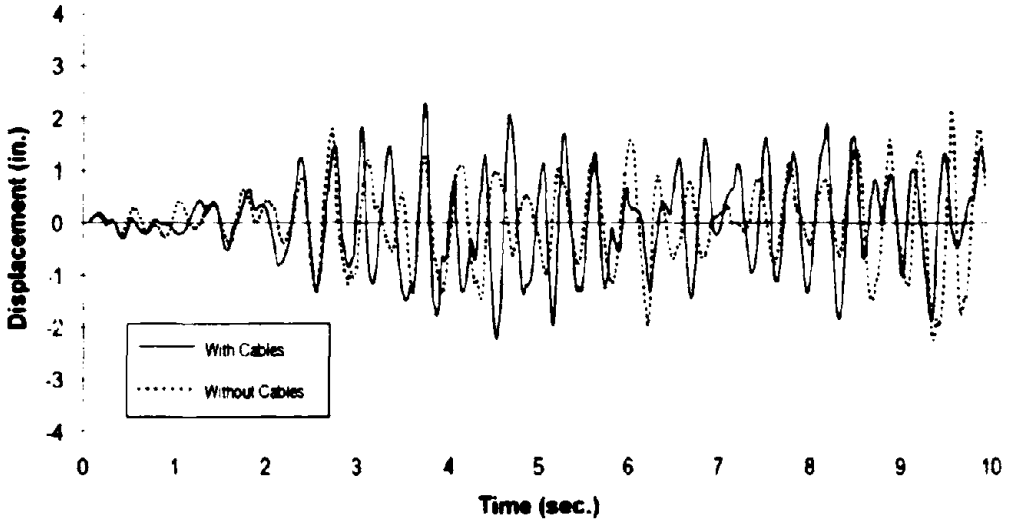

Figure 4-9. Midspan (Node 9) Longitudinal Response—0.65-g, without Hinge Bolts.

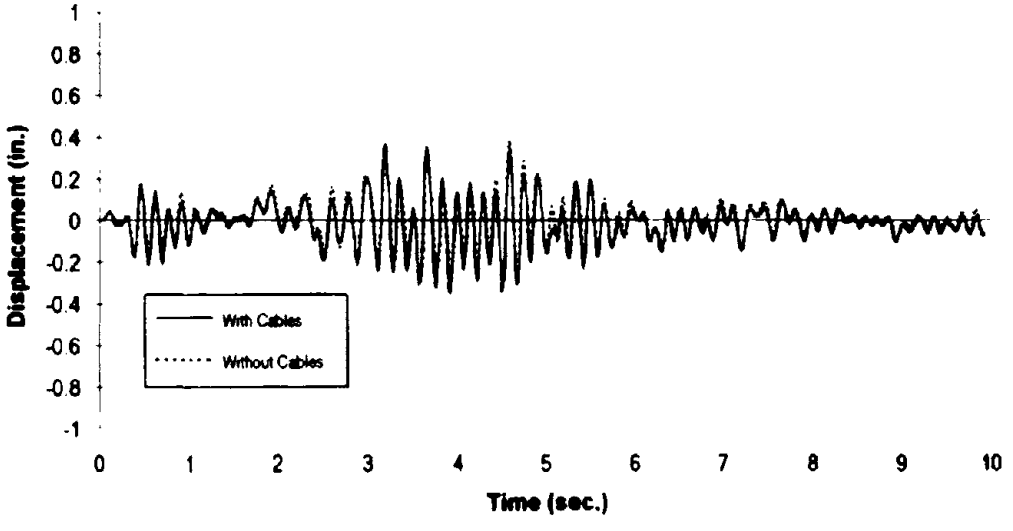

Figure 4-10. Midspan (Node 9) Transverse Response—0.65-g, without Hinge Bolts.

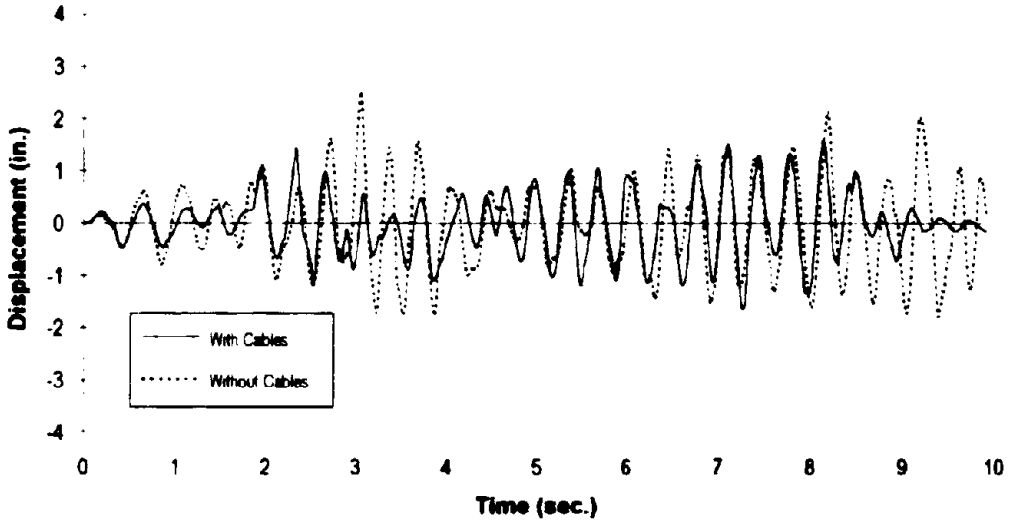

Figure 4-11. Midspan (Node 9) Longitudinal Response—0.5-g, with Hinge Bolts.

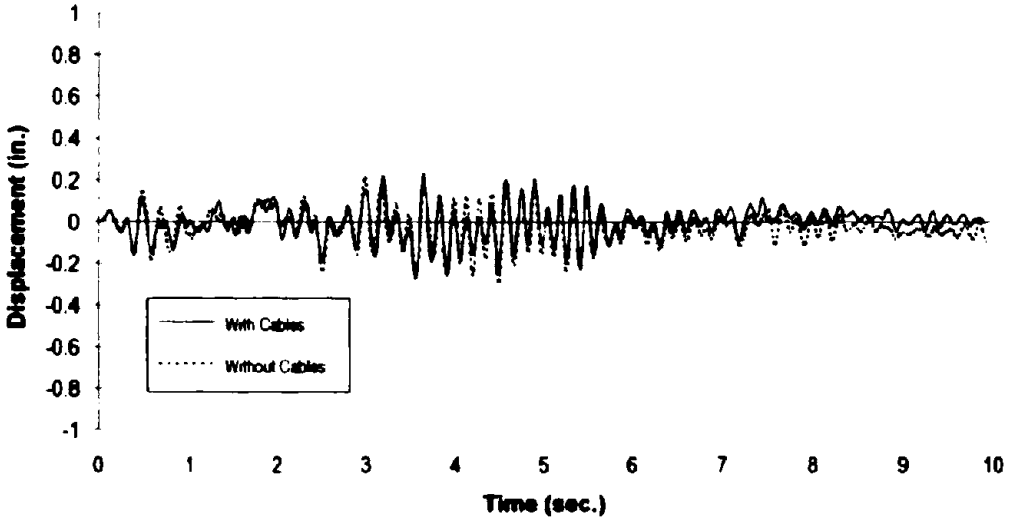

Figure 4-12. Midspan (Node 9) Transverse Response—0.5-g, with Hinge Bolts.

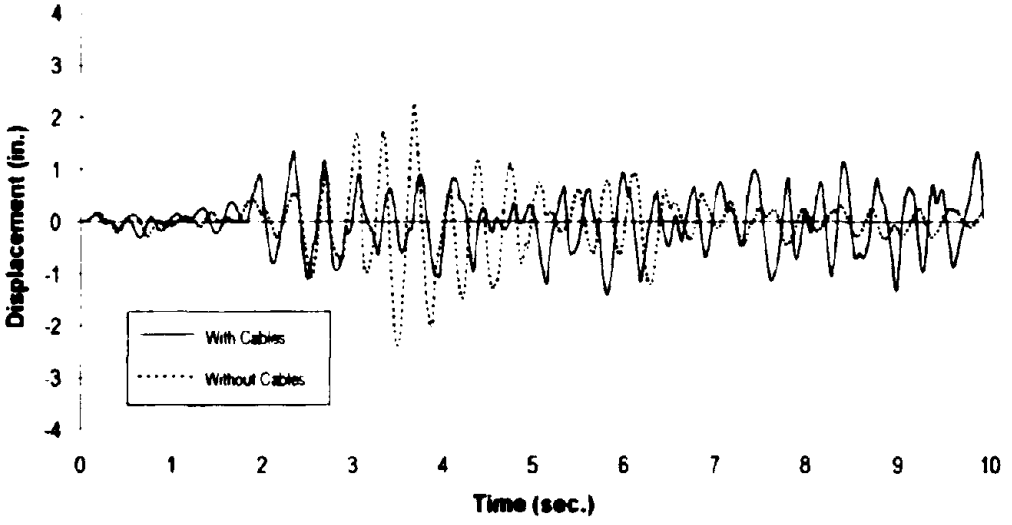

Figure 4-13. Midspan (Node 9) Longitudinal Response—0.5-g; without Hinge Bolts.

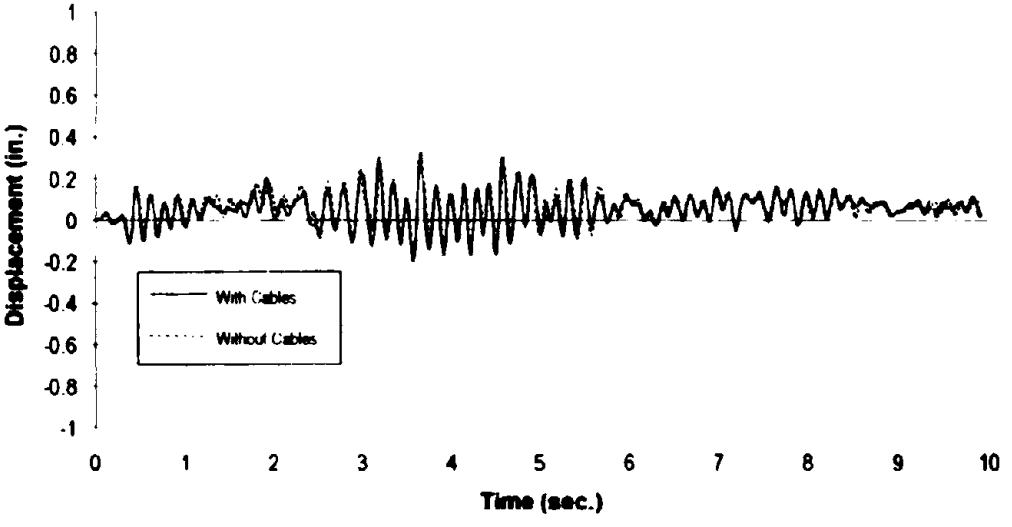

Figure 4-14. Midspan (Node 9) Transverse Response—0.5-g; without Hinge Bolts.

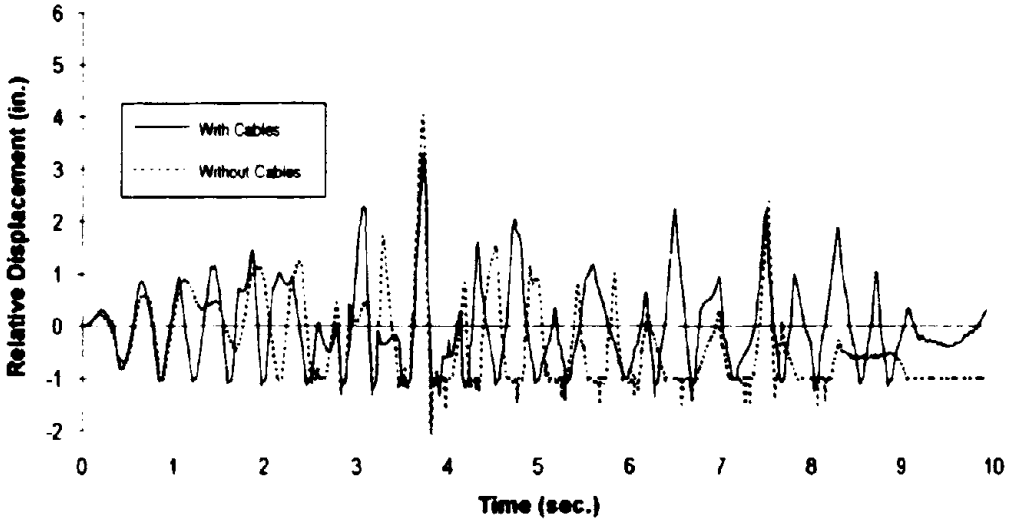

Figure 4-15. South Abutment Expansion Joint (Nodes 1 and 2) Longitudinal Relative Displacement—0.65-g; with Hinge Bolts.

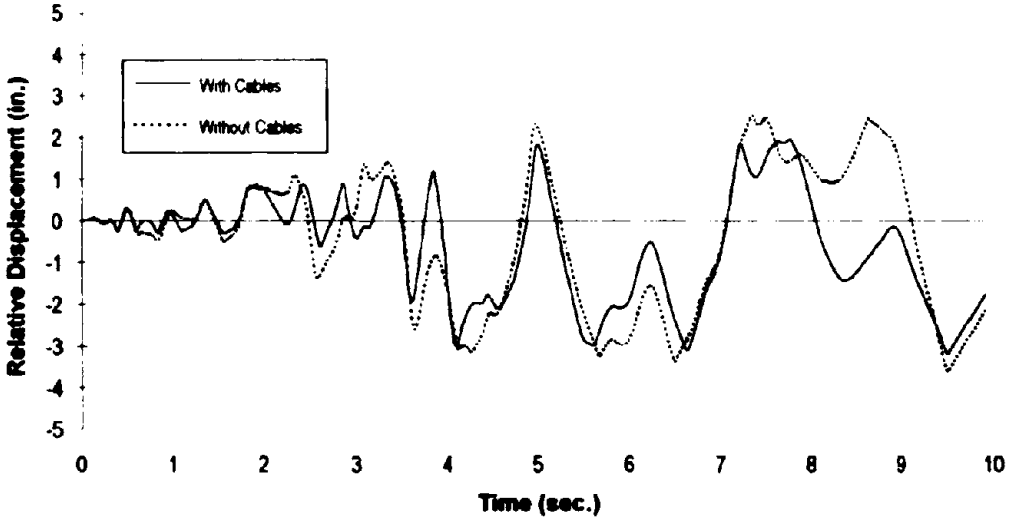

Figure 4-16. South Abutment Expansion Joint (Nodes 1 and 2) Transverse Relative Displacement—0.65-g; with Hinge Bolts.

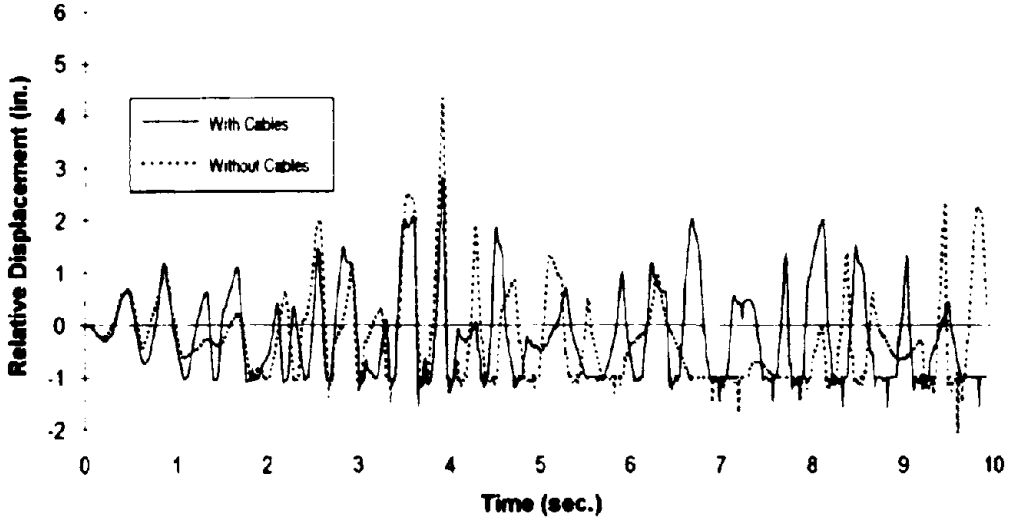

Figure 4-17. North Abutment Expansion Joint (Nodes 16 and 17) Longitudinal Relative Displacement—0.65-g; with Hinge Bolts.

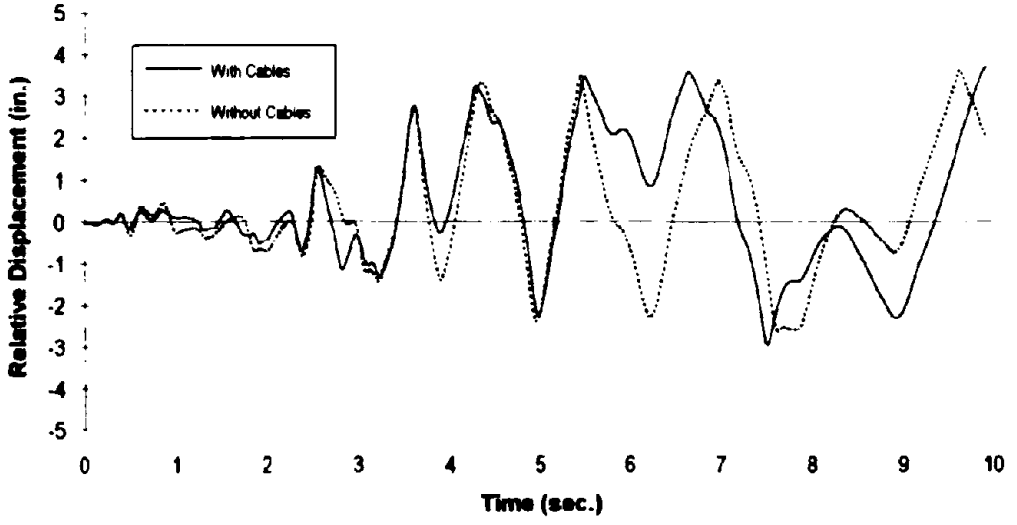

Figure 4-18. North Abutment Expansion Joint (Nodes 16 and 17) Transverse Relative Displacement—0.65-g; with Hinge Bolts.

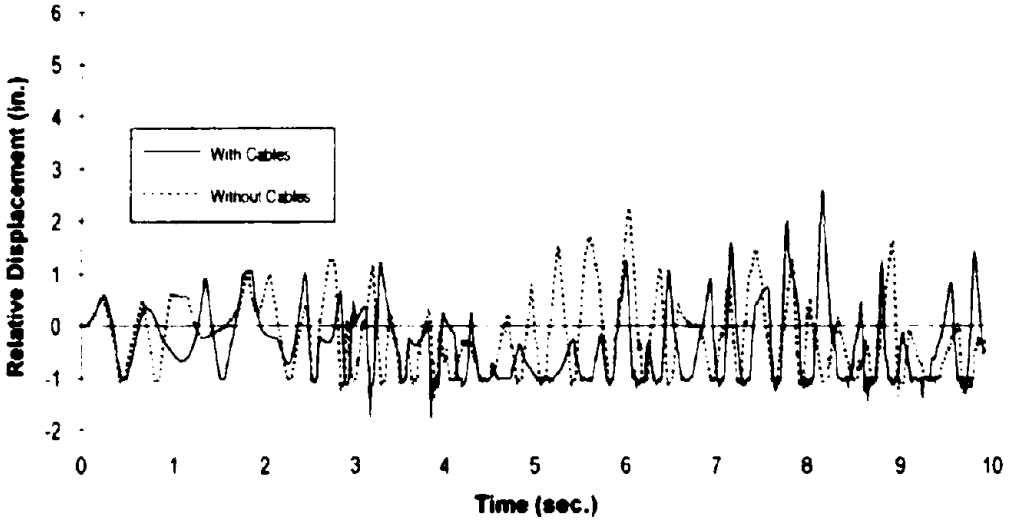

Figure 4-19. South Abutment Expansion Joint (Nodes 1 and 2) Longitudinal Relative Displacement—0.65-g, without Hinge Bolts.

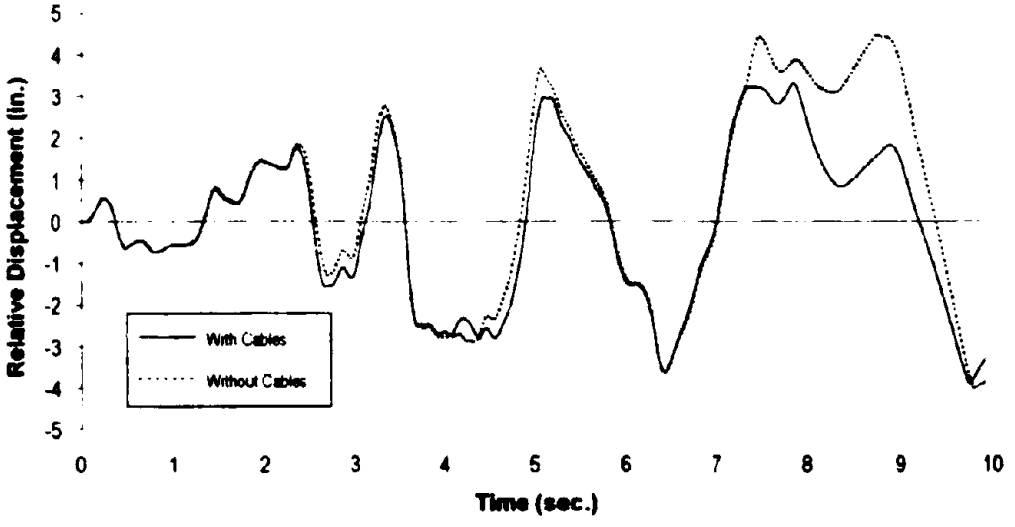

Figure 4-20. South Abutment Expansion Joint (Nodes 1 and 2) Transverse Relative Displacement—0.65-g, without Hinge Bolts.

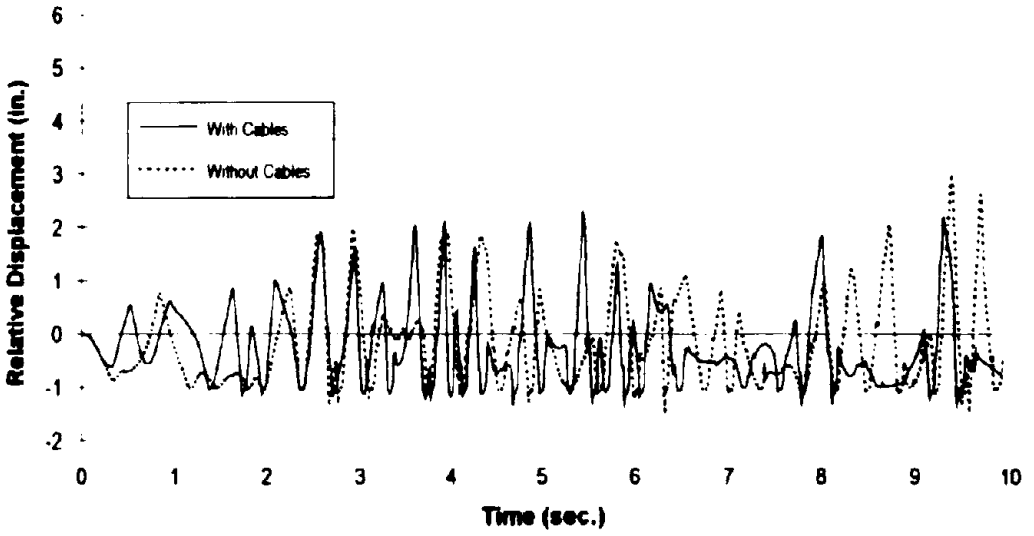

Figure 4-21. North Abutment Expansion Joint (Nodes 16 and 17) Longitudinal Relative Displacement—0.65-g; without Hinge Bolts.

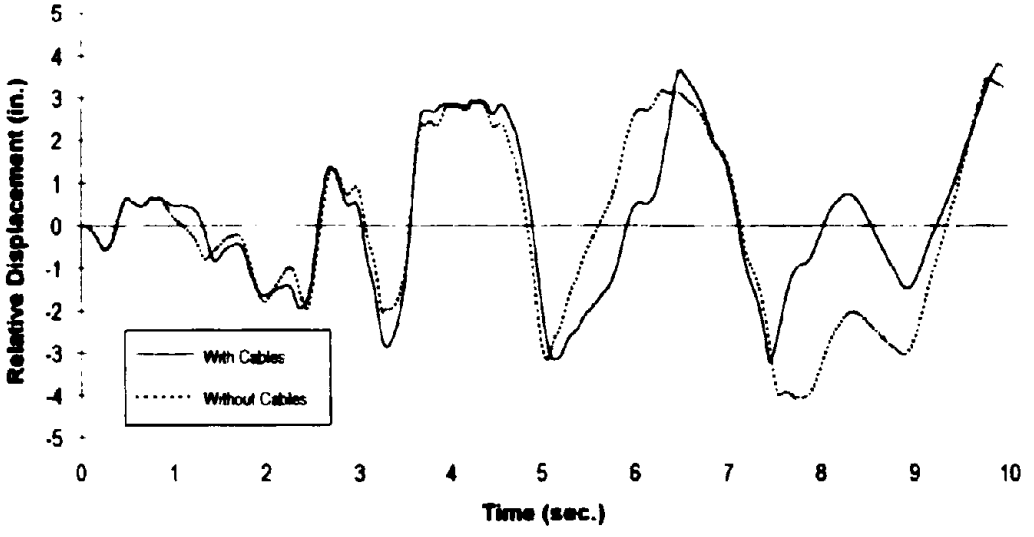

Figure 4-22. North Abutment Expansion Joint (Nodes 16 and 17) Transverse Relative Displacement—0.65-g; without Hinge Bolts.

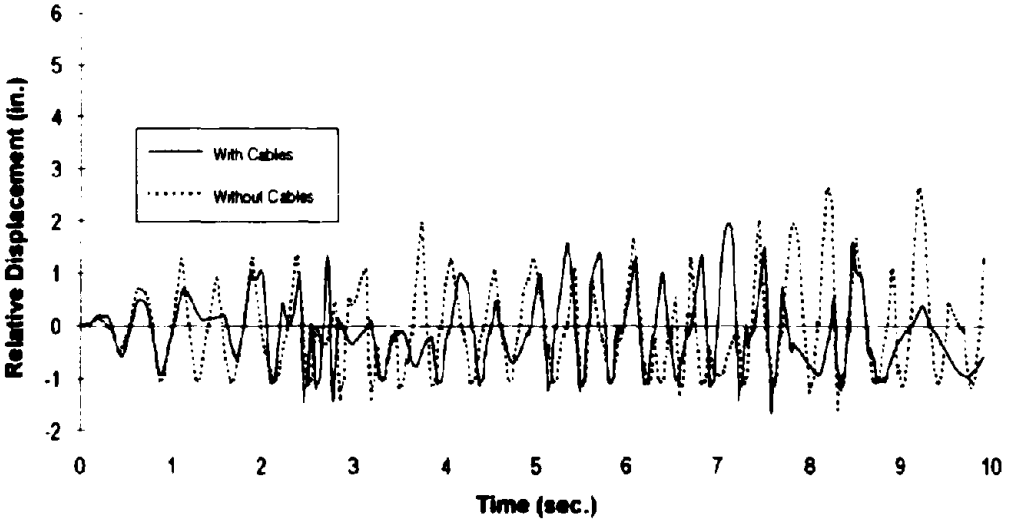

Figure 4-23. South Abutment Expansion Joint (Nodes 1 and 2) Longitudinal Relative Displacement—0.5-g; with Hinge Bolts.

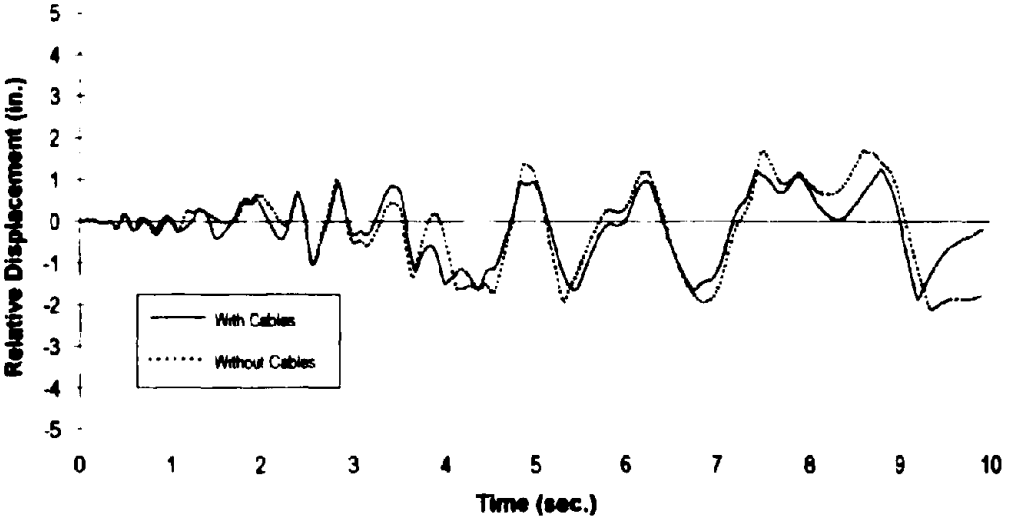

Figure 4-24. South Abutment Expansion Joint (Nodes 1 and 2) Transverse Relative Displacement—0.5-g; with Hinge Bolts.

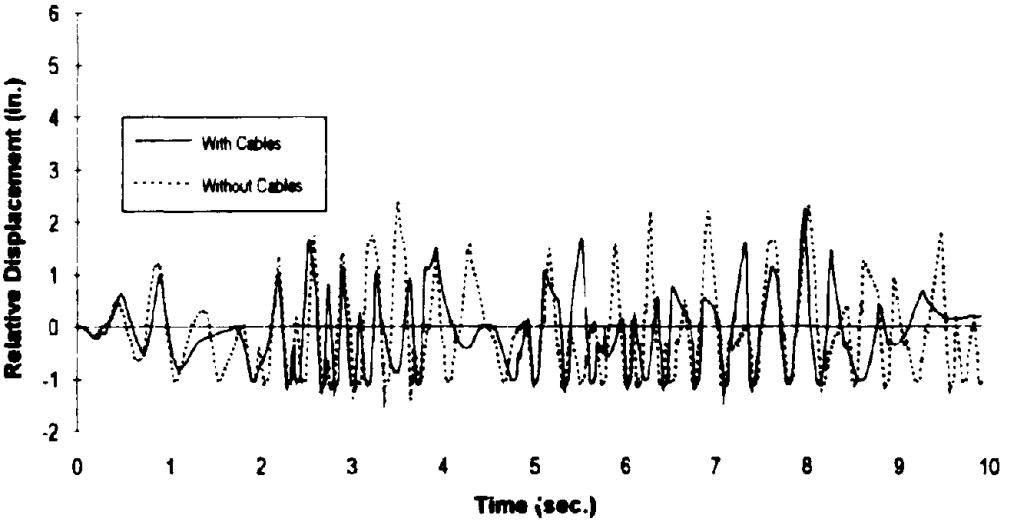

Figure 4-25. North Abutment Expansion Joint (Nodes 16 and 17) Longitudinal Relative Displacement—0.5-g; with Hinge Bolts.

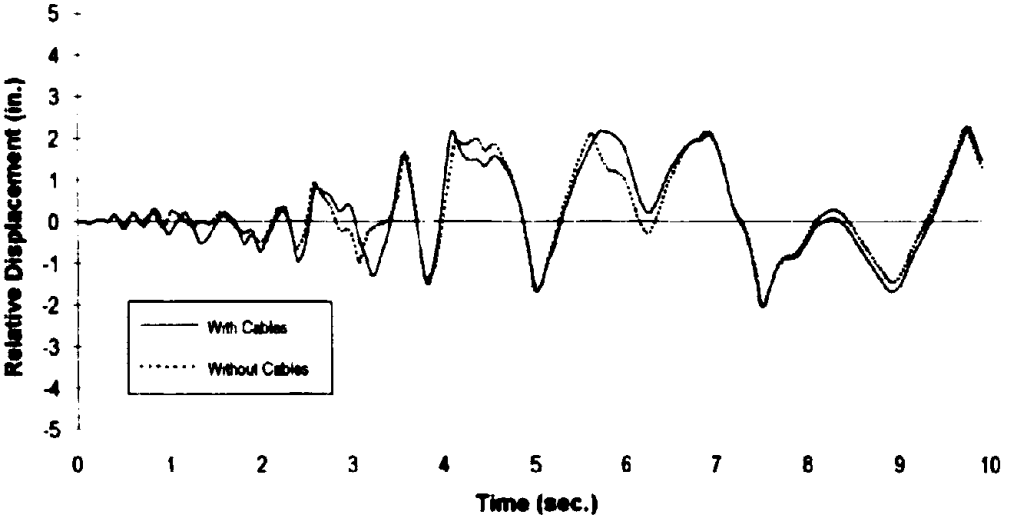

Figure 4-26. North Abutment Expansion Joint (Nodes 16 and 17) Transverse Relative Displacement—0.5-g; with Hinge Bolts.

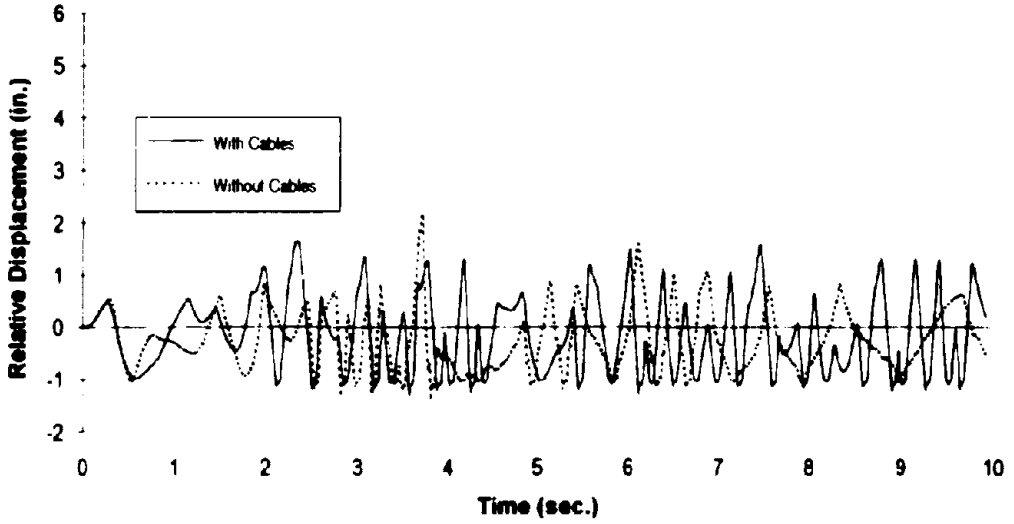

Figure 4-27. South Abutment Expansion Joint (Nodes 1 and 2) Longitudinal Relative Displacement—0.5-g, without Hinge Bolts.

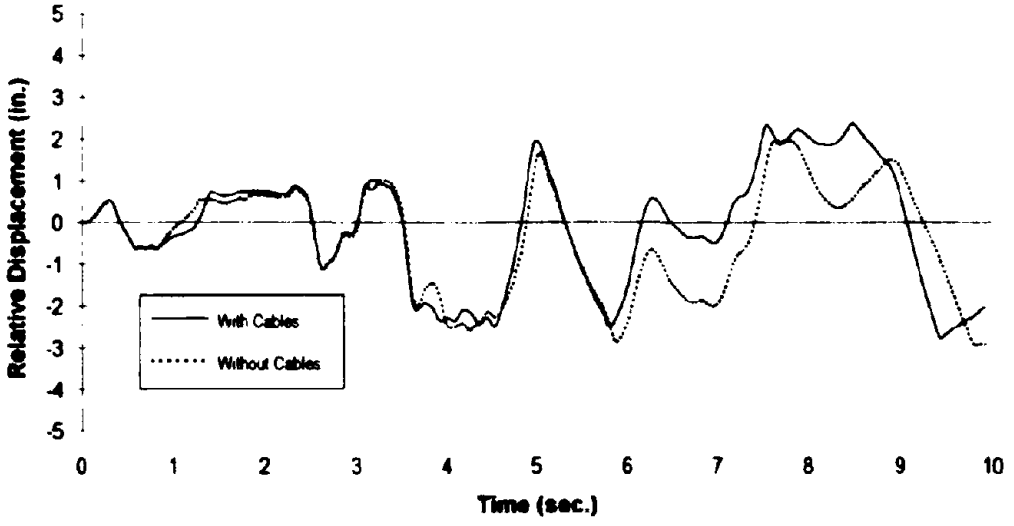

Figure 4-28. South Abutment Expansion Joint (Nodes 1 and 2) Transverse Relative Displacement—0.5-g, without Hinge Bolts.

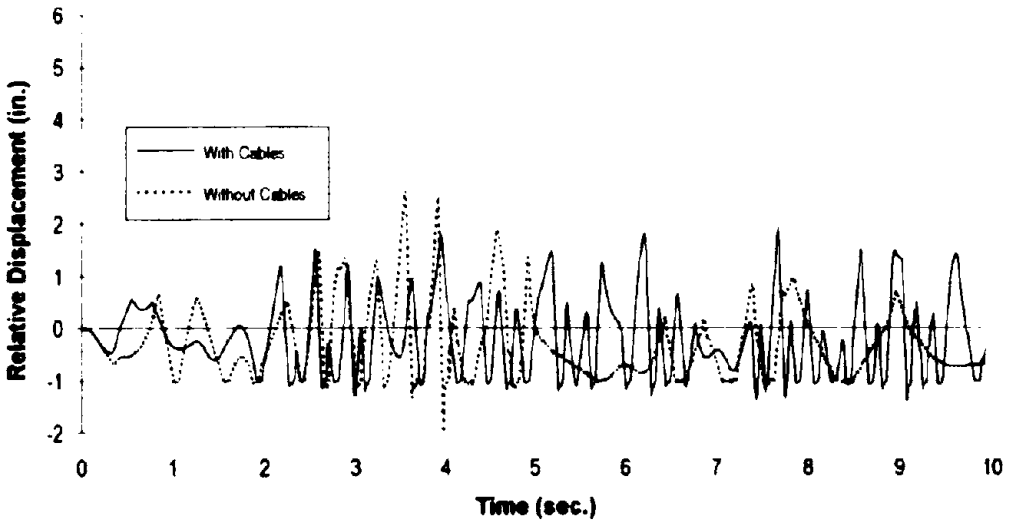

Figure 4-29. North Abutment Expansion Joint (Nodes 16 and 17) Longitudinal Relative Displacement—0.5-g, without Hinge Bolts.

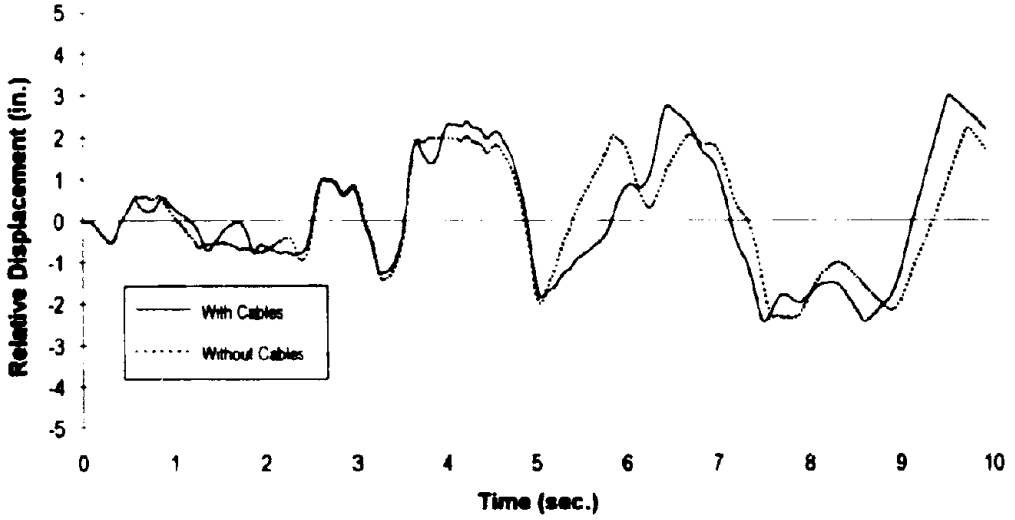

Figure 4-30. North Abutment Expansion Joint (Nodes 16 and 17) Transverse Relative Displacement—0.5-g, without Hinge Bolts.

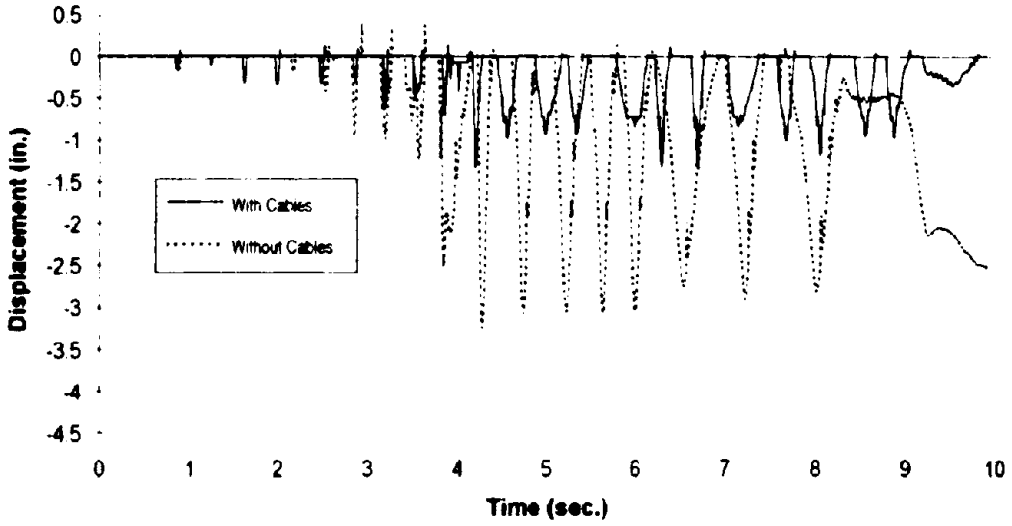

Figure 4-31. South Abutment (Node 1) Longitudinal Displacement—0.65-g; with Hinge Bolts.

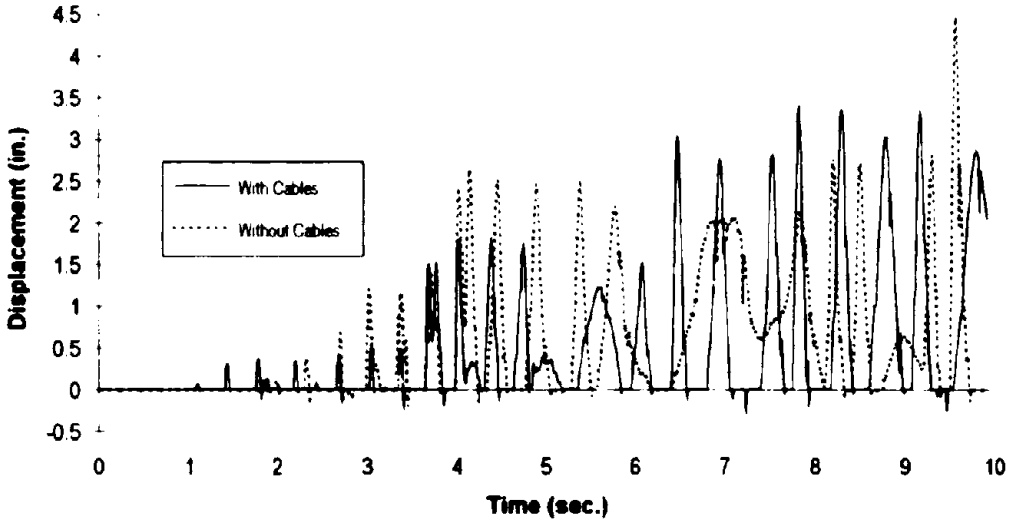

Figure 4-32. North Abutment (Node 17) Longitudinal Displacement—0.65-g; with Hinge Bolts.

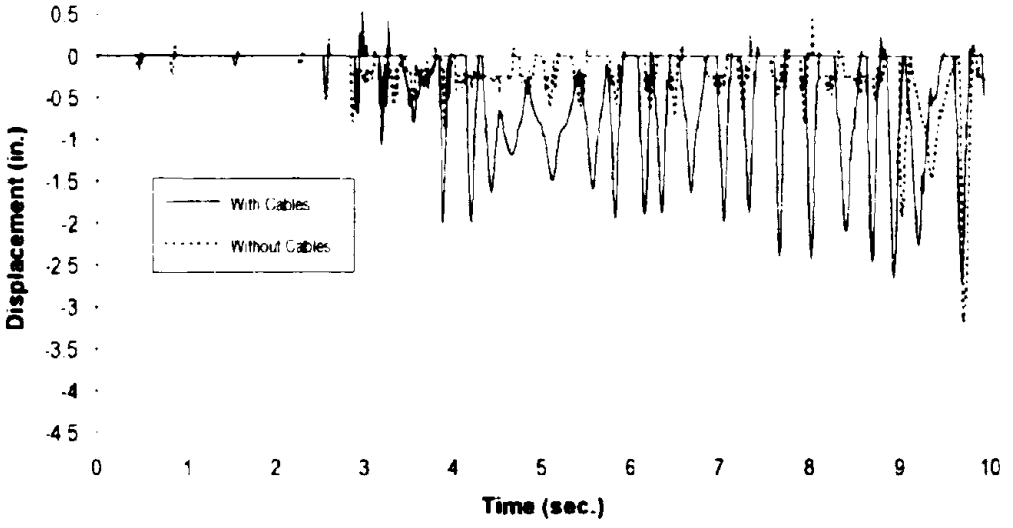

Figure 4-33. South Abutment (Node 1) Longitudinal Displacement—0.65-g, without Hinge Bolts

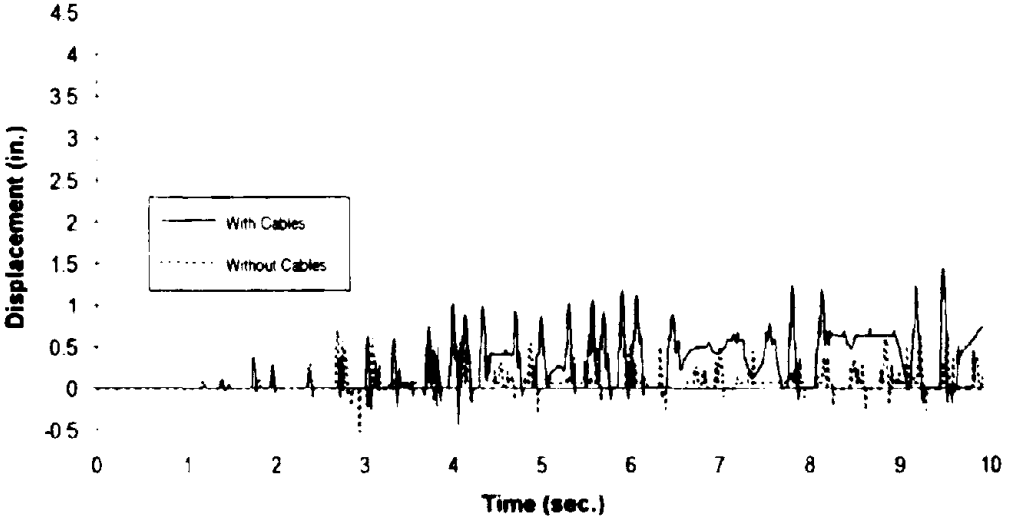

Figure 4-34. North Abutment (Node 17) Longitudinal Displacement—0.65-g, without Hinge Bolts

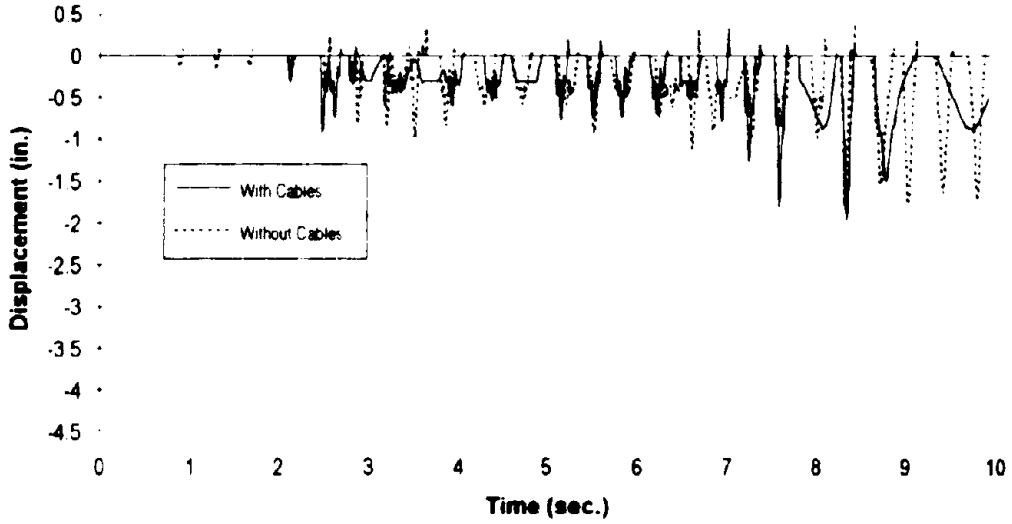

Figure 4-35. South Abutment (Node 1) Longitudinal Displacement—0.5-g, with Hinge Bolts

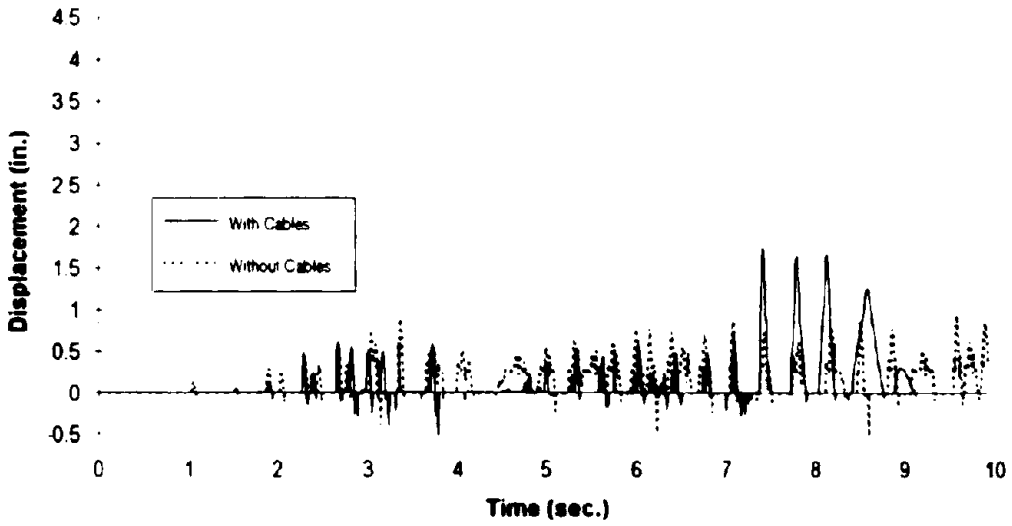

Figure 4-36. North Abutment (Node 17) Longitudinal Displacement—0.5-g, with Hinge Bolts

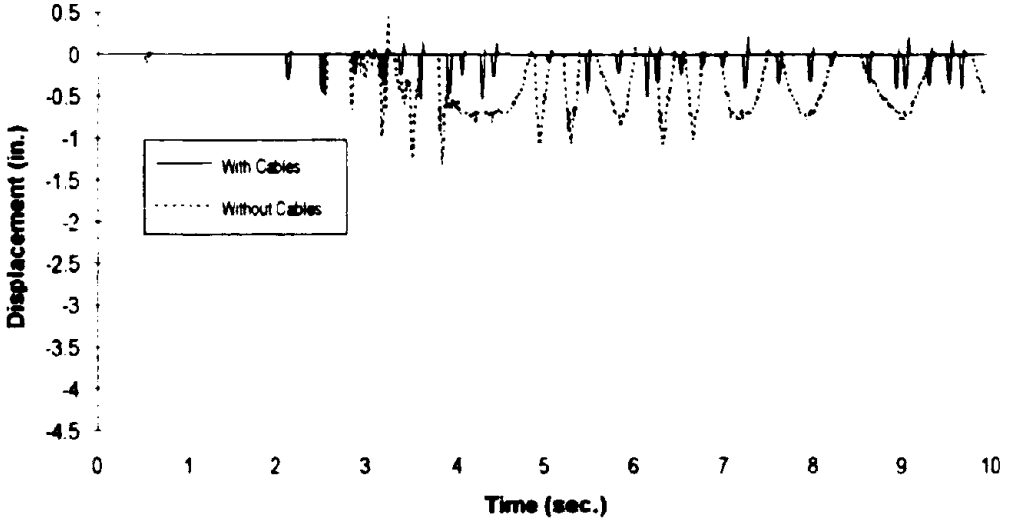

Figure 4-37. South Abutment (Node 1) Longitudinal Displacement—0.5-g; without Hinge Bolts.

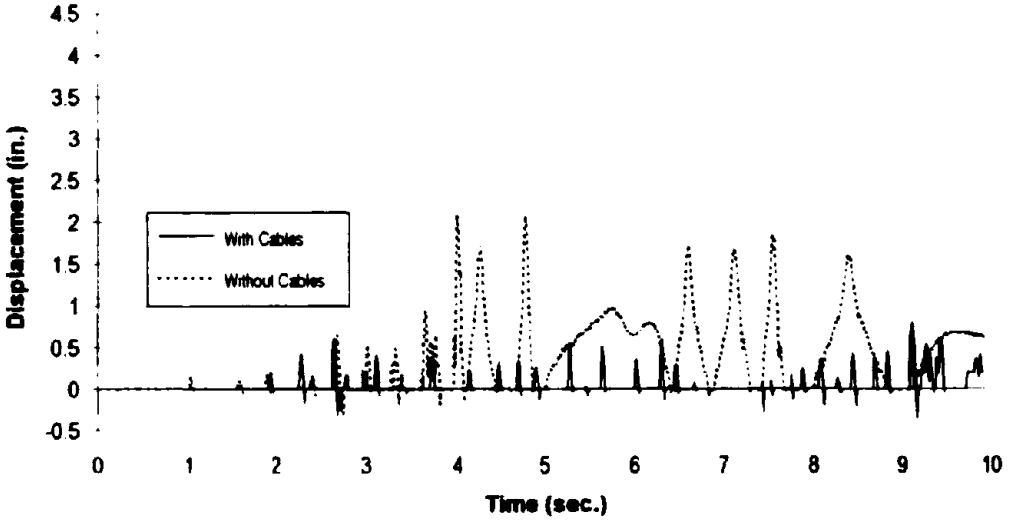

Figure 4-38. North Abutment (Node 17) Longitudinal Displacement—0.5-g; without Hinge Bolts.

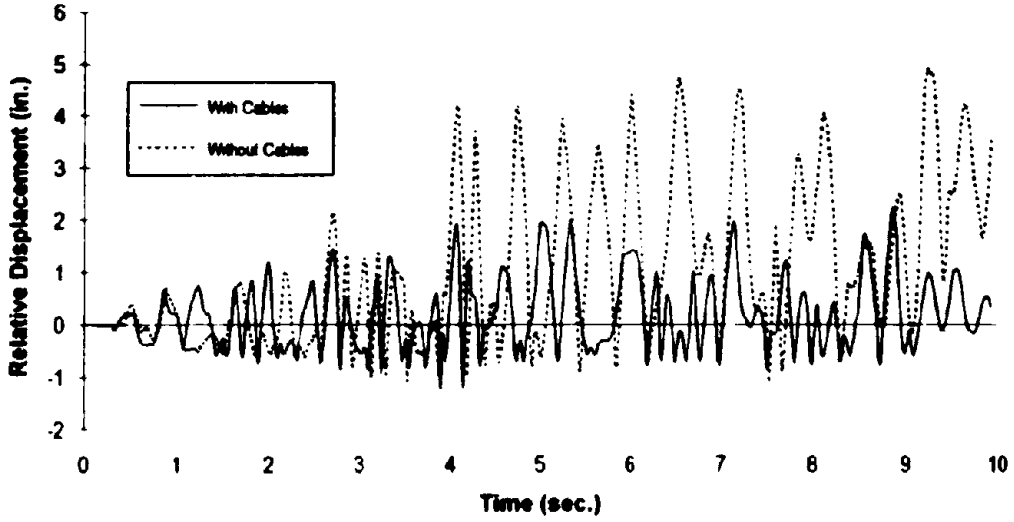

Figure 4-39. South Intermediate Hinge (Nodes 5 and 6) Longitudinal Relative Displacement—0.65-g; with Hinge Bolts

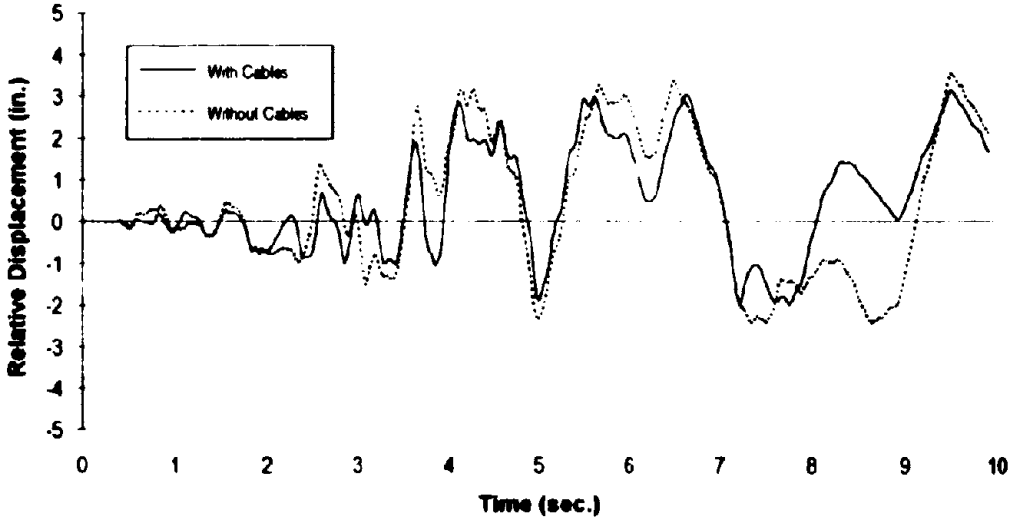

Figure 4-40. South Intermediate Hinge (Nodes 5 and 6) Transverse Relative Displacement—0.65-g; with Hinge Bolts.

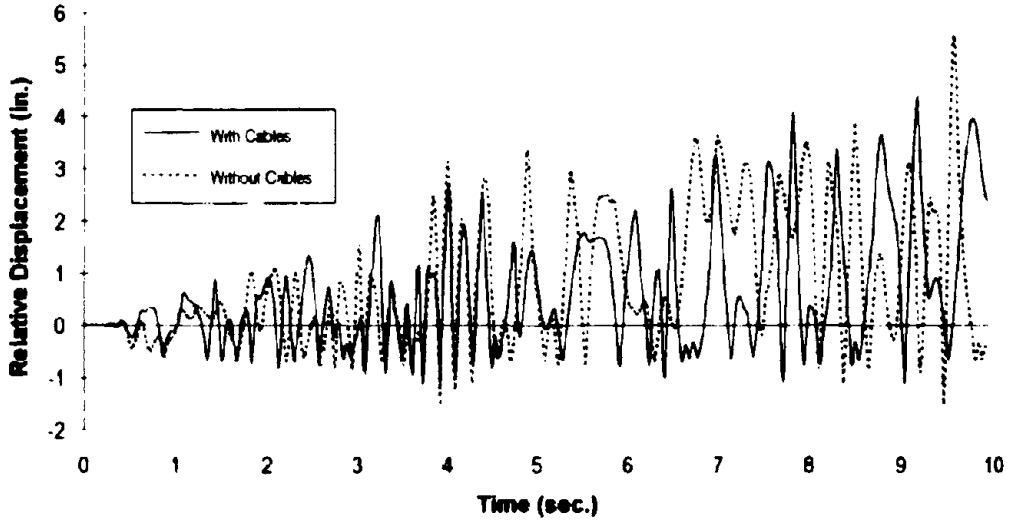

Figure 4-41. North Intermediate Hinge (Nodes 12 and 13) Longitudinal Relative Displacement—0.65-g; with Hinge Bolts.

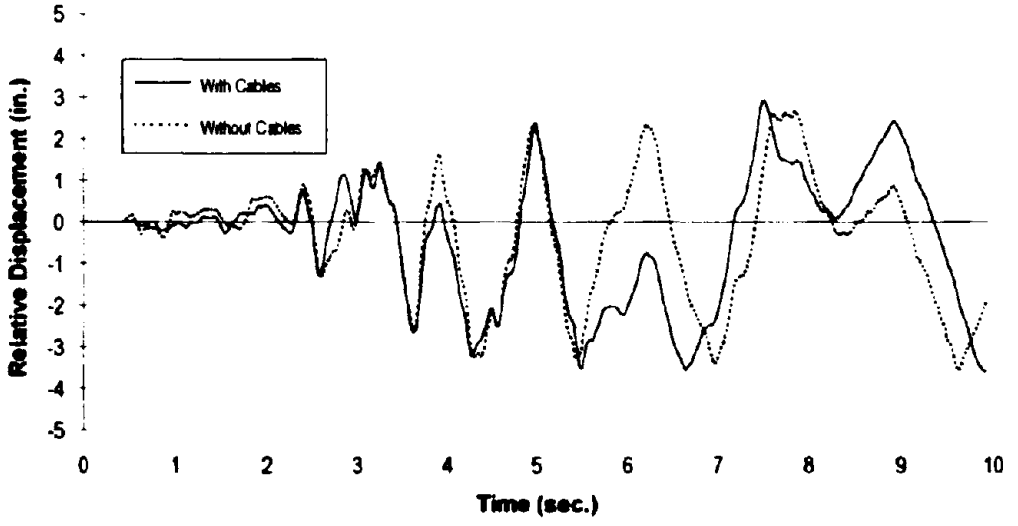

Figure 4-42. North Intermediate Hinge (Nodes 12 and 13) Transverse Relative Displacement—0.65-g; with Hinge Bolts.

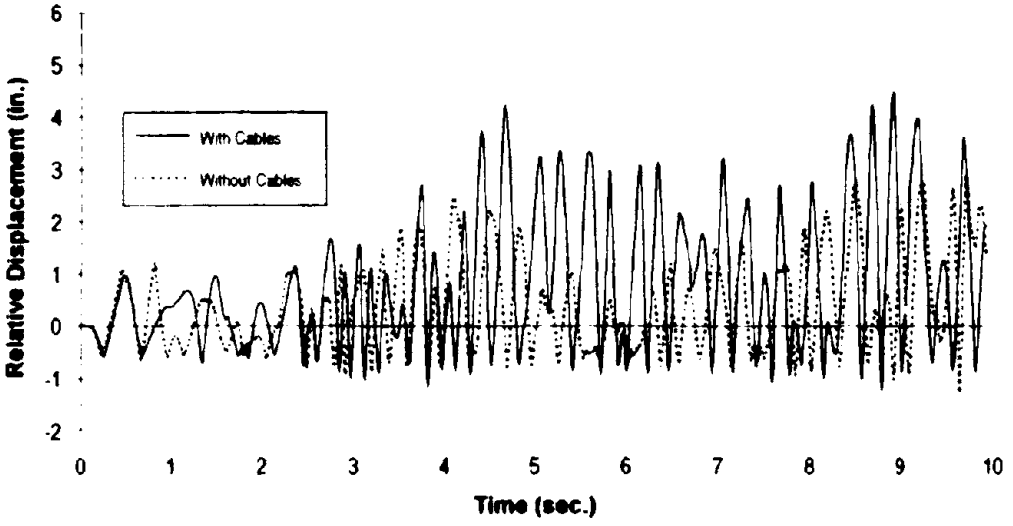

Figure 4-43. South Intermediate Hinge (Nodes 5 and 6) Longitudinal Relative Displacement—0.65-g, without Hinge Bolts.

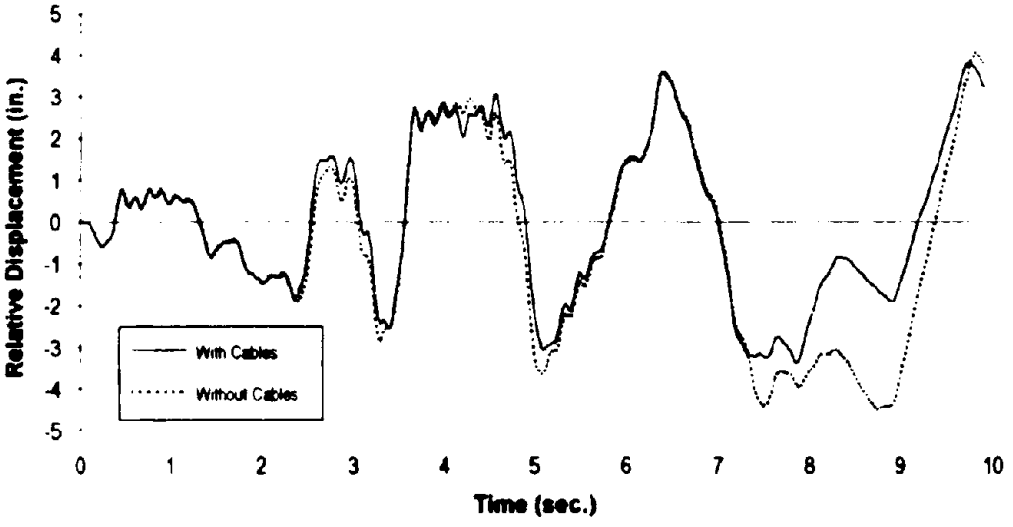

Figure 4-44. South Intermediate Hinge (Nodes 5 and 6) Transverse Relative Displacement—0.65-g, without Hinge Bolts.

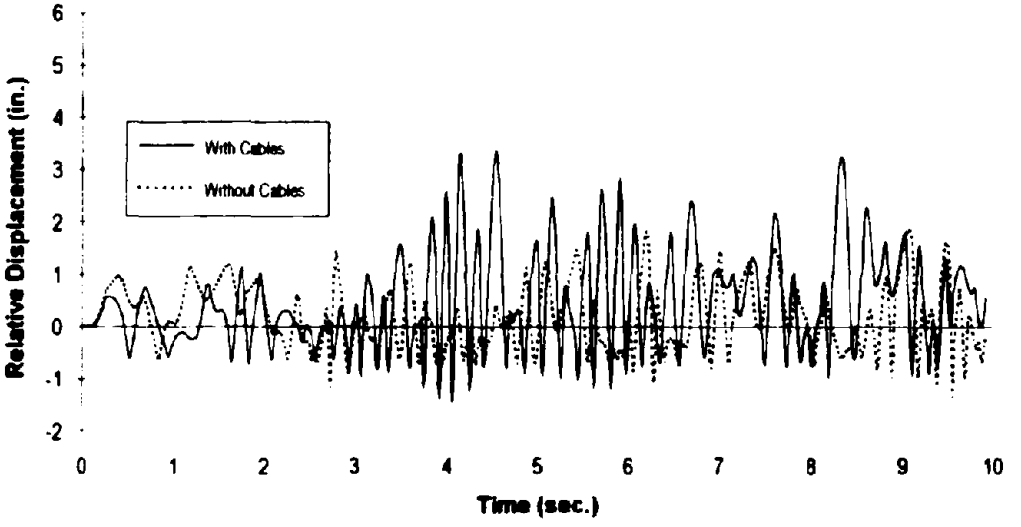

Figure 4-45. North Intermediate Hinge (Nodes 12 and 13) Longitudinal Relative Displacement—0.65-g; without Hinge Bolts.

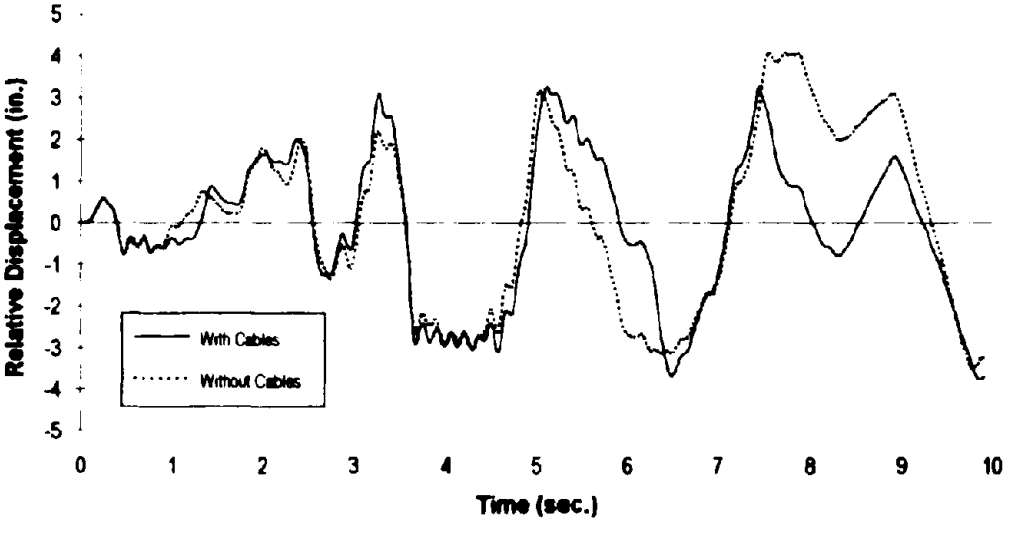

Figure 4-46. North Intermediate Hinge (Nodes 12 and 13) Transverse Relative Displacement—0.65-g; without Hinge Bolts.

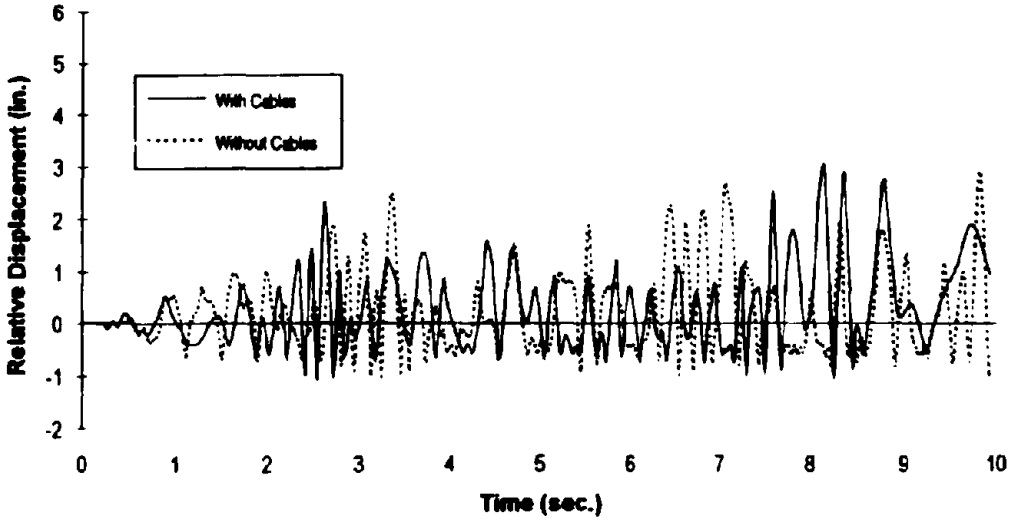

Figure 4-47. South Intermediate Hinge (Nodes 5 and 6) Longitudinal Relative Displacement—0.5-g; with Hinge Bolts.

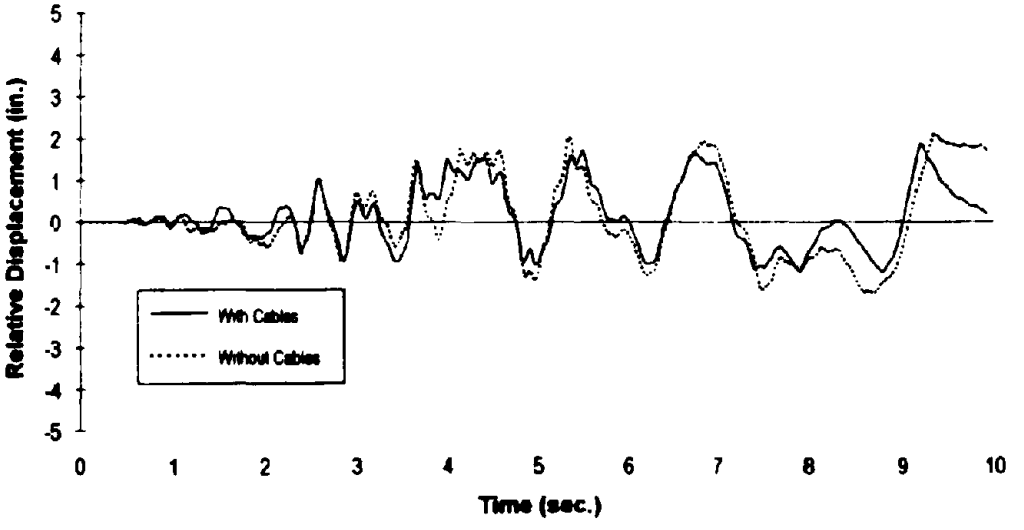

Figure 4-48. South Intermediate Hinge (Nodes 5 and 6) Transverse Relative Displacement—0.5-g; with Hinge Bolts.

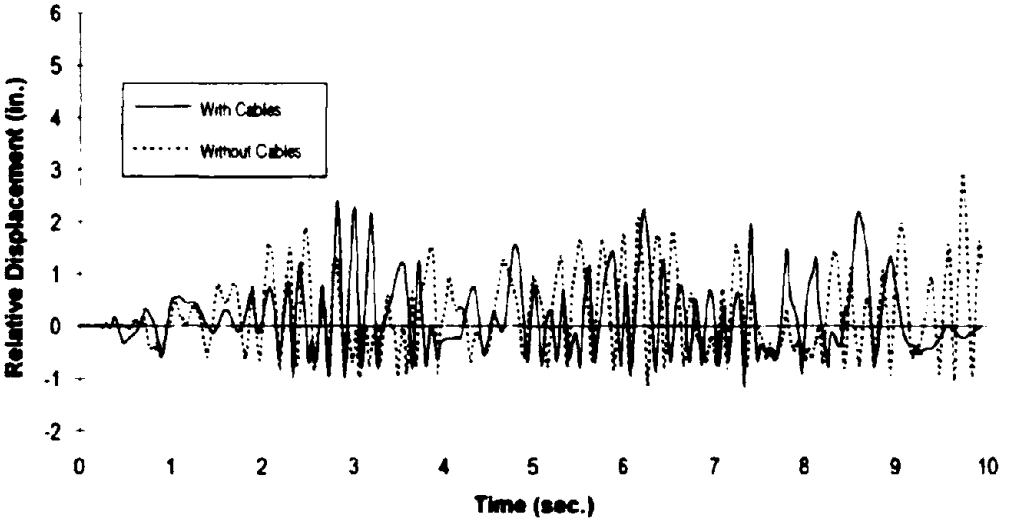

Figure 4-49. North Intermediate Hinge (Nodes 12 and 13) Longitudinal Relative Displacement—0.5-g, with Hinge Bolts.

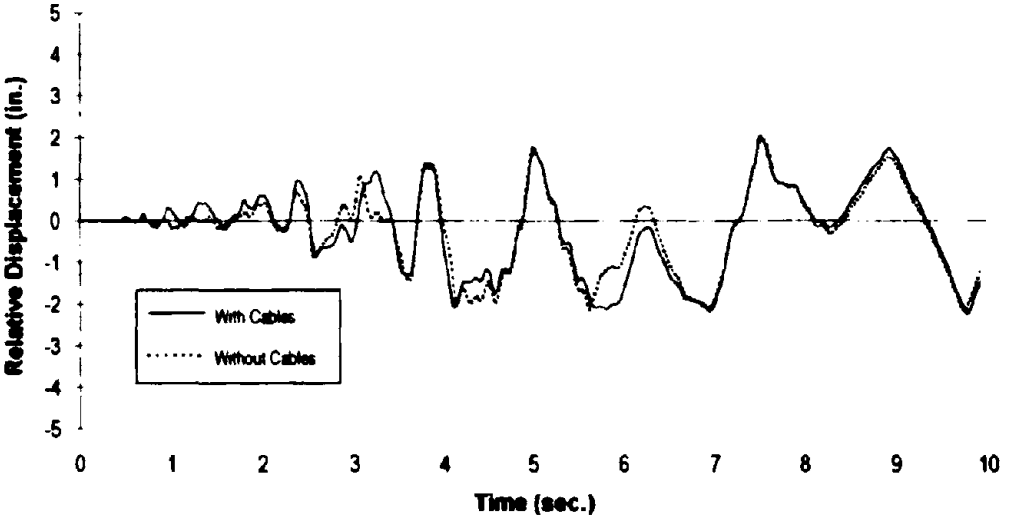

Figure 4-50. North Intermediate Hinge (Nodes 12 and 13) Transverse Relative Displacement—0.5-g, with Hinge Bolts.

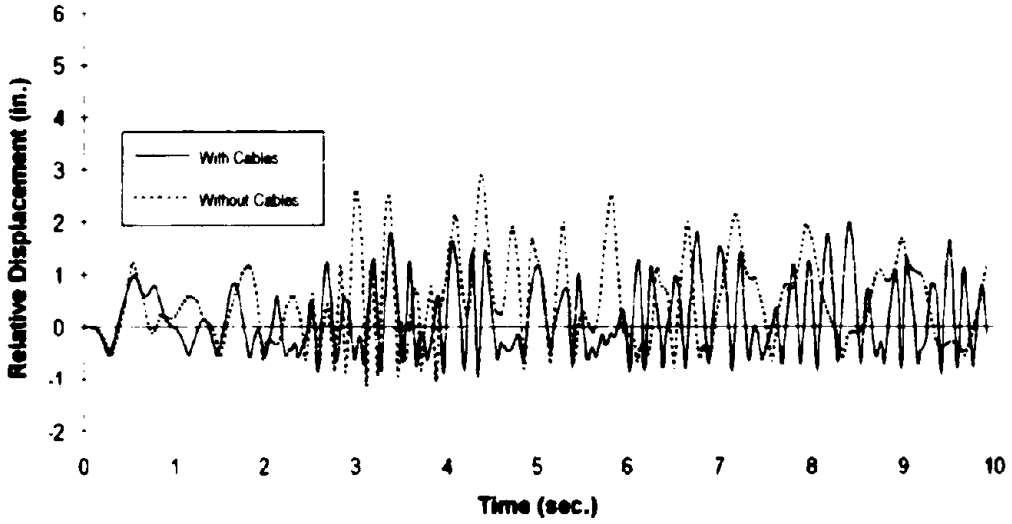

Figure 4-51. South Intermediate Hinge (Nodes 5 and 6) Longitudinal Relative Displacement—0.5-g; without Hinge Bolts.

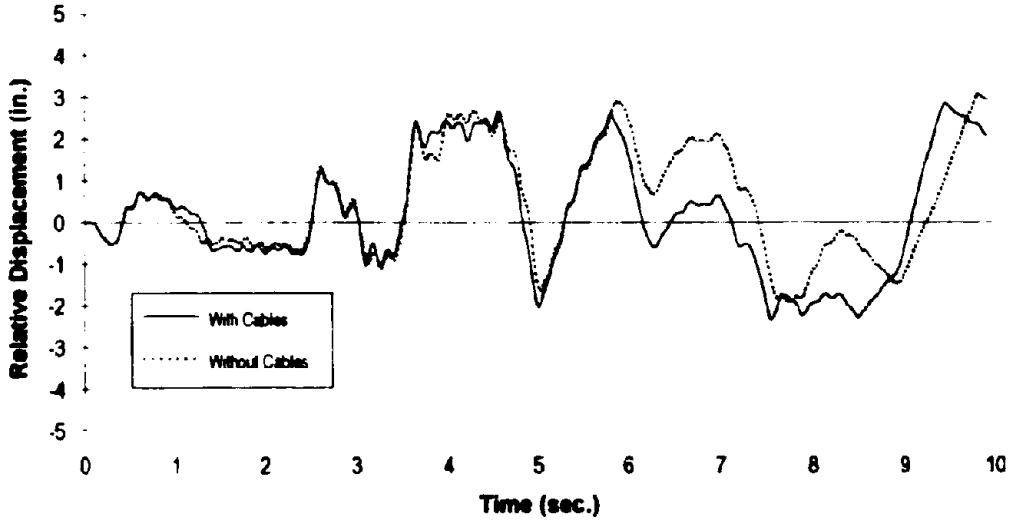

Figure 4-52. South Intermediate Hinge (Nodes 5 and 6) Transverse Relative Displacement—0.5-g; without Hinge Bolts.

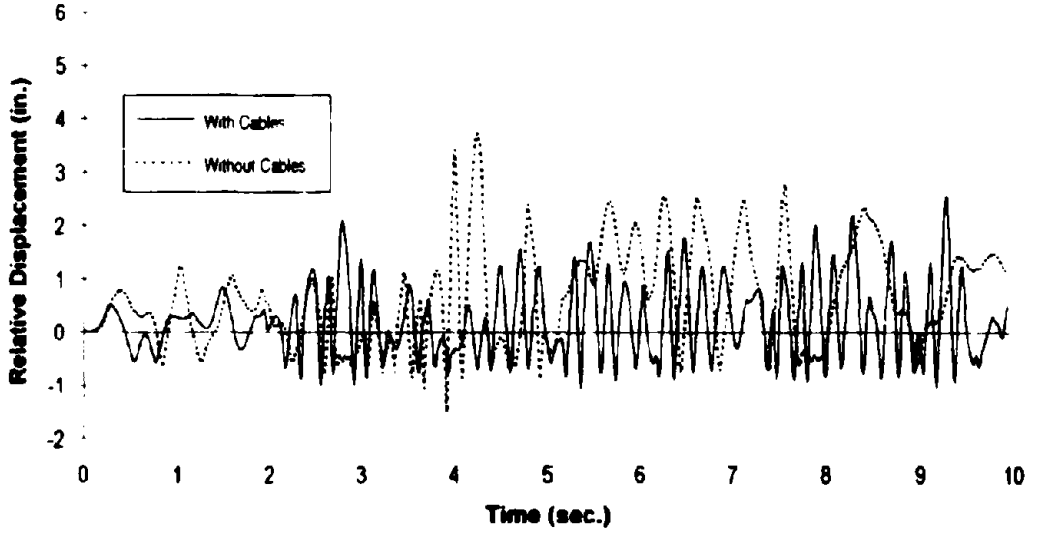

Figure 4-53. North Intermediate Hinge (Nodes 12 and 13) Longitudinal Relative Displacement—0.5-g; without Hinge Bolts.

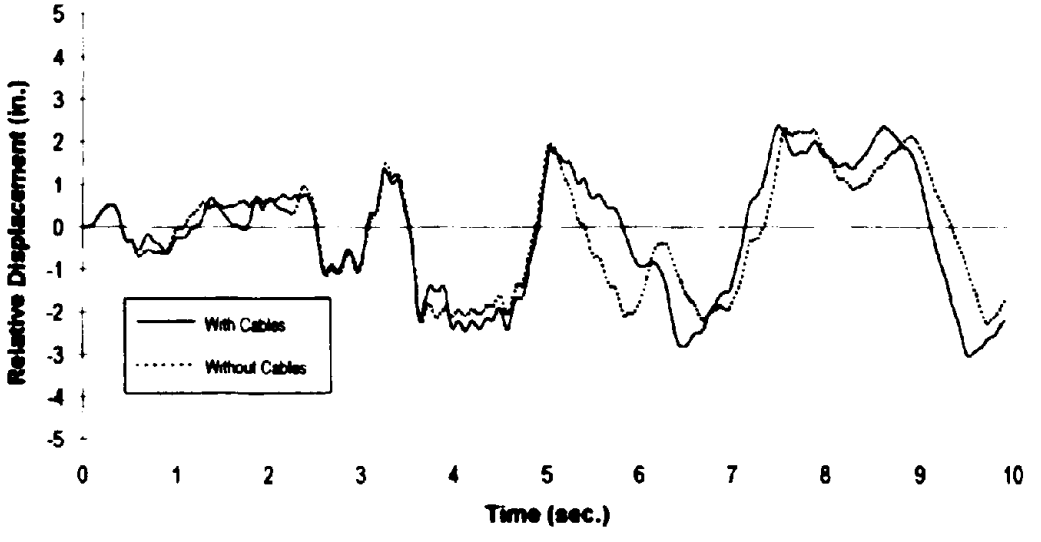

Figure 4-54. North Intermediate Hinge (Nodes 12 and 13) Transverse Relative Displacement—0.5-g; without Hinge Bolts.

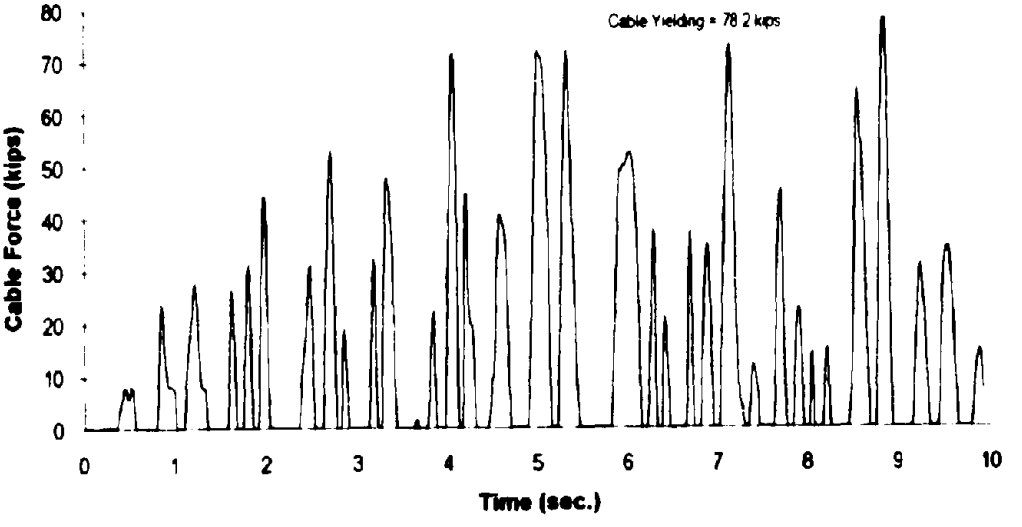

Figure 4-55. South Intermediate Hinge Restrainer Cable Force –0.65-g; with Hinge Bolts.

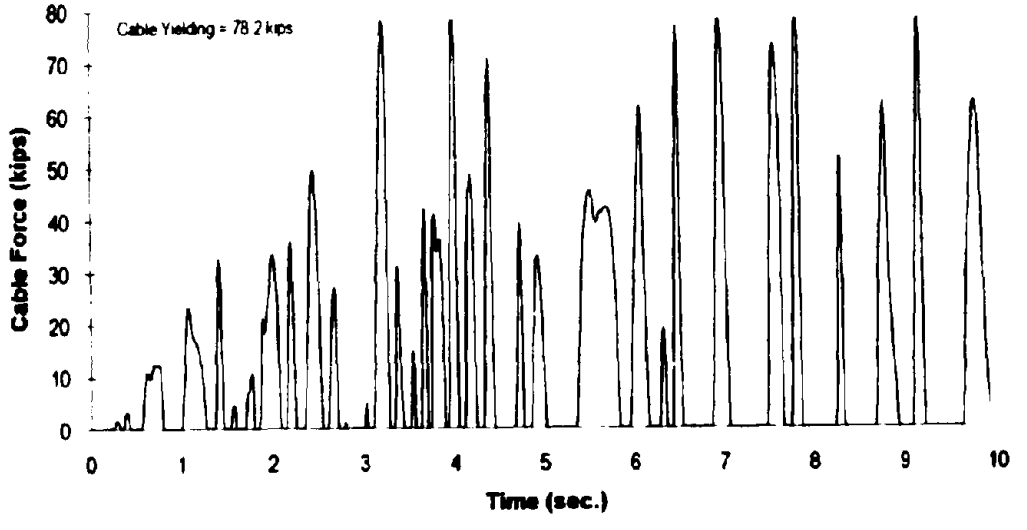

Figure 4-56. North Intermediate Hinge Restrainer Cable Force—0.65-g; with Hinge Bolts.

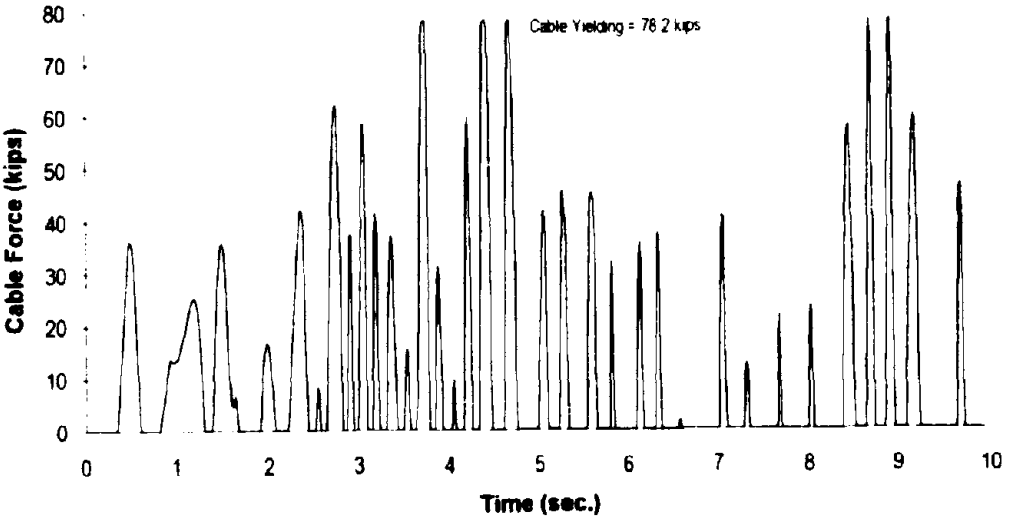

Figure 4-57. South Intermediate Hinge Restrainer Cable Force—0.65-g; without Hinge Bolts.

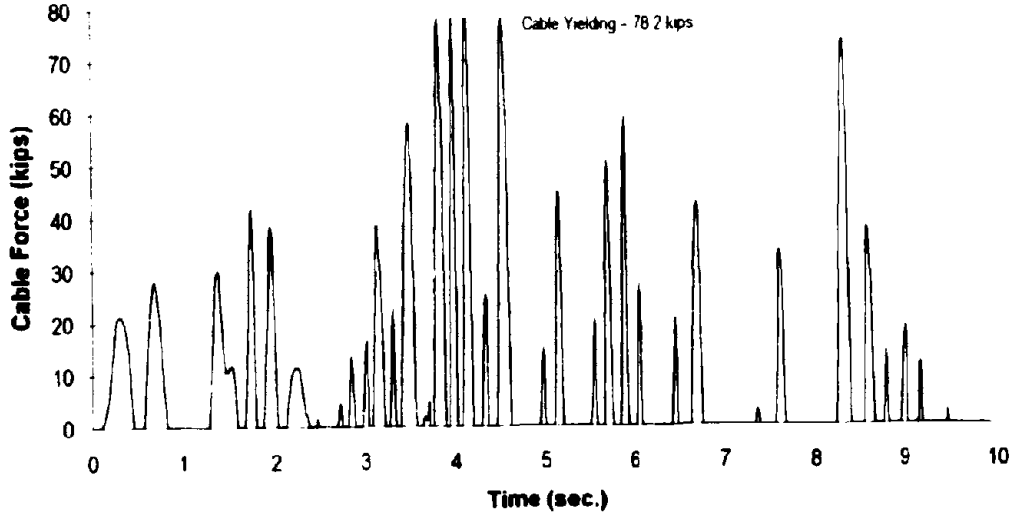

Figure 4-58. North Intermediate Hinge Restrainer Cable Force—0.65-g; without Hinge Bolts.

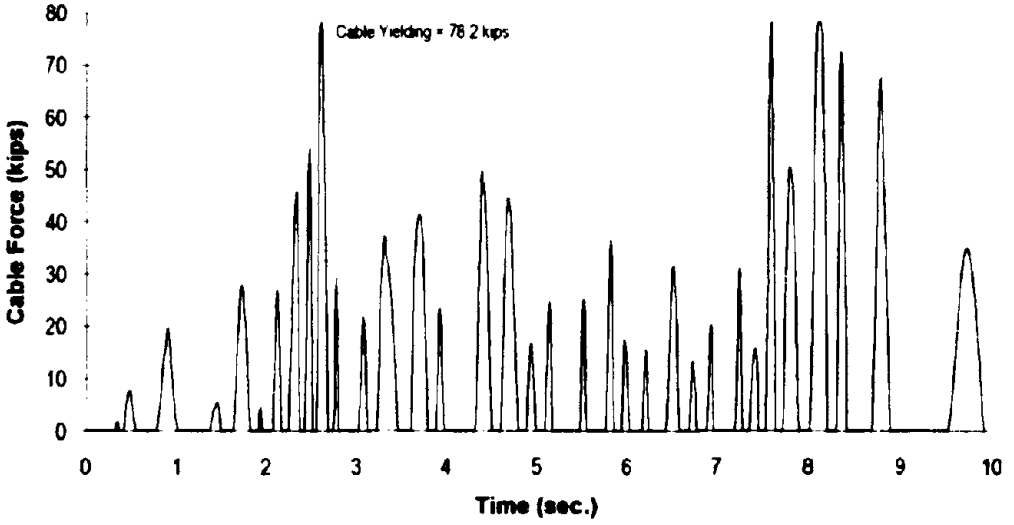

Figure 4-59. South Intermediate Hinge Restrainer Cable Force—0.5-g; with Hinge Bolts.

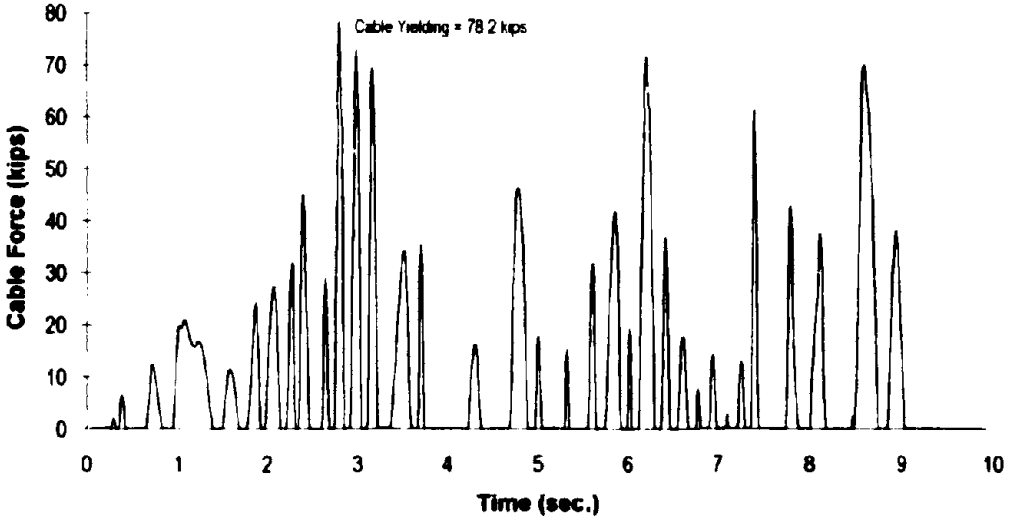

Figure 4-60. North Intermediate Hinge Restrainer Cable Force—0.5-g; with Hinge Bolts.

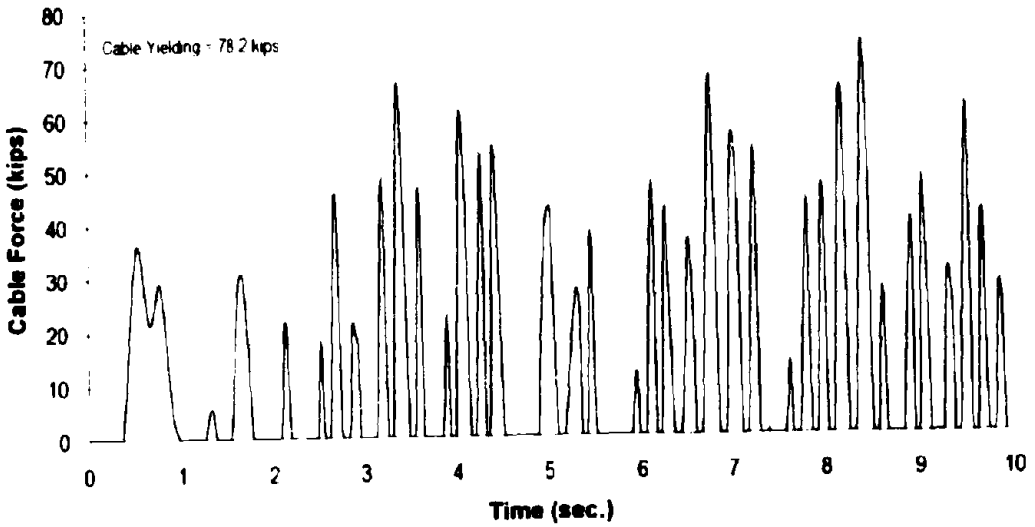

Figure 4-61. South Intermediate Hinge Restrainer Cable Force—0.5-g; without Hinge Bolts.

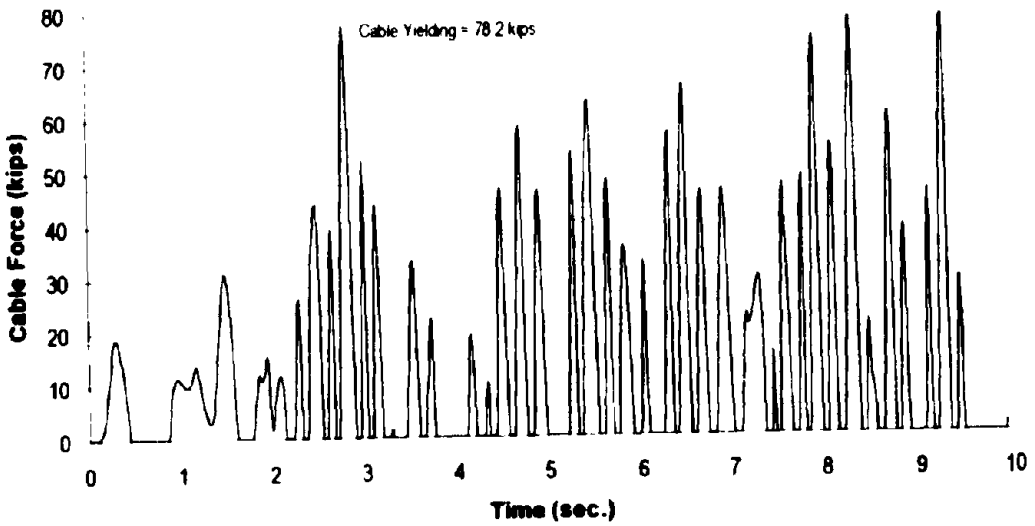

Figure 4-62. North Intermediate Hinge Restrainer Cable Force—0.5-g; without Hinge Bolts.

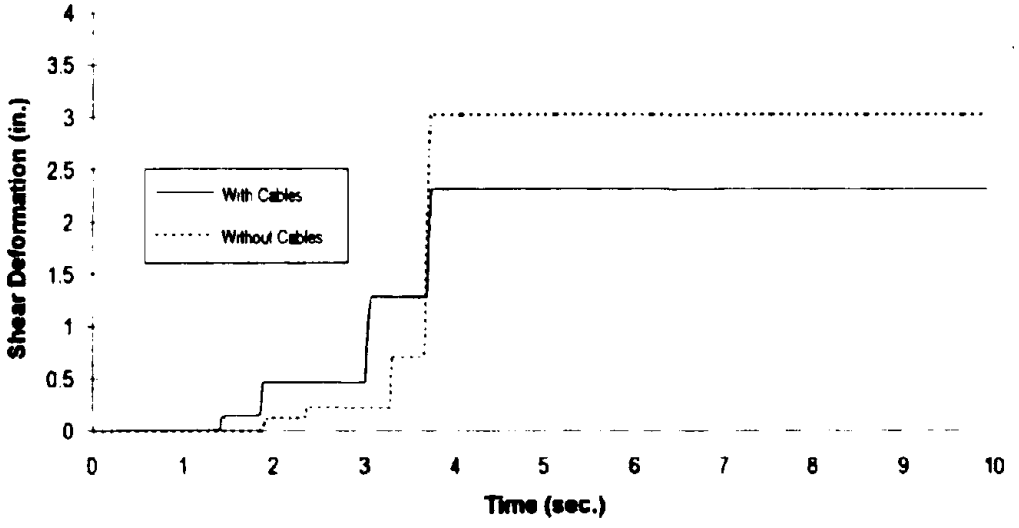

Figure 4-63. South Abutment Shear Block Longitudinal Deformation—0.65-g; with Hinge Bolts.

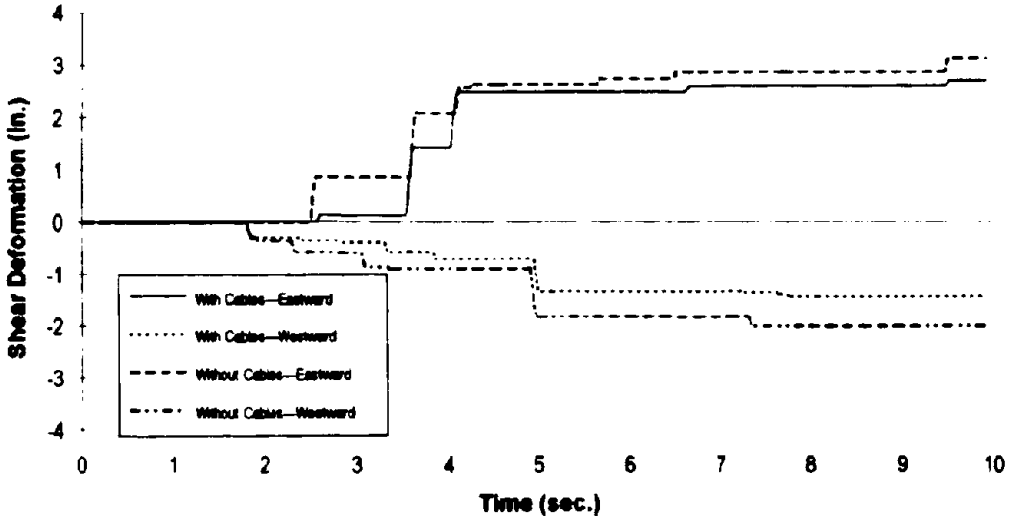

Figure 4-64. South Abutment Shear Block Transverse Deformation—0.65-g; with Hinge Bolts.

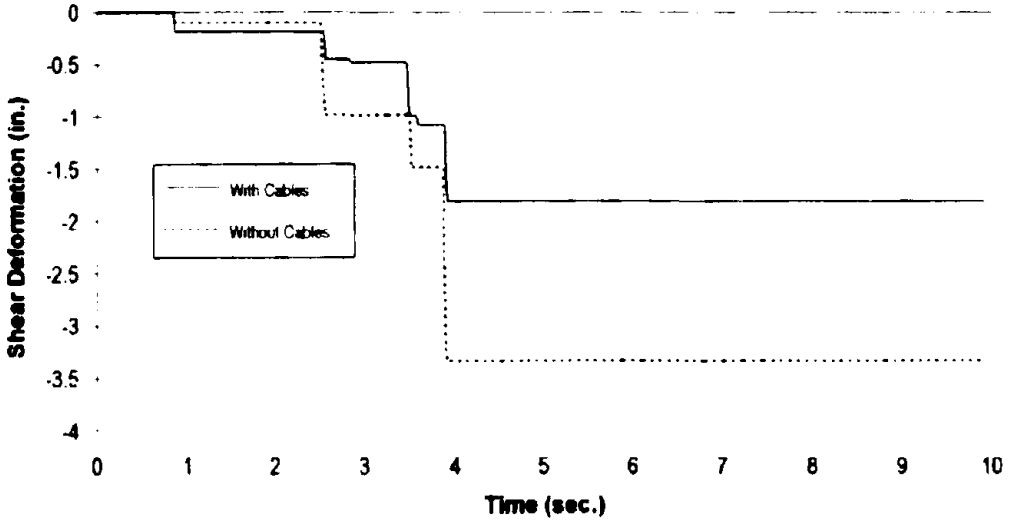

Figure 4-65. North Abutment Shear Block Longitudinal Deformation—0.65-g, with Hinge Bolts.

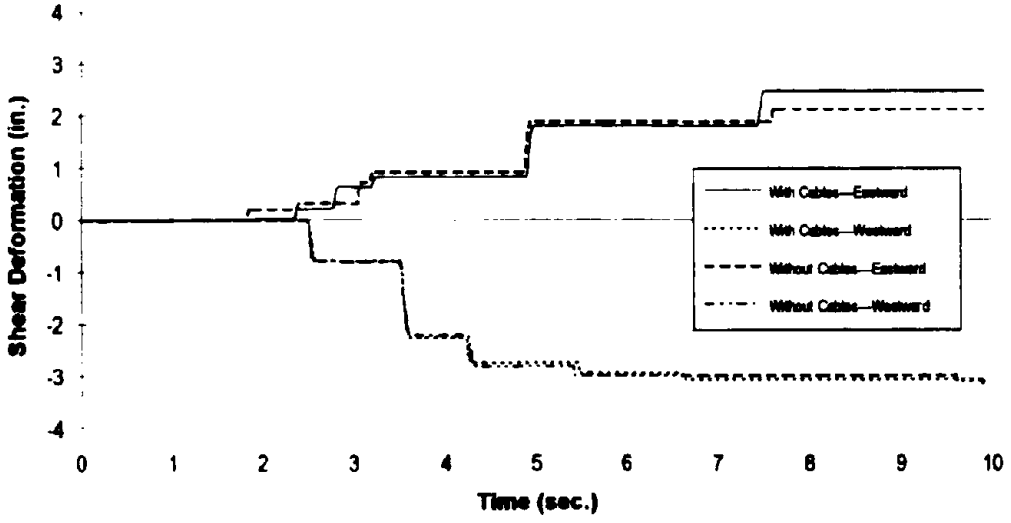

Figure 4-66. North Abutment Shear Block Transverse Deformation—0.65-g, with Hinge Bolts.

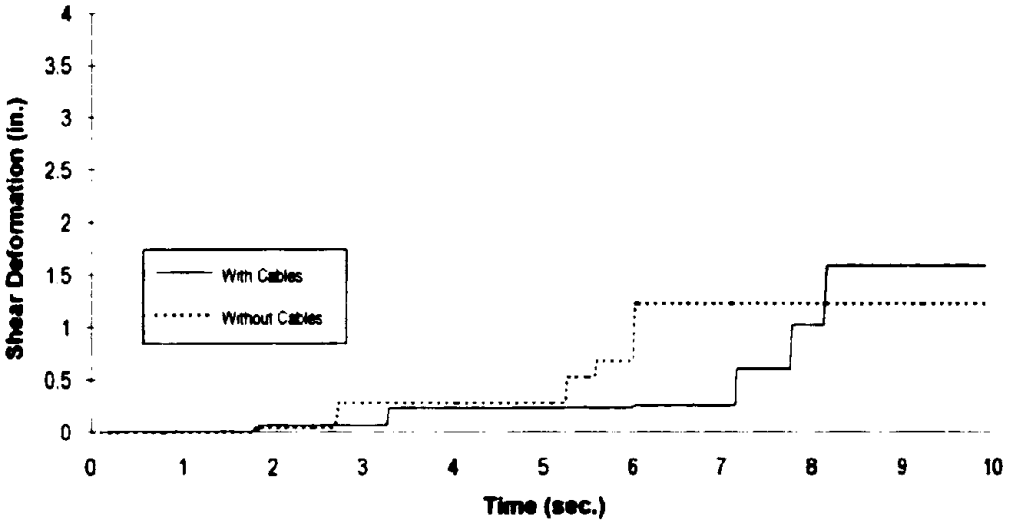

Figure 4-67. South Abutment Shear Block Longitudinal Deformation—0.65-g, without Hinge Bolts.

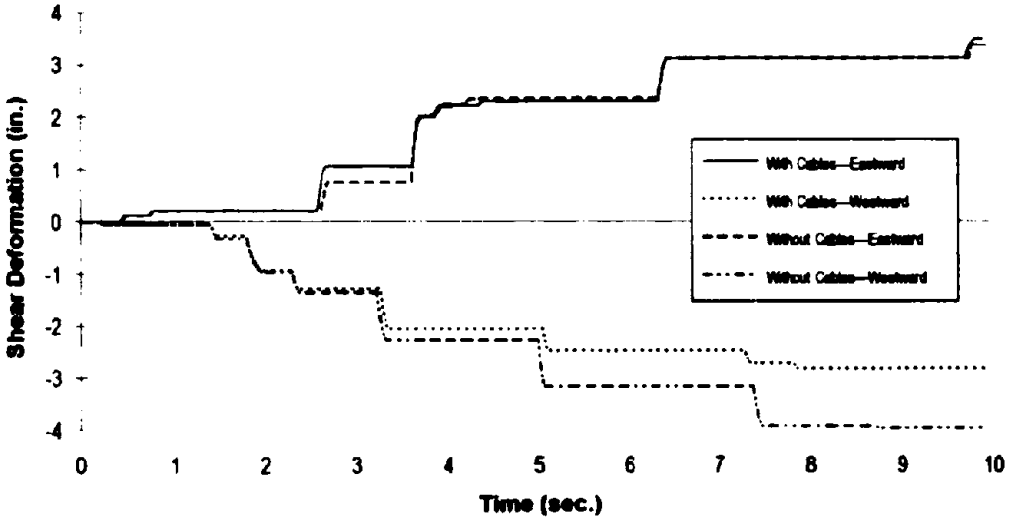

Figure 4-68. South Abutment Shear Block Transverse Deformation—0.65-g, without Hinge Bolts.

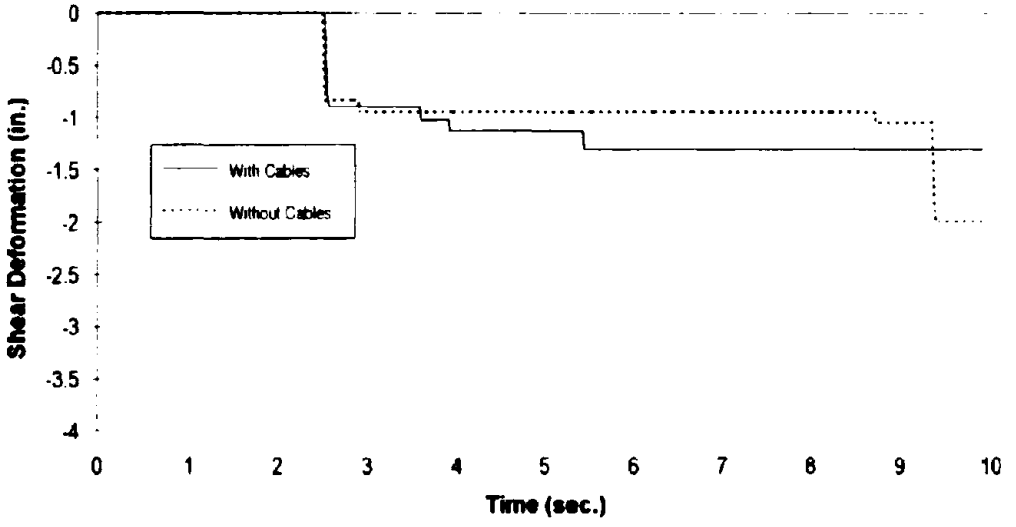

Figure 4-69. North Abutment Shear Block Longitudinal Deformation—0.65-g; without Hinge Bolts.

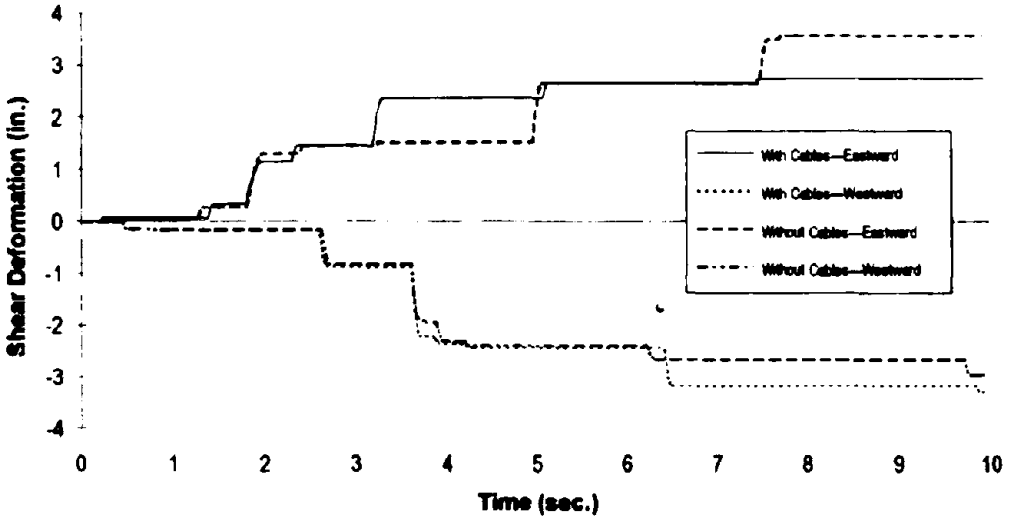

Figure 4-70. North Abutment Shear Block Transverse Deformation—0.65-g; without Hinge Bolts.

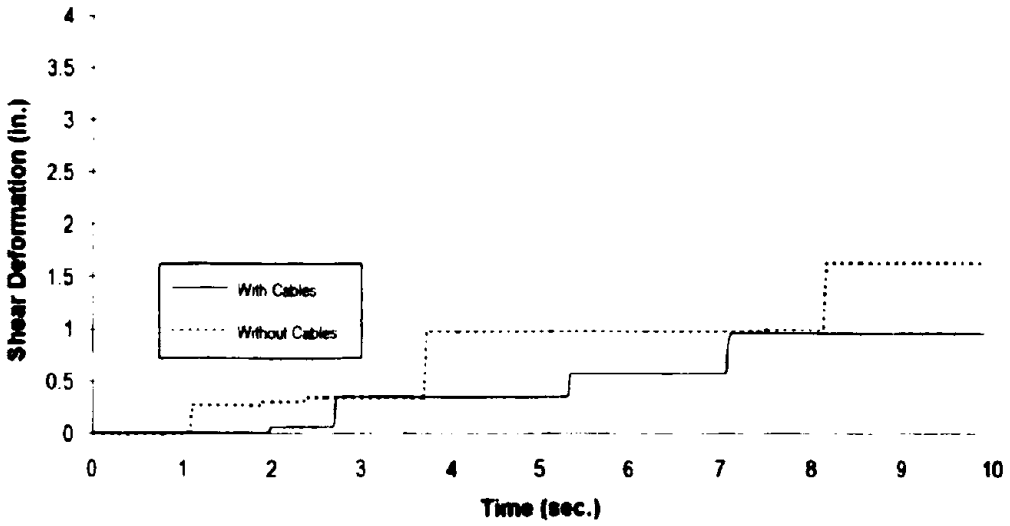

Figure 4-71. South Abutment Shear Block Longitudinal Deformation—0.5-g; with Hinge Bolts.

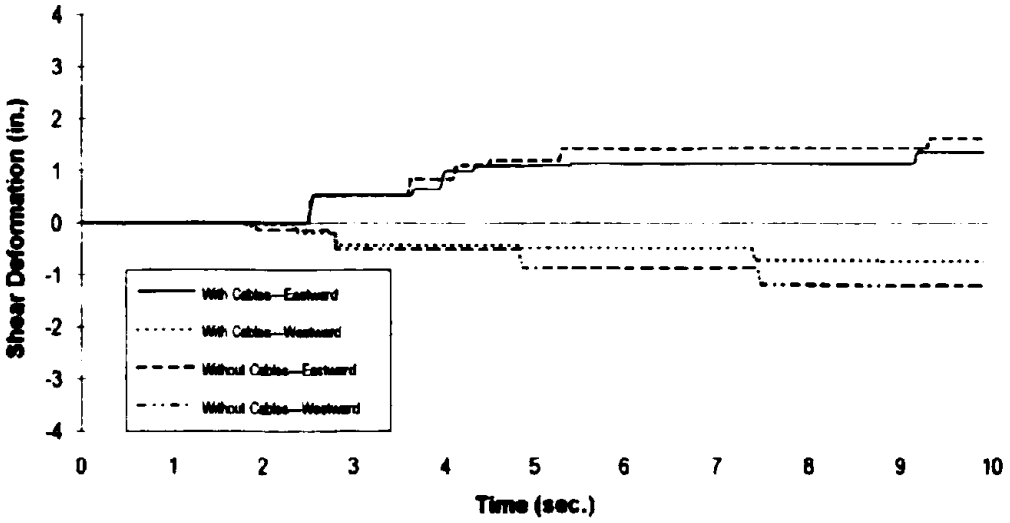

Figure 4-72. South Abutment Shear Block Transverse Deformation—0.5-g; with Hinge Bolts.

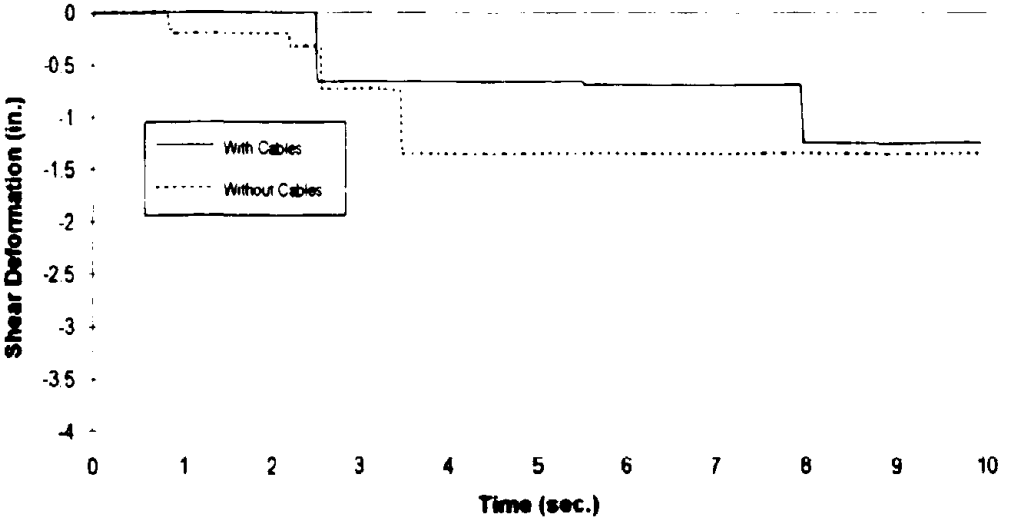

Figure 4-73. North Abutment Shear Block Longitudinal Deformation—0.5-g, with Hinge Bolts.

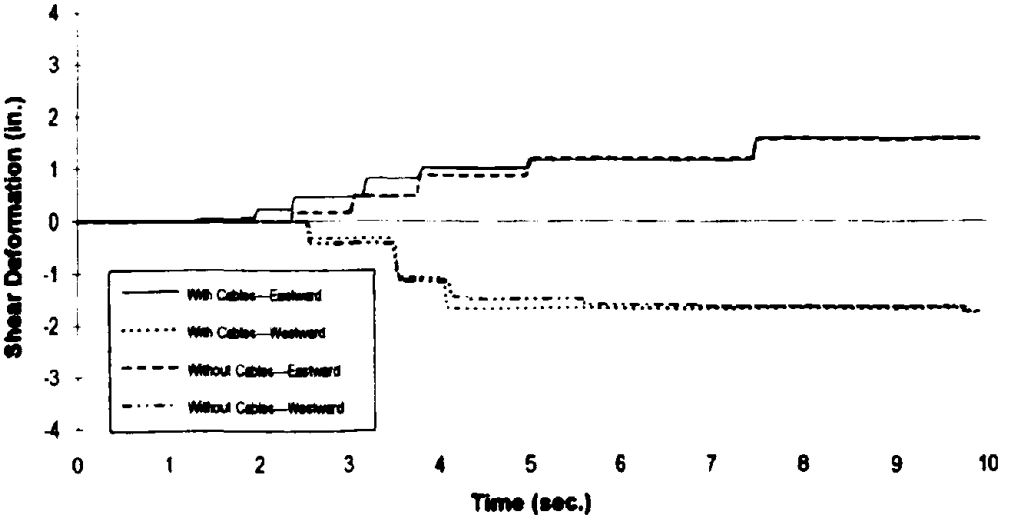

Figure 4-74. North Abutment Shear Block Transverse Deformation—0.5-g; with Hinge Bolts.

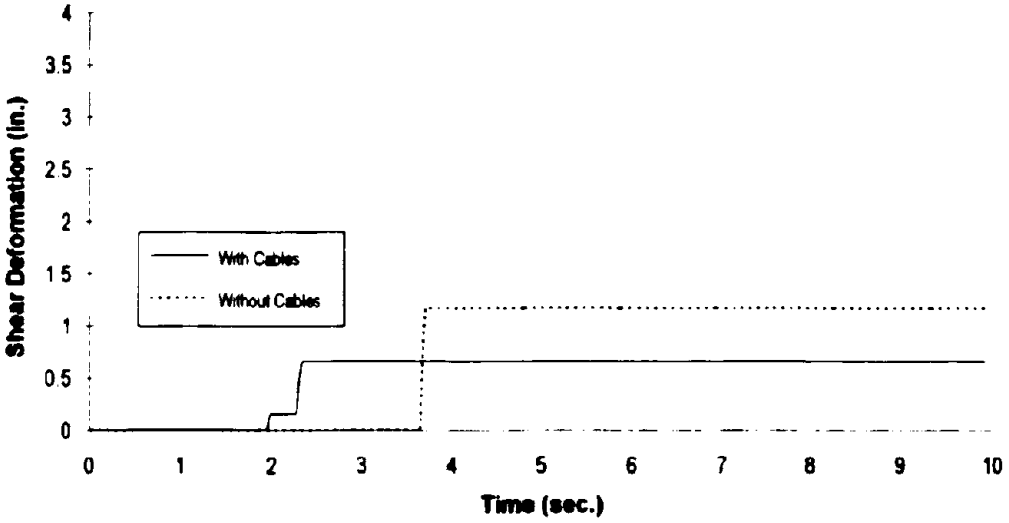

Figure 4-75. South Abutment Shear Block Longitudinal Deformation—0.5-g; without Hinge Bolts.

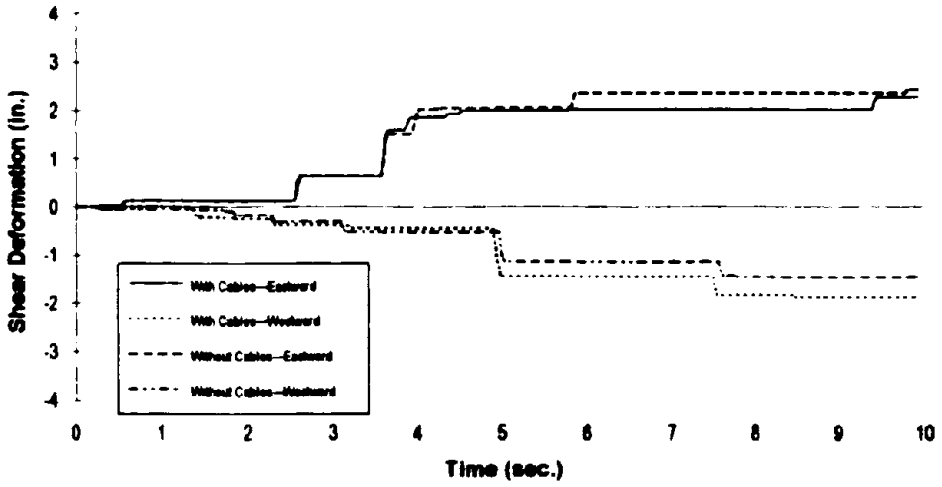

Figure 4-76. South Abutment Shear Block Transverse Deformation—0.5-g; without Hinge Bolts.

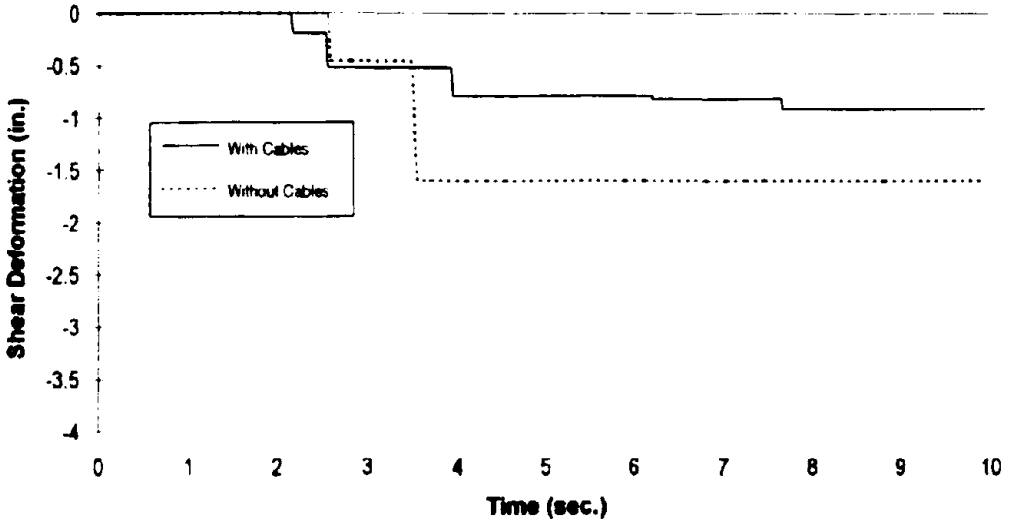

Figure 4-77. North Abutment Shear Block Longitudinal Deformation—0.5-g; without Hinge Bolts.

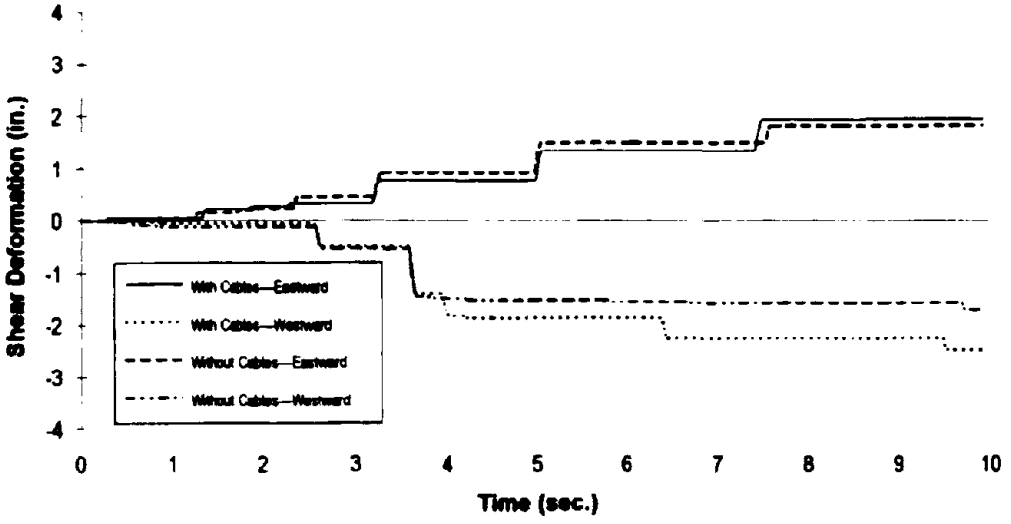

Figure 4-78. North Abutment Shear Block Transverse Deformation—0.5-g; without Hinge Bolts.

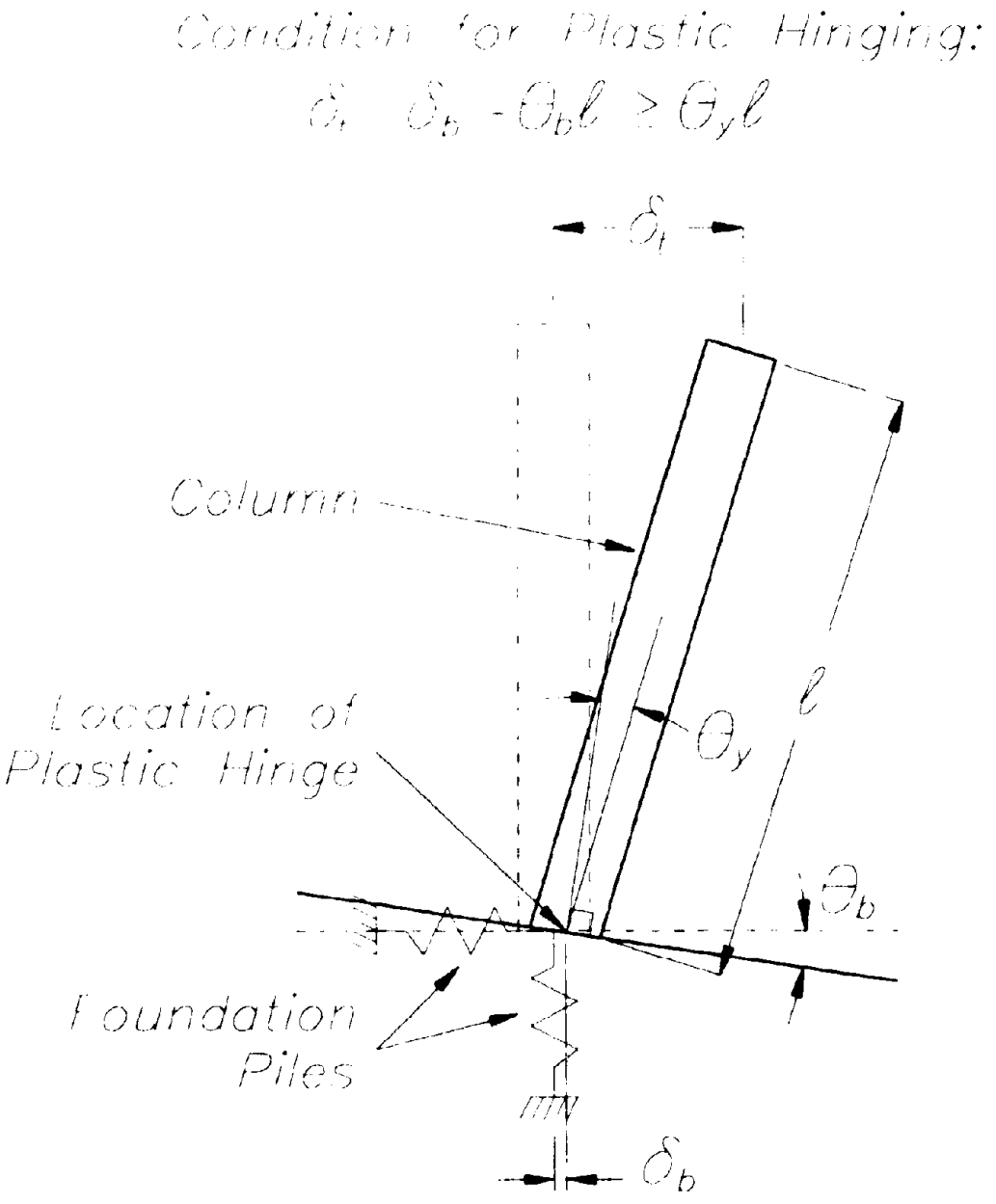

Figure 4-79. Plastic Hinging (Yielding) of Column Base in *NEABS* Model.

List of CCEER Publications

Report No.	Publication
CCEER-84-1	Saiidi, M., and R. A. Lawver. "User's manual for LZAK-C64, a computer program to implement the Q-model on Commodore 64." *Report number CCEER-84-1.* Reno: University of Nevada, Department of Civil Engineering. January 1984.
CCEER-84-2	Douglas, B. M., and T. Iwasaki. "Proceedings of the first USA-Japan bridge engineering workshop," held at the Public Works Research Institute, Tsukuba, Japan. *Report number CCEER-84-2.* Reno: University of Nevada, Department of Civil Engineering. April 1984.
CCEER-84-3	Saiidi, M., J. D. Hart, and B. M. Douglas. "Inelastic static and dynamic analysis of short R/C bridges subjected to lateral loads." *Report number CCEER-84-3.* Reno: University of Nevada, Department of Civil Engineering. July 1984.
CCEER-84-4	Douglas, B. "A proposed plan for a national bridge engineering laboratory." *Report number CCEER-84-4.* Reno: University of Nevada, Department of Civil Engineering. December 1984.
CCEER-85-1	Norris, G. M., and P. Abdollaholiaee. "Laterally loaded pile response: Studies with the strain wedge model." *Report number CCEER-85-1.* Reno: University of Nevada, Department of Civil Engineering. April 1985.
CCEER-86-1	Ghusn, G. E., and M. Saiidi. "A simple hysteretic element for biaxial bending of R/C columns and implementation in NEABS-86." *Report number CCEER-86-1.* Reno: University of Nevada, Department of Civil Engineering. July 1986.
CCEER-86-2	Saiidi, M., R. A. Lawver, and J. D. Hart. "User's manual of ISADAB and SIBA, computer programs for nonlinear transverse analysis of highway bridges subjected to static and dynamic lateral loads." *Report number CCEER-86-2.* Reno: University of Nevada, Department of Civil Engineering. September 1986.
CCEER-87-1	Siddharthan, R. "Dynamic effective stress response of surface and embedded footings in sand." *Report number CCEER-87-1.* Reno: University of Nevada, Department of Civil Engineering. June 1987.
CCEER-87-2	Norris, G., and R. Sack. "Lateral and rotational stiffness of pile groups for seismic analysis of highway bridges." *Report number CCEER-87-2.* Reno: University of Nevada, Department of Civil Engineering. June 1987.
CCEER-88-1	Orie, J., and M. Saiidi. "A preliminary study of one-way reinforced concrete pier hinges subjected to shear and flexure." *Report number CCEER-88-1.* Reno: University of Nevada, Department of Civil Engineering. January 1988.
CCEER-88-2	Orie, D., M. Saiidi, and B. Douglas. "A micro-CAD system for seismic design of regular highway bridges." *Report number CCEER-88-2.* Reno: University of Nevada, Department of Civil Engineering. June 1988.

CCEER-88-3 Orie, D., and M. Saiidi. "User's manual for Micro-SARB, a microcomputer program for seismic analysis of regular highway bridges." *Report number CCEER-88-3.* Reno: University of Nevada, Department of Civil Engineering. October 1988.

CCEER-89-1 Douglas, B., M. Saiidi, R. Hayes, and G. Holcomb. "A comprehensive study of the loads and pressures exerted on wall forms by the placement of concrete." *Report number CCEER-89-1.* Reno: University of Nevada, Department of Civil Engineering. February 1989.

CCEER-89-2a Richardson, J., and B. Douglas. "Dynamic response analysis of the Dominion Road Bridge test data." *Report number CCEER-89-2.* Reno: University of Nevada, Department of Civil Engineering. March 1989.

CCEER-89-2b Vrontinos, S., M. Saiidi, and B. Douglas. "A simple model to predict the ultimate response of R/C beams with concrete overlays." *Report number CCEER-89-2.* Reno: University of Nevada, Department of Civil Engineering. June 1989.

CCEER-89-3 Ebrahimpour, A., and P. Jagadish. "Statistical modeling of bridge traffic loads: A case study." *Report number CCEER-89-3.* Reno: University of Nevada, Department of Civil Engineering. December 1989.

CCEER-89-4 Shields, J., and M. Saiidi. "Direct field measurement of prestress losses in box girder bridges." *Report number CCEER-89-4.* Reno: University of Nevada, Department of Civil Engineering. December 1989.

CCEER-90-1 Saiidi, M., E. Maragakis, G. Ghusn, Jr., Y. Jiang, and D. Schwartz. "Survey and evaluation of Nevada's transportation infrastructure, task 7.2—highway bridges, final report." *Report number CCEER-90-1.* Reno: University of Nevada, Department of Civil Engineering. October 1990.

CCEER-90-2 Abdel-Ghaffar, S., E. Maragakis, and M. Saiidi. "Analysis of the response of reinforced concrete structures during the Whittier earthquake of 1987." *Report number CCEER-90-2.* Reno: University of Nevada, Department of Civil Engineering. October 1990.

CCEER-91-1 Saiidi, M., E. Hwang, E. Maragakis, and B. Douglas. "Dynamic testing and analysis of the Flamingo Road Interchange." *Report number CCEER-91-1.* Reno: University of Nevada, Department of Civil Engineering. February 1991.

CCEER-91-2 Norris, G., R. Siddharthan, Z. Zafir, S. Abdel-Ghaffar, and P. Gowda. "Soil-foundation-structure behavior at the Oakland Outer Harbor Wharf." *Report number CCEER-91-2.* Reno: University of Nevada, Department of Civil Engineering. July 1991.

CCEER-91-3 Norris, G. M. "Seismic lateral and rotational pile foundation stiffness at Cypress." *Report number CCEER-91-3.* Reno: University of Nevada, Department of Civil Engineering. August 1991.

CCEER-91-4 O'Connor, D. N., and M. Saiidi. "A study of protective overlays for highway bridge decks in Nevada, with emphasis on polyester-styrene polymer concrete." *Report number CCEER-91-4.* Reno: University of Nevada, Department of Civil Engineering. October 1991.

CCEER-91-5 O'Connor, D. N., and M. Saiidi. "Laboratory studies of polyester-styrene polymer concrete engineering properties." *Report number CCEER-91-5.* Reno: University of Nevada, Department of Civil Engineering. November 1991.

CCEER-92-1 Straw, D. L., and M. "Saiid" Saiidi. "Scale model testing of one-way reinforced concrete pier hinges subjected to combined axial force, shear and flexure." *Report number CCEER-92-1,* ed. by D. N. O'Connor. Reno: University of Nevada, Department of Civil Engineering. March 1992.

CCEER-92-2 Wehbe, N., M. Saiidi, and F. Gordaninejad. "Basic behavior of composite sections made of concrete slabs and graphite epoxy beams." *Report number CCEER-92-2.* Reno: University of Nevada, Department of Civil Engineering. August 1992.

CCEER-92-3 Saiidi, M., and E. Hutchens. "A study of prestress changes in a post-tensioned bridge during the first 30 months." *Report number CCEER-92-3.* Reno: University of Nevada, Department of Civil Engineering. April 1992.

CCEER-92-4 Saiidi, M., B. Douglas, S. Feng, E. Hwang, and E. Maragakis. "Effects of axial force on frequency of prestressed concrete bridges." *Report number CCEER-92-4.* Reno: University of Nevada, Department of Civil Engineering. August 1992.

CCEER-92-5 Siddharthan, R., and Zafir, Z. "Response of layered deposits to traveling surface pressure waves." *Report number CCEER-92-5.* Reno: University of Nevada, Department of Civil Engineering. September 1992.

CCEER-92-6 Norris, G., and Zafir, Z. "Liquefaction and residual strength of loose sands from drained triaxial tests." *Report number CCEER-92-6.* Reno: University of Nevada, Department of Civil Engineering. September 1992.

CCEER-92-7 Douglas, B. "Some thoughts regarding the improvement of the University of Nevada, Reno's national academic standing." *Report number CCEER-92-7.* Reno: University of Nevada, Department of Civil Engineering. September 1992.

CCEER-92-8 Saiidi, M., E. Maragakis, and S. Feng. "An evaluation of the current Caltrans seismic restrainer design method." *Report number CCEER-92-8.* Reno: University of Nevada, Department of Civil Engineering. October 1992.

CCEER-92-9 O'Connor, D. N., M. Saiidi, and E. A. Maragakis. "Effect of hinge restrainers on the response of the Madrone Drive Undercrossing during the Loma Prieta earthquake." *Report number CCEER-92-9.* Reno: University of Nevada, Department of Civil Engineering. February 1993.

CCEER-92-10 O'Connor, D. N., and M. Saiidi. "Laboratory studies of polyester concrete: Compressive strength at elevated temperatures and following temperature cycling, bond strength to portland cement concrete, and modulus of elasticity." *Report number CCEER-92-10.* Reno: University of Nevada, Department of Civil Engineering. December 1992.